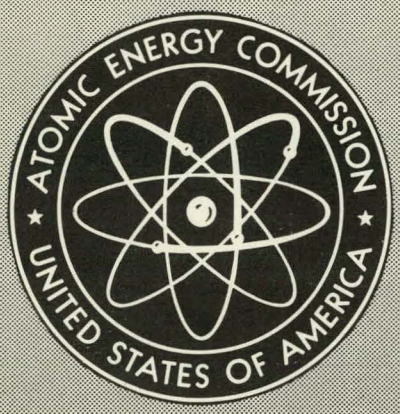

GA-3053

EXPERIMENTAL BERYLLIUM OXIDE REACTOR PROGRAM

Quarterly Progress Report for the Period
January 1, through March 31, 1962

April 25, 1962

General Atomic Division
General Dynamics Corporation
San Diego, California

UNITED STATES ATOMIC ENERGY COMMISSION • DIVISION OF TECHNICAL INFORMATION

DISCLAIMER

LEGAL NOTICE

This report has been reproduced directly from the best available copy.

Printed in USA. Price $2.25. Available from the Office of Technical Services, Department of Commerce, Washington 25, D. C.

USAEC Division of Technical Information Extension, Oak Ridge, Tennessee

GENERAL ATOMIC

DIVISION OF

GENERAL DYNAMICS

JOHN JAY HOPKINS LABORATORY FOR PURE AND APPLIED SCIENCE

P.O. BOX 608. SAN DIEGO 12. CALIFORNIA

GA-3053

REACTOR TECHNOLOGY

EXPERIMENTAL BERYLLIUM OXIDE REACTOR PROGRAM

QUARTERLY PROGRESS REPORT

for the period January 1, through March 31, 1962

U.S. Atomic Energy Commission

Contract AT(04-3)-187

April 25, 1962

PREVIOUS REPORTS IN THIS SERIES

GA-2372 – April, May, June, 1961

GA-2568 – July, August, September, 1961

GA-2847 – October, November, December, 1961

FOREWORD

The Experimental Beryllium Oxide Reactor (EBOR) Program, formerly the Maritime Gas-cooled Reactor (MGCR) Program, was initiated February 17, 1958, under Contract AT(04-3)-187 between the U. S. Atomic Energy Commission–Maritime Administration and General Dynamics Corporation. In December of 1960, formal authorization was received to reorient the program to include as an intermediate stage the design, construction, and test operation of a 10-Mw(t) reactor experiment for the purpose of determining the operating characteristics of BeO-moderated, gas-cooled systems and of lending greater assurance of success to the subsequent prototype plant. This reactor experiment is known as the Experimental Beryllium Oxide Reactor. The over-all project responsibility is assigned to the General Atomic Division of General Dynamics Corporation, and the project is being carried out by a staff of technical personnel from General Atomic.

The objective of the EBOR program is to develop a gas-cooled, BeO-moderated reactor which can be used in conjunction with a closed-cycle gas turbine or a steam cycle for a small land-based or a maritime power plant. Design objectives for the power plant are high thermodynamic efficiency, simplicity of design with attendant ease of operation, low maintenance costs, and maximum efficiency of operation over a wide range of power settings.

THIS PAGE

WAS INTENTIONALLY

LEFT BLANK

SUMMARY

REACTOR DEVELOPMENT

During the present reporting period, a series of steady-state and transient thermal stress tests on BeO moderator blocks was completed. In general, there was excellent correlation between the modulus-of-rupture values for the material tested and the stresses which caused failure.

The problem of preventing possible interlocking of adjacent fuel elements because of rotation of BeO moderator blocks during operation has been studied. As a result, the moderator-block design has been slightly altered to incorporate BeO dowels which will prevent such rotation. A honeycomb-type structure was selected for the blades of the cruciform control element in preference to the previously favored tube-type design, primarily because of the better dimensional control associated with the honeycomb design.

The life-cycling tests of the control-rod drives were completed after five life cycles--the equivalent of ten years of reactor operation--with the drives still functioning satisfactorily. Changes prompted by the experiences gained in the environmental testing, and those resulting from the change in the fuel-handling concept, have been incorporated into the control-rod-drive production drawings.

The core component handling concept has been developed to the degree that the equipment specifications for modification of the STF instrument bridge and for fabrication of the portable shield shutter and the core-component transfer cask have been released for procurement action.

The essential design of the instrument conduits and their anchors has been completed, and a purchase equipment specification has been prepared for use by the architect-engineer in procuring these components.

REACTOR PHYSICS

The experimental program on dry-core critical assemblies resembling the EBOR in composition and complexity was initiated following completion of the new critical-assembly building. Criticality was achieved in the first core of the series on January 12, 1962. A summary of the

experimental results obtained to date, an analysis of these results, and their correlations with respect to EBOR nuclear design are presented in this report. As in the previous series of experiments, excellent agreement between experimental results and analytical predictions is indicated.

The development of methods and analytical techniques for the solution of static EBOR physics problems has been essentially completed. Minor modifications were made to a few codes in order to assure their compatibility with General Atomic's IBM-7090, which has recently been placed in operation.

A detailed temperature-coefficient study for the EBOR has been completed. This study, in which temperature increments in various components of the heterogeneous core were considered as a function of time, revealed a fairly strong prompt negative coefficient due to fuel-pin heating, a small but negative delayed coefficient due to core moderator heating, and a positive delayed coefficient due to reflector heating. Several other calculations pertaining to the nuclear design of the EBOR were initiated during the quarter, and the results to date are summarized in this report.

In the reactor-physics effort supporting the EBOR nuclear design, a reactivity calculation of one of the highly loaded, uranium–beryllium oxide, bare, critical assemblies constructed at Livermore was completed. This calculation, in which essentially the same data and analytical techniques were used as were employed in EBOR calculations, verified the adequacy of our present methods. In addition, crystalline scattering kernels for beryllium oxide were calculated and incorporated into our compilation of data. An effort was also begun on the calculation of U^{235} resonance absorption with the resonance-theory prescriptions outlined by L. W. Nordheim and generally used for U^{238} resonance absorption.

Work has been completed on the calculation of flux-depression and spectra data for the MGCR-2 capsule to be irradiated in the General Electric Test Reactor (GETR), and similar calculations for the MGCR-7 capsule to be irradiated in the Westinghouse Testing Reactor (WTR) are nearing completion. The results of these calculations are summarized in this report.

MATERIALS DEVELOPMENT

Work on the development of BeO-coated BeO-UO_2 fuel compacts was resumed during the quarter.

The irradiation of the MGCR-4 and MGCR-BRR-9 fuel capsules was continued in the Materials Test Reactor (MTR). Peak fuel-cladding

surface temperatures of approximately 1640°F and 1600°F, respectively, are being maintained for the MGCR-4 and the MGCR-BRR-9.

The fabrication of BeO specimens for the MGCR-2 capsule has been completed at General Atomic, and the specimens are being ground to the required finished dimensions by a vendor. The thermal diffusivities of the capsule and the control specimens are being measured.

The MGCR-7 capsule for the irradiation of control-rod absorber materials has been completed. A refined strain-gauge technique for measuring the residual strain in the cladding of creep-shrunk fuel pins was developed. The results of measurements obtained with this technique indicate that a stress of approximately 28, 600 psi is introduced as a result of the creep-shrink operation.

The initial results of self-welding studies indicate that at a temperature of 1200°F and a contact pressure of 100 psi, A-212B carbon steel exhibits significant self-welding after 100 hr in helium, while 18/18 stainless steel bonds to itself after 100 hr at 1500°F and a contact pressure of 500 psi.

The initial test results from the fission-product plateout study indicate that the plateout of iodine is roughly inversely proportional to the absolute temperature. This plateout appears to be relatively insensitive to the nature of the substrate materials that have been studied (304 stainless steel, SA-387B low-alloy steel, and AISI 1030 carbon steel).

THIS PAGE

WAS INTENTIONALLY

LEFT BLANK

TENTATIVE EBOR DATA SHEET

Site	
Location	NRTS, Idaho
Operating Data	
Reactor thermal power, Mw	10
Reactor heat flux (max.), Btu/(hr)(ft^2)	210,000
Reactor heat flux (avg.), Btu/(hr)(ft^2)	77,100
Reactor inlet coolant pressure, psia	1117
Reactor outlet coolant pressure, psia	1085
Reactor inlet coolant temperature, ^oF	750
Reactor outlet coolant temperature, ^oF	1300
Maximum cladding temperature (hot spot), ^oF	1500
Coolant mass flow rate (through core), lb/sec	13.88
Coolant maximum velocity, ft/sec	240
Reactor Pressure Vessel	
Inside diameter, in.	116
Inside height, in.	280
Total weight of pressure vessel and internals, lb	440,000
Reactor Core	
Approximate dimensions, in.	23.3 × 23.3 × 76.0 high
Reflector thickness, in. BeO	~7
Number of fuel elements	36
Number of control rods	4
Loadings, kg	
U^{235}	100
U^{238}	60
Be:U^{235} atom ratio	117
Composition (with fuel element in core), vol-%	
UO_2-BeO fuel compacts	11.8
Cladding and spacers	3.0
Shroud	0.6
Fuel cooling void	11.0
Instrument tube and void	1.6
Moderator spine and outer block	63.6
Outer spacing gap	8.4

Fuel Element (annular ring of rods)

Number of rods	18
Number of fueled rods	18
Rod outside diameter, in.	0.375
Structural material	Hastelloy X
Amount of diluent (BeO) in fuel body, vol-%	76.0
Fueled length, in.	76.0
Over-all length of assembly, in.	82.5
Design life at full power, hr	10,000
Burnup at end of life, Mw-day/ton of U	2×10^4

Nuclear Data

Core nuclear constants at operating temperatures	
Median fission energy, ev	34
Age to indium resonance energy, cm^2	131
Infinite medium resonance-escape probabilities to 2 ev	
P_{28}	0.839
P_{total}	0.147
Reactivities (unrodded)	
Hot, clean	1.05
Cold, clean	1.07
Control-rod worth, % $\delta k/k$	
Hot, clean reactor, all four rods	25
Power distributions (normal)	
Axial maximum to average factor	2.2
Radial maximum to average factor	1.2
Core-element maximum to average factor	1.03

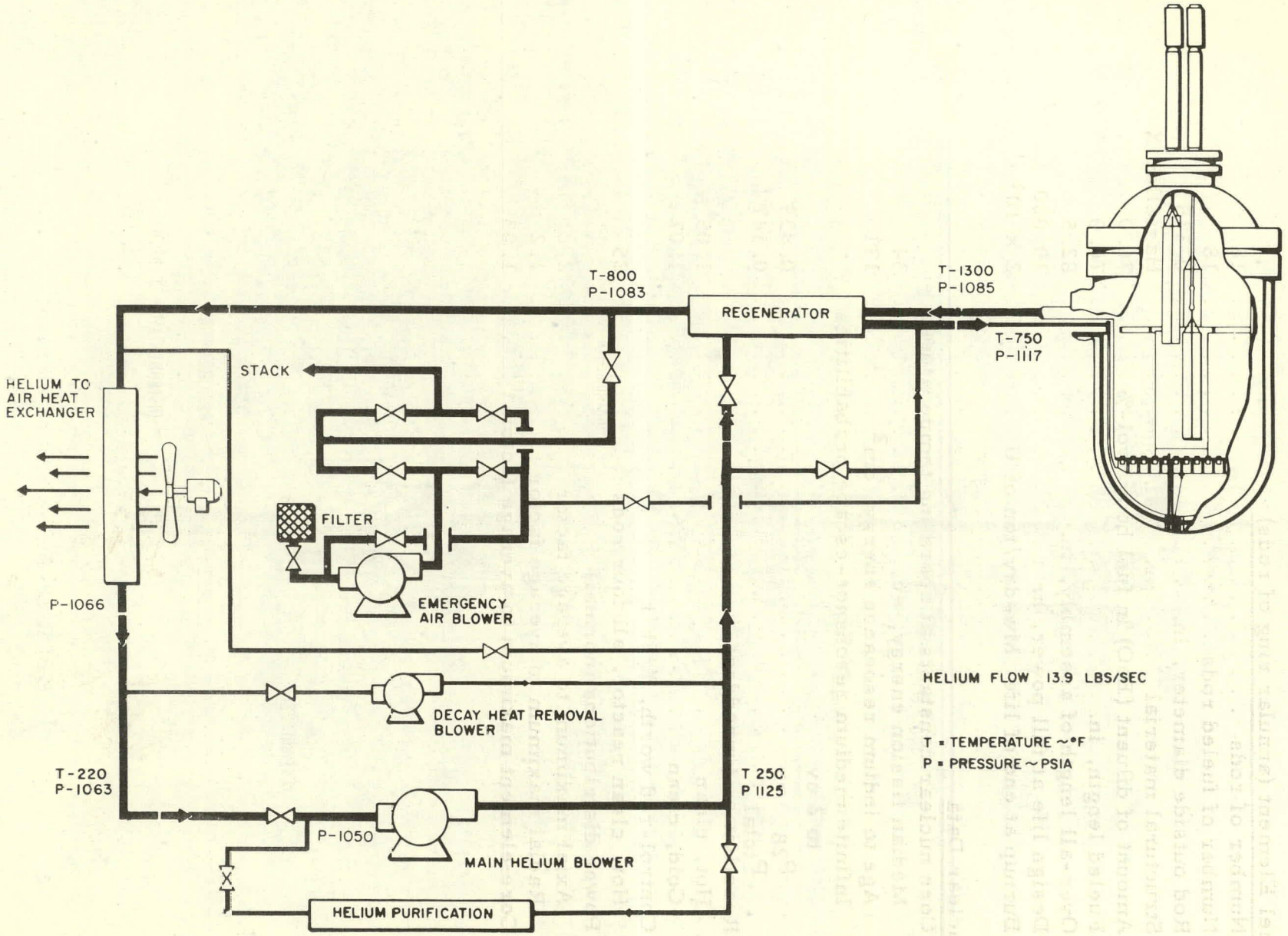

EBOR flow diagram

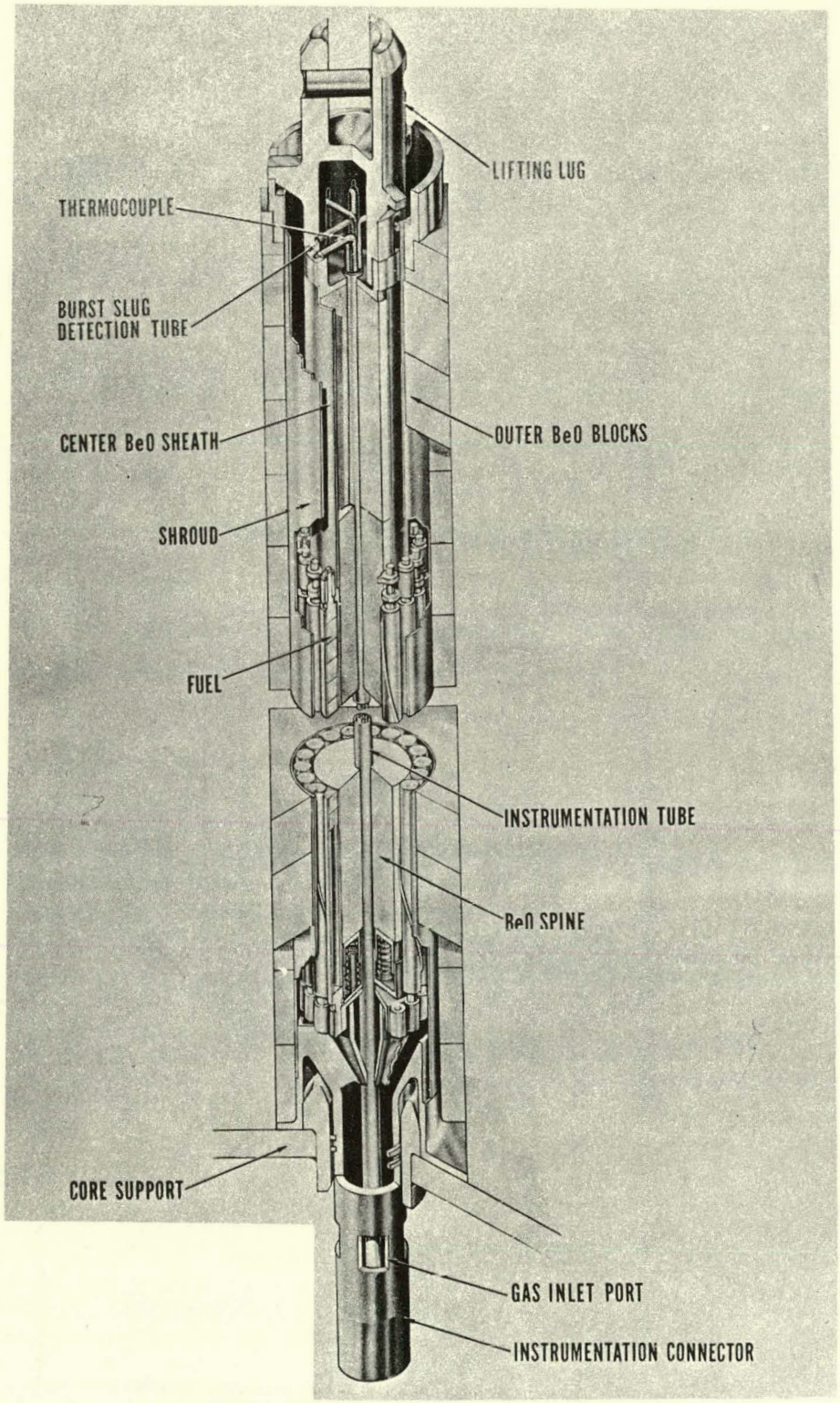

EBOR 18-fuel-pin core element

CONTENTS

I. REACTOR DEVELOPMENT

CORE AND ASSOCIATED COMPONENTS (K. A. Trickett, R. W. Bean)

Research and Development (Task 07)

Heat-transfer Experiments (R. Katz, G. J. Malek)

The final phase of experiments for determining the friction and heat-transfer correlations for the EBOR 18-pin fuel element has been started. The purpose of this work is to extend existing information from the design-point Reynolds number of about 20,000 to a Reynolds number of approximately 2,000. Data thus obtained will be applicable to reactor operation at partial power under shutdown or emergency cooling conditions. Tests with smooth rods in the element have been completed, and tests with rods having helical spacers are in progress.

A test is being initiated to determine the orifice coefficient for the reflector element. This test will permit accurate sizing of the orifice configuration for the EBOR so that the proper coolant flow will be directed to the reflector elements. The work statement which outlines the program and test procedures has been written, and work is proceeding on the assembly of the experimental apparatus.

BeO Thermal Stress Analysis (D. R. Buttemer)

Steady-state Thermal Stress Tests. The steady-state thermal stress test series utilizing the EBOR mockup blocks (approximately 98 wt-% BeO, 0.04 wt-% SiO_2, 1.4 wt-% Al_2O_3, and 0.3 wt-% MgO) has been completed. Since the tests were conducted using step increases in the power level into the blocks, the exact power (and corresponding stress level) at which fracture occurred in each block is not known. However, by careful examination of the blocks at each power increment, the stress range within which each fracture occurred was determined. These values, which are presented in Table 1.1, may be compared with an average modulus of rupture of 17,700 psi obtained at General Atomic[1]* for specimens of the same composition at a comparable temperature. The generally excellent correlation shows that, for the geometry tested, modulus of rupture is an acceptable strength criterion for thermal loading. Testing will be continued during the next reporting period on blocks containing a 1 wt-% bentonite additive.

---

*References are listed at the end of each section.

Table 1. 1

RESULTS OF STEADY-STATE BeO THERMAL STRESS TESTS ON EBOR MOCKUP BLOCKS

Test Block	Maximum Tensile Thermal Stress Developed	
	Before Fracture (psi)	After Fracture (psi)
C	15,000	16,500
D	14,300	16,200
E	17,500	(*)
F	18,900	(*)
G	17,700	18,600

*Specimens were not fractured owing to limitations of the test facility.

A brief description of the test setup and the calculational method is given in the previous quarterly progress report.[2]

BeO Quench Tests. Quench tests of the square-annular beryllia blocks of EBOR mockup composition have been completed. These tests have as their objective the specification of the allowable temperature difference between the beryllia in a spent core element and the storage-pool water such that additional damage to the beryllia will not occur during handling prior to examination.

To provide close control of the water temperature during the test, boiling water was used for the quench. The test results, including the initial block temperature for which cracking was noted and the temperature at which complete fracture occurred, are summarized in Fig. 1. 1 for each of the eight blocks tested. In each case, the initial temperature difference between the block and the water may be obtained by subtracting 212°F from the initial block temperature. The average temperature difference for which cracking occurred was found to be 152°F and the minimum difference was found to be 128°F. The maximum thermal stress for the 152°F average temperature difference was calculated to be 19,800 psi tension. The average measured modulus of rupture for the same blocks at room temperature is 18,600 psi.[1]

Two additional tests were conducted using quench water at room temperature. The results were inconclusive, primarily because of the small heat capacity of the test apparatus, which resulted in a significant change in the quench-water temperature during the test. Since the storage pool will be an essentially infinite heat sink, the test conditions were considered to be so unrealistic that further tests to determine the effect of using subcooled water have been temporarily discontinued.

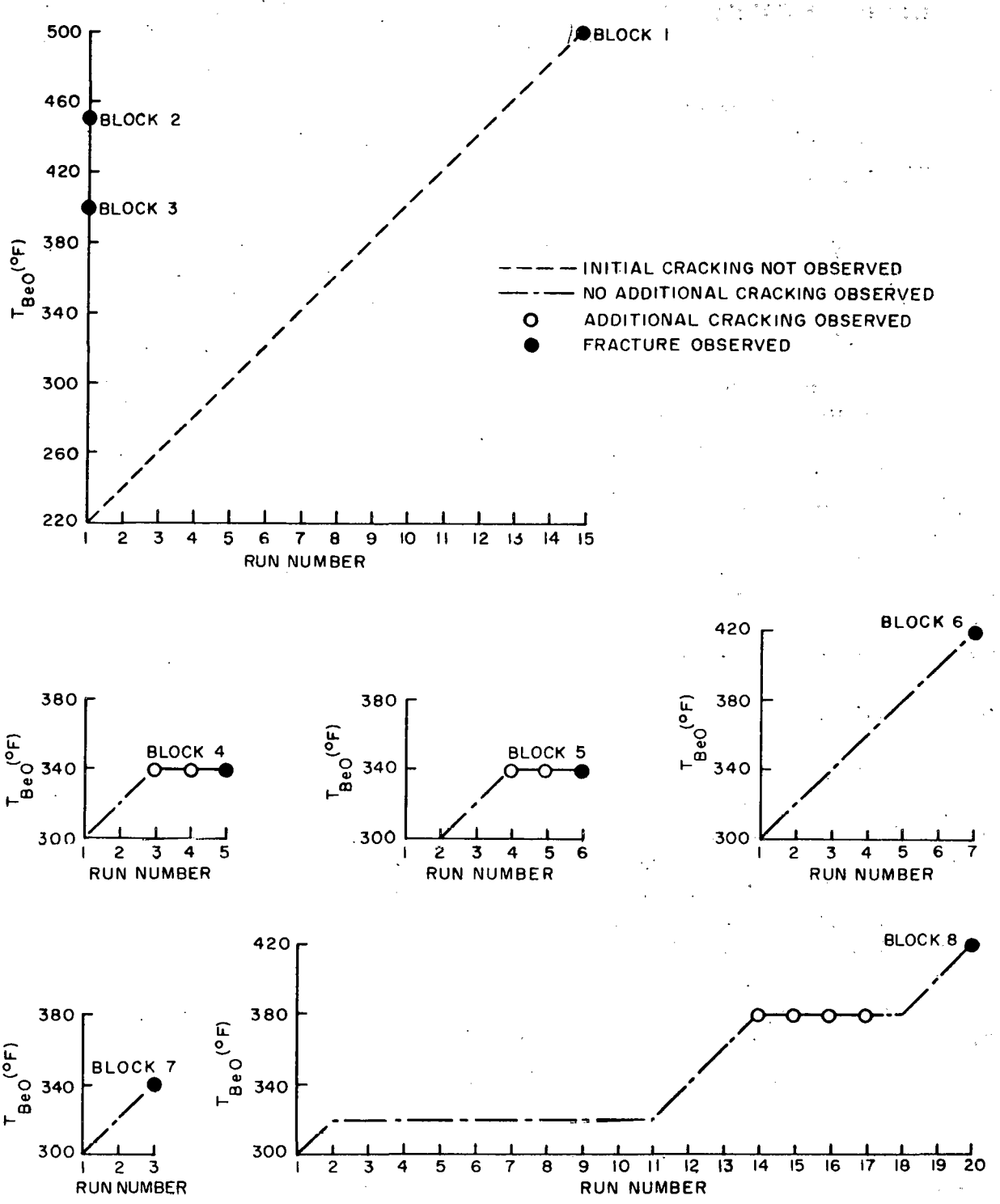

Fig. 1.1--Quench-test results; temperature difference = T_{BeO} - 212°F

Further testing using boiling quench water and blocks containing a 1 wt-% bentonite additive are planned for the next reporting period. Preliminary results from two such tests already completed give an initial block temperature for cracking of 400°F--an increase of 36°F over the average obtained with blocks of the previous mockup composition.

Core-element Flow and Dynamic Test (R. Katz, G. P. Young)

A flow and dynamic test for the EBOR core element has been initiated. The purpose of the test is twofold: the first phase will be a flow test which will yield data on the core-element orifice coefficient, inlet and exit pressure losses, and over-all pressure drop; the second phase will determine the flow-induced vibration characteristics of the element under conditions simulating reactor operation.

The element used for these tests will be the second full-scale mockup, which is currently nearing completion. The test stand for the element (see Fig. 1.2) has been designed and fabricated. All necessary equipment for the flow-test phase is on hand and is being assembled into the test stand. During the flow tests, a second oct of fuel rods (obtained from the first mockup) will be instrumented with strain gauges for vibration measurements so as to be ready for installation in the test element after completion of the flow tests. This procedure eliminates from the flow tests the perturbing effects of the strain-gauge instrumentation.

Seal-ring Leakage Test (G. J. Malek)

Seal rings are used with the core and reflector elements of the EBOR to prevent bypass leakage of the coolant gas. An experiment has been designed to demonstrate the suitability of the basic ring design and to determine the optimum combination of rings for minimum leakage. Tests will be performed with air as the working fluid and with the rings maintained at 850°F and 1000°F, which are the inlet temperatures corresponding to the two reactor outlet gas temperatures, 1300°F and 1500°F, respectively. The test variables will include the following:

1. Ring material--Hastelloy C and Type 420 stainless steel.
2. Number of rings--two rings and three rings.
3. Ring arrangement--rings installed in single grooves and rings installed in double grooves.

Leakage determinations will be made by the time-pressure decay method for the various ring combinations subjected to pressure differentials up to 35 psi and with the discharge pressure equal to atmospheric pressure.

The test rings have been procured and the test fixture is being fabricated. It is anticipated that testing will begin shortly.

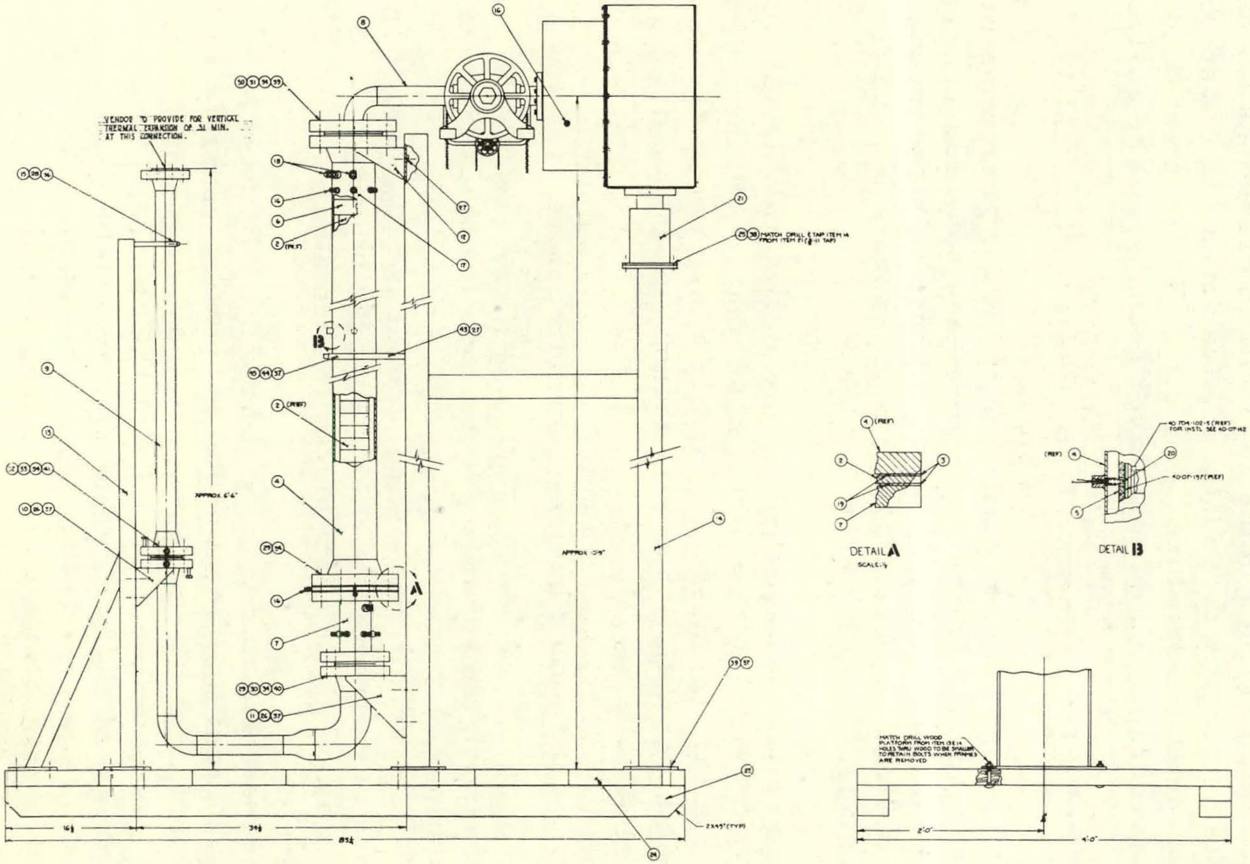

GENERAL NOTES:

1. SWAGELOK-CRAWFORD FITTING CO., CLEVELAND, OHIO
2. CONAX-JENSEN INSTRUMENT CO., LOS ANGELES, CALIF
3. UNITED AIRCRAFT PRODUCTS INC., DAYTON, OHIO
4. GRINNEL-McJUNKIN CORP., CHARLESTON, W. VA.
5. TUBE TURN, INC., LOS ANGELES, CALIF
6. BENTLY NEVADA CORP., P.O. BOX 157 MINDEN, NEV
7. DESIGN PER ASME CODE SECTION VIII
8. WORKING PRESSURE 250 PSI AT 700°F
9. DESIGN PRESSURE 400 PSI AT 800°F

REQUIRED	ITEM	PART NO.	DESCRIPTION	MATL	MATL SPEC
2	45		SOCKET HD CAP SCREW [illegible] LG	STL	COML
1	44	40-704-103-26	CLAMP		
1	43	40-704-103-25	SUPPORT 5"		
1	42	R-23	2" SEAL		
1	41	R-34	3½" SEAL		
1	40	R-41	5" SEAL		
16	39		CARRIAGE BOLT ⅝ X 2½	STL	COML
4	38		L'WASHER ⅝		COML
26	37		L'WASHER ⅞		COML
2	36		L'WASHER ¾		COML
8	35		NUT ¾-10		ASTM-A194 GR 2H
24	34		NUT ⅞-9		ASTM-A194 GR 2H
5	33		BOLT-HEX HD ¾-10 X 4" LG		ASTM-A193 GR B7
3	32		BOLT-HEX HD ¾-10 X 5 [illegible] LG		
3	31		BOLT-HEX HD ⅞-9 X 4 [illegible] LG		
10	30		BOLT-HEX HD ⅞-9 X 4 [illegible] LG		
11	29		BOLT-HEX HD ⅞-9 X 4 [illegible] LG		ASTM-A193 GR B7
2	28		SOCKET HD CAP SCREW ¼-20 X 2 LG		COML
4	27		SOCKET HD SHOULDER SCREW [illegible] SHOULDER LG [illegible]		COML
8	26		BOLT-HEX HD ⅝-16 X [illegible] LG		COML
4	25		BOLT-HEX HD ⅝-11 X [illegible] LG	STL	COML
[illegible]	24		PLATFORM 2 X 12 X 32'-0"	WOOD	
2	23		SKID 4 X 4 X 85¼	WOOD	
1	21	TYPE F [illegible]	SPRING HANGER		
2	20	H3-042-6	DISTANCE DETECTOR		
2	19	U2412-0775-SE	METALLIC "O" RING		
2	18	TG-20-A-LG	PACKING GLAND		
3	17	MICRO	PACKING GLAND-SEALANT TO BE LAVA		
7	16	*200-1-2	CONNECTOR		
1	15	40-704-103-24	CLAMP		
1	14	40-704-103-5	FRAME-12"		
1	13	40-704-103-4	FRAME-7"		
1	12	40-704-103-3	SUPPORT-5"		
1	11	40-704-103-2	SUPPORT-3½"		
1	10	40-704-103-1	SUPPORT-2"		
1	9	40-704-104-4	SECTION-PIPING		
1	8	40-704-104-1	SECTION-VALVE		
1	7	40-704-101-1	ASSEMBLY-AIR FLOW		
1	6	40-704-102-13	SPACER BLOCK		
1	5	40-704-102-11	BeO BLOCK		
1	4	40-704-102-4	SHELL-OUTER		
2	3	40-704-102-12	SPACER-SEAL		
1	2	40-704-102-1	ELEMENT-FUEL		
	-1		ASSEMBLY		
-1					

LIST OF MATERIAL

Fig. 1.2--Core-element dynamic test facility

Design for Construction (Tasks 27, 29, 54)

Thermal Performance (R. Katz, G. J. Malek)

A detailed evaluation has been made of the effect on core thermal performance of the core-element flow control orifice over the available range of orifice openings. As a result of this evaluation, the positioning device has been redesigned to permit finer adjustment in the low flow range (discussed below under "Design" under "Core and Reflector Elements").

A transient code for the IBM-7090 is being developed for the purpose of determining the core-element component temperatures during transient operating conditions. Included in the code will be provisions for determining the component temperatures as a function of variations in power, coolant flow, and coolant inlet temperature. The effects of transient conditions such as start-up, scram, and normal power changes will be analyzed.

Core and Reflector Elements (T. B. Pearson, G. J. Malek, D. R. Buttemer)

Design. A design study of various methods for preventing rotation of the BeO square-annular blocks in the core- and reflector-element assemblies has been completed. The antirotation device selected mechanically prevents angular block movement during reactor operation and during removal and replacement of elements.

The design criteria established for the antirotation device were that it (1) must prevent block rotation to the extent that interlocking of adjacent elements cannot occur, (2) must not result in a major increase in BeO cost, (3) must not result in a major change in design, and (4) must not significantly affect core physics.

The various antirotation devices considered were as follows:

1. Roof topping, in which the upper and lower surfaces of the block are shaped in a manner to prevent relative block rotation or translation.
2. A metallic barrier, consisting of angle bars located at opposite corners of the element and extending the full length of the element.
3. Dowels attaching adjacent blocks to each other.

Of the three alternatives, roof topping and the metallic barrier were rejected because of the BeO cost increment and added poison, respectively, and dowels were selected as offering the best compromise among the several design criteria. Dowelling will be accomplished by locating two through holes on one diagonal of the block, each approximately midway between the central hole and the corner. This location was selected to put the holes in a low compressive-stress field so as to minimize the effects of the resulting

stress concentration (see "Structural Analysis" below). The dowel material will be BeO.

An evaluation of the bids on the BeO moderator and reflector blocks has resulted in redesign in several areas in order to reduce costs:

1. A probable change in reference composition from a 1 wt-% bentonite additive to a 1% alkaline earth aluminum silicate additive.
2. Combining of the reflector-element spine and sleeve into an enlarged spine, thus eliminating two machined surfaces.
3. Relaxation of the square-annular-block hole tolerance to the as-fired tolerance (±1/2% on the diameter) in the reflector only, where the heating rates are relatively low.

The core-element variable inlet orifice has been redesigned to provide finer adjustment in the low flow range and, additionally, to reduce costs. Changes introduced were (1) elimination of the spring-loaded-ratchet arrangement and the valve-sleeve serrations, and substitution of a setscrew or a clamping device which is infinitely variable, and (2) use of round orifice holes in the valve sleeve operating in conjunction with rectangular holes in the nozzle body. This arrangement results in a slight reduction in adjustment sensitivity for the smaller openings and eliminates completely the fixed incremental settings attendant upon the ratchet arrangement.

Structural Analysis (Steady-state Thermal Stress Analysis of Square-annular BeO Block). The tangential-stress intensity at the inside surface of a dowel hole in the square-annular block has been calculated. The dowel-hole location is shown in Fig. 1.3. By locating the holes in a compressive-stress field, the tangential stresses around the hole are held to a maximum of 5240 psi and are everywhere compressive. These stresses are not expected to result in any damage to the block and do not impose limitations on the design.

Control Element (N. H. Davison, G. P. Young)

Design. The drawings and specifications for the cruciform control element have been completed and released for element fabrication.

The design selected (see Figs. 1.4 and 1.5) consists of a Hastelloy X square-lattice structure containing rectangular tiles composed of Dy_2O_3 in Al_2O_3. Hastelloy X facing sheets on each side of the blade retain the tiles in position within the structure and protect them against damage. These facing sheets are butt-welded to each of the longitudinal stringers in the lattice framework and are spot-welded to the horizontal stringers. Each facing sheet contains a drilled hole near the bottom of each cell to equalize the control-element internal pressure with system pressure. The active section of the element is of a sufficient length that the active section of the

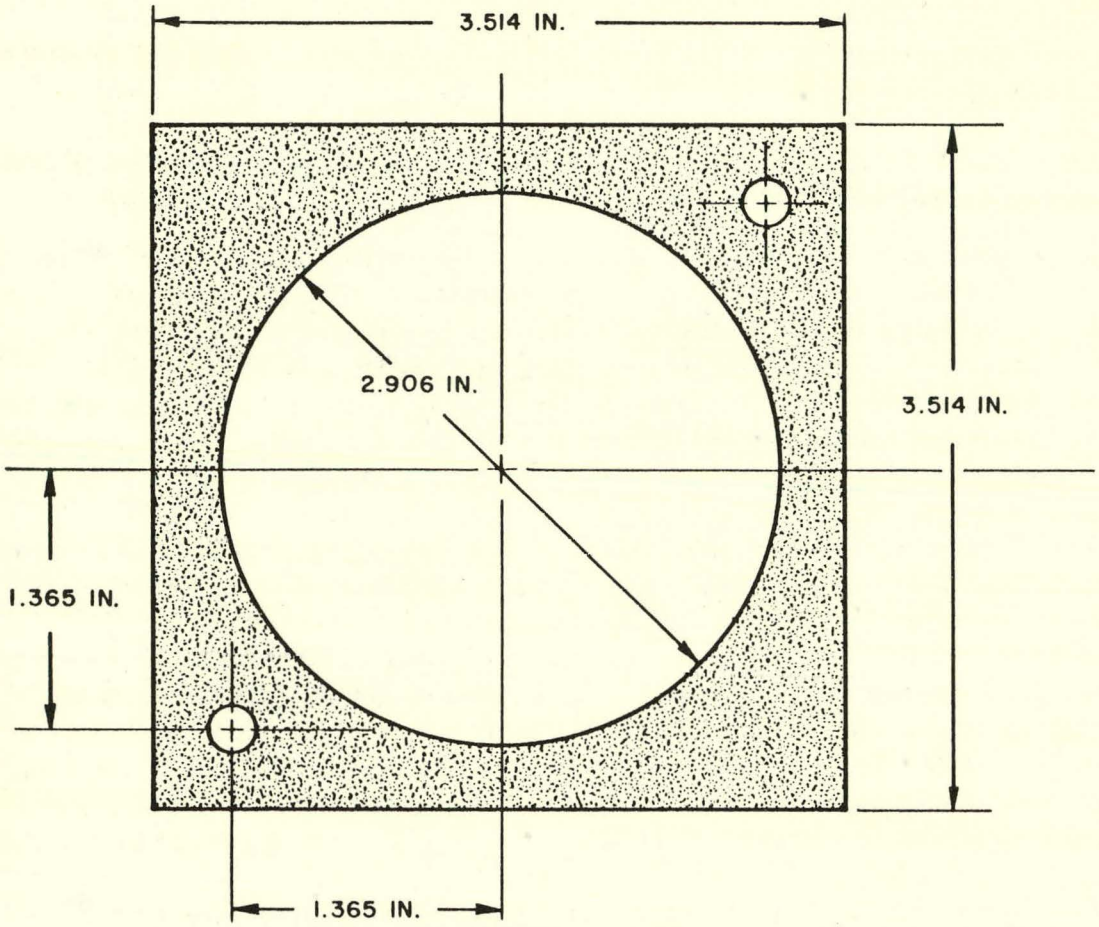

Fig. 1.3--Location of dowel holes in BeO block

core remains covered with the rod in the normal full-in position or in the disconnected position.

Square-gusset plates containing multiple lightning holes are provided at the top of each blade to support the central column against axial-buckling loads and to continue the smooth blade surface through the top-reflector region regardless of rod position. Two longitudinal spacer strips on each blade face ensure a minimum gap for coolant flow for all conditions of operation.

The top of the central Hastelloy X column terminates in a cruciform-shaped spherical segment which engages the disconnect on the drive line shafting.

The selection of a honeycomb design in preference to the previously favored rod-type reference design was based on the following factors:

1. Improved dimensional control during fabrication afforded by the honeycomb design.

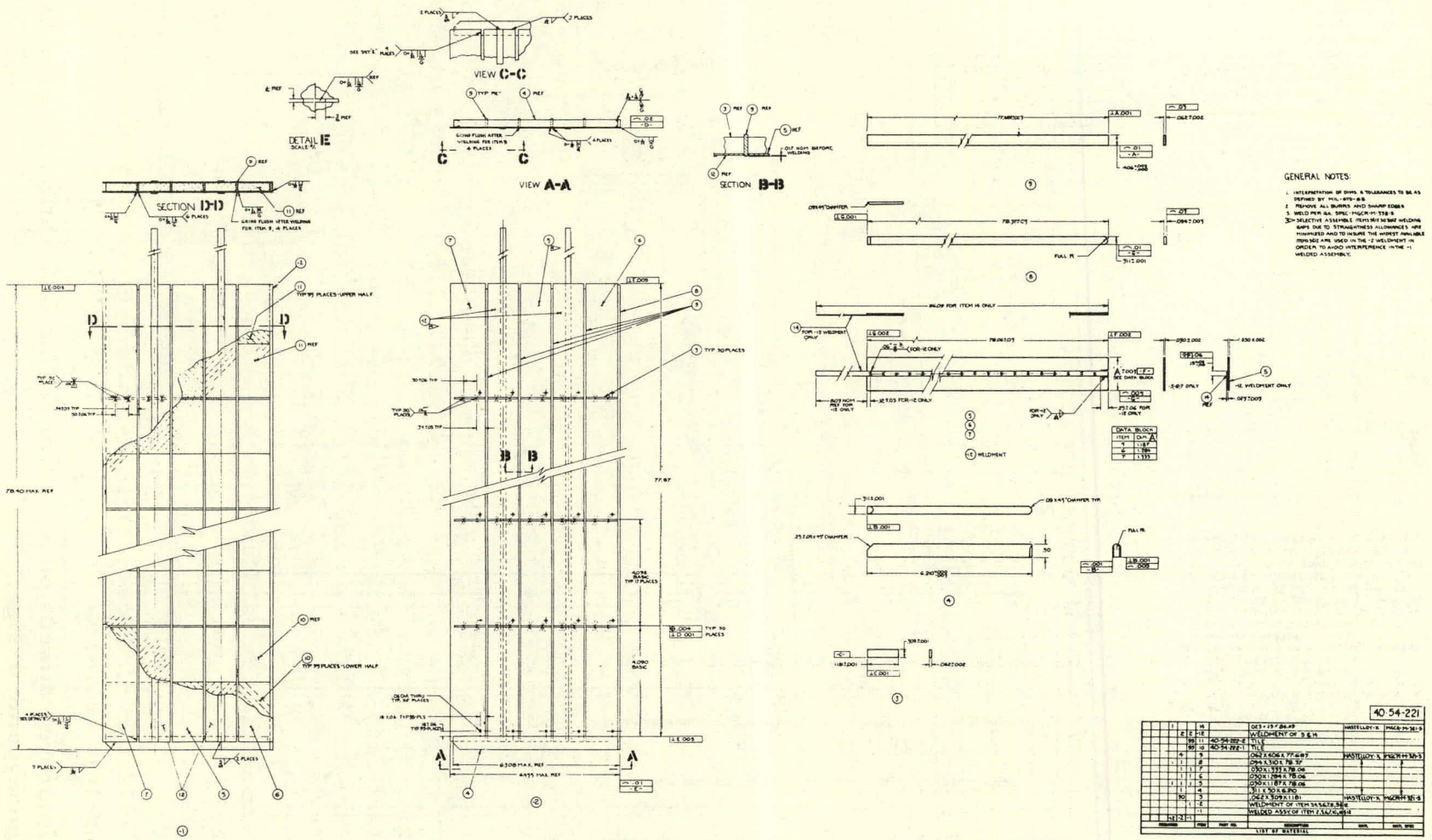

Fig. 1.4--EBOR control-element panel assembly

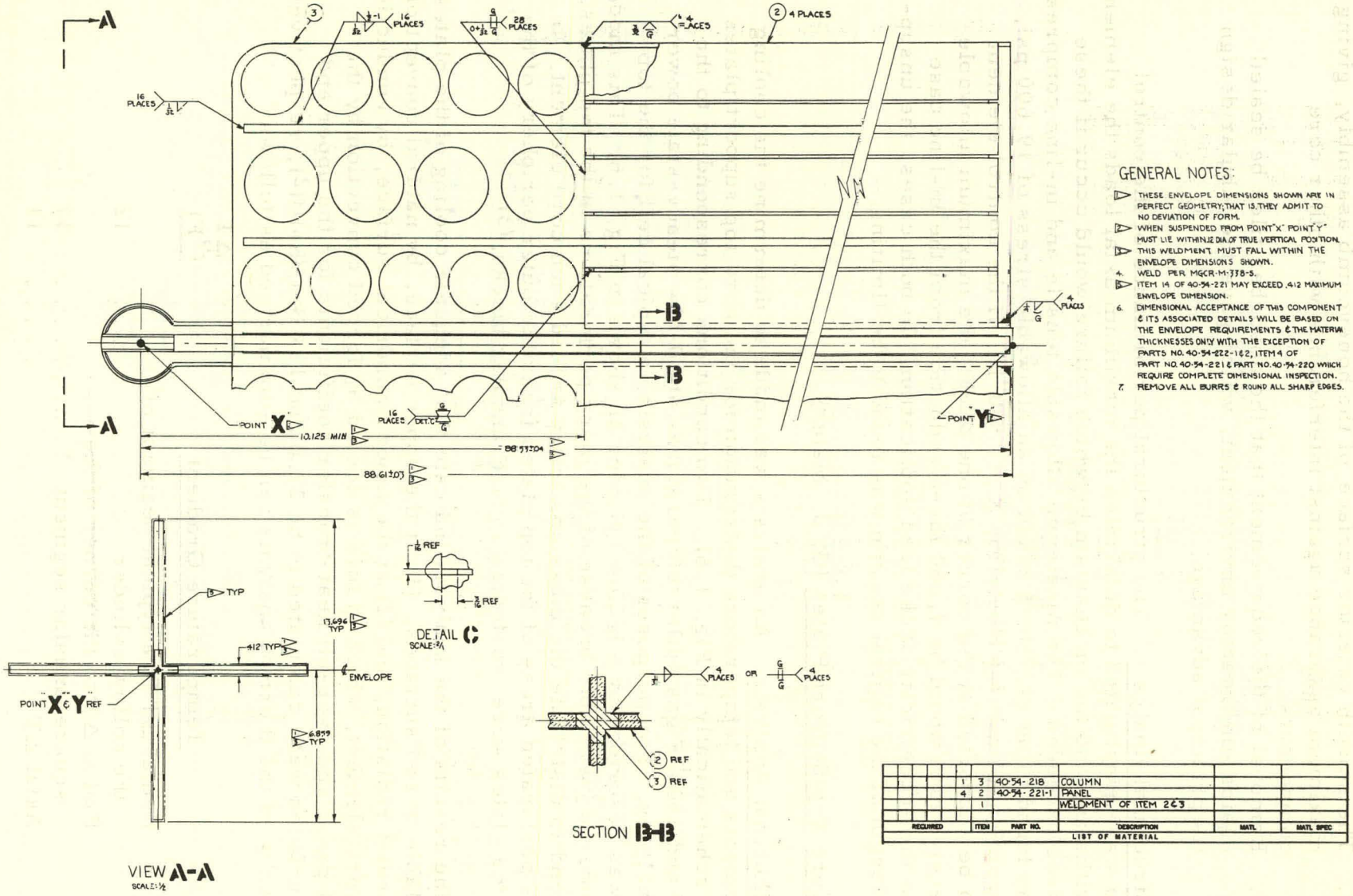

Fig. 1.5--EBOR control-element assembly

2. The smooth exterior surface of the honeycomb assembly, giving maximum assurance against interference with other core components.
3. Removal of the requirement that the absorber tiles be sealed against the reactor environment, which gave the tubular design its principal advantage.

Structural Analysis. The structural performance of the control element was investigated to determine the maximum axial loads the element could withstand and the mechanism by which failure would occur if these loads were exceeded. The maximum allowable tensile and in-line compressive load was found to be 11,760 lb based on an allowable stress of 19,600 psi, the proportional limit for Hastelloy X at 1,500°F. If the control element were to be supported at the corner of one blade, the maximum allowable compressive load would be 4,680 lb--a reduction from the in-line case owing to the eccentricity of the load application. In both cases, the unsupported length of the central column was found to be limiting.

Core Top Support Plates (G. J. Malek)

Thermal Analysis. An analysis was made to determine the cooling requirements and temperature distribution for the core top support plates (shown schematically in Fig. 1.6). Two conditions corresponding to the 1300°F and 1500°F gas outlet temperatures at 10-Mw steady-state power were analyzed. For purposes of the analysis, a typical cell for the top plates was described by a hollow cylinder as shown in Fig. 1.6. This model is considered justifiable because of the many perforations in the top plates, which tend to distribute the mass uniformly around each core element. In the less perforated areas of the top plates (near the outer periphery of the core), the plates were treated as square-annular blocks.[3]

The results of the analysis indicate that adequate cooling of the plates is available at two surfaces: (1) at the upper surface, by natural convection and thermal radiation, and (2) at the inner cylindrical surface, by conduction to the core element, which in turn is cooled by forced convection by the exhaust gas. The over-all heat-transfer coefficients for the upper and inner surfaces were calculated to be 27.6 and 113 Btu/(hr)(ft^2), respectively. The results of the thermal analysis can be summarized as follows:

Temperature Gradient	ΔT (°F)
Radial ΔT in a typical segment of the hollow cylinder	12
Radial ΔT to the corner of the square-annular segment	37
Axial ΔT	11

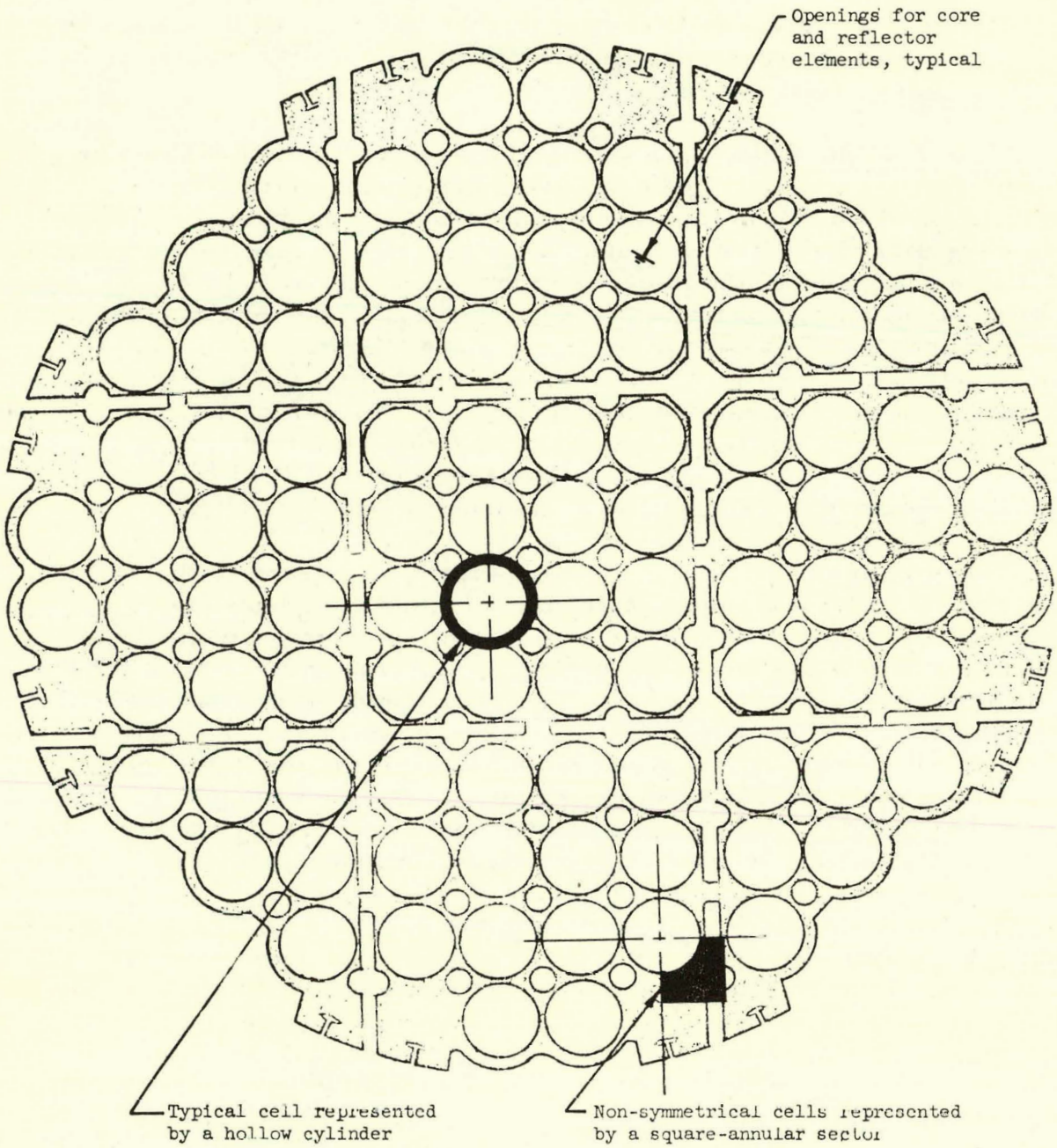

Fig. 1.6 -Core top support plates, plan view

Temperature Level (max.)	T_{max} (°F)
1300°F core-element outlet temperature (design case)	1445
1500°F core-element outlet temperature (design case)	1650

PRESSURE VESSEL AND ASSOCIATED COMPONENTS (K. A. Trickett, C. O. Peinado)

Research and Development (Task 08) (C. O. Peinado, V. H. Pierce)

In order to complete the design of the EBOR pressure-vessel components and ensure their safe operation within design temperatures, it is necessary to ensure that the components are adequately cooled. Component cooling is dependent on the development of an adequate surface heat-transfer coefficient, which in turn depends on the local coolant velocity and, therefore, on the distribution of the coolant within the coolant passages. Accurate prediction of coolant distribution within the passages cannot be accomplished by analytical methods alone because of the dependence of the coolant distribution on the location of the inlet nozzle and on the variation of the coolant-channel size with the longitudinal and circumferential co-ordinates. Therefore, it is proposed that the adequacy of the cooling be determined experimentally through the use of a flow model. The model would be a reduced scale model of the EBOR pressure-vessel components shown in Fig. 1.22 of the previous quarterly progress report.[2]

The flow-model test would yield experimentally: (1) a visual record of the coolant-flow direction at longitudinal and circumferential positions along the passages, (2) a determination of the spiral baffle design for adequate coolant distribution within the inlet region, (3) a determination of the orifice sizes for proper flow split between passages, (4) differential-pressure data throughout the model, and (5) the flow distribution of the final geometry for the predicted reactor operating range. A test specification to cover this work is now being written for use in obtaining bids and awarding a contract.

Design for Construction (Task 52) (C. O. Peinado, V. H. Pierce)

Vendor Engineering

The equipment specification for the pressure vessel and internals was revised to incorporate the changes (listed on page 34 of the previous quarterly progress report[2]) which resulted from a change in the fuel-handling concept. Invitations to bid were extended to eight pressure-vessel vendors, and three bids were received from which a vendor will be selected.

General Atomic Engineering – Review of Phase I Analysis

Additional results obtained from the PACECO Phase I analysis of the predicted-pressure-drop data for the EBOR pressure-vessel design made prior to the fuel-handling modification are shown in Fig. 1.7. These data are based on a coolant distribution between the main inlet nozzle and the reactor top head of 30% and 70%, respectively, and a total mass flow of 15.6 lb/sec. Within the reactor coolant passages above the main nozzle, a flow distribution of 70% to the inner passage (between the thermal shield and the core barrel) and 30% to the outer passage (between the pressure vessel and the thermal shield) would be necessary. The internal flow split would be accomplished by the flow-split ring on the top edge of the thermal-shield top head. The coolant from these two passages is combined at the primary flange. Below this flange, the flow split is accomplished by the wedge-shaped top edges of the thermal-shield shell. These wedges are arranged so as to direct the coolant below the primary flange to either the inner passage or the outer passage as required for the flow split. The coolant from the main nozzle is added to the system at the upper shell region of the reactor. A flow split of 70% and 30% between the inner and outer channels would be required in the lower reactor shell region. The total coolant is combined in the bottom head and is passed to the unused core supports or the core supports of the EBOR core as required.

The pressure drop across the core-support riser (see Fig. 1.7) was calculated for the EBOR central core-support risers, which carry the maximum coolant of 1.57 lb/sec to the core. From these data a conservative maximum pressure drop from the reactor inlet to the core inlet was predicted to be 0.2472 psi.

Several areas of the analysis are not complete or are lacking in detail (see Fig. 1.8):

Area A: The centerline temperature distribution of the core-barrel seal plate and the thermal-shield flat head was not analyzed.

Area B: The pressure-drop analysis in the region of the flow-split ring requires more detail.

Area C: The analysis of the pressure drop where the coolant from the inner and outer passages combine and flow through the core-barrel shell flange could not be checked owing to lack of a sufficiently illustrated model. The pressure-drop calculation for the redistribution of the coolant below the flange to the inner and outer passages requires more detail. In addition, the analysis of the core-barrel shell temperature for a coolant dead spot between holes in the core-barrel shell flange requires more explanation and model detail. A similar calculation was not made for the pressure-vessel shell in this region.

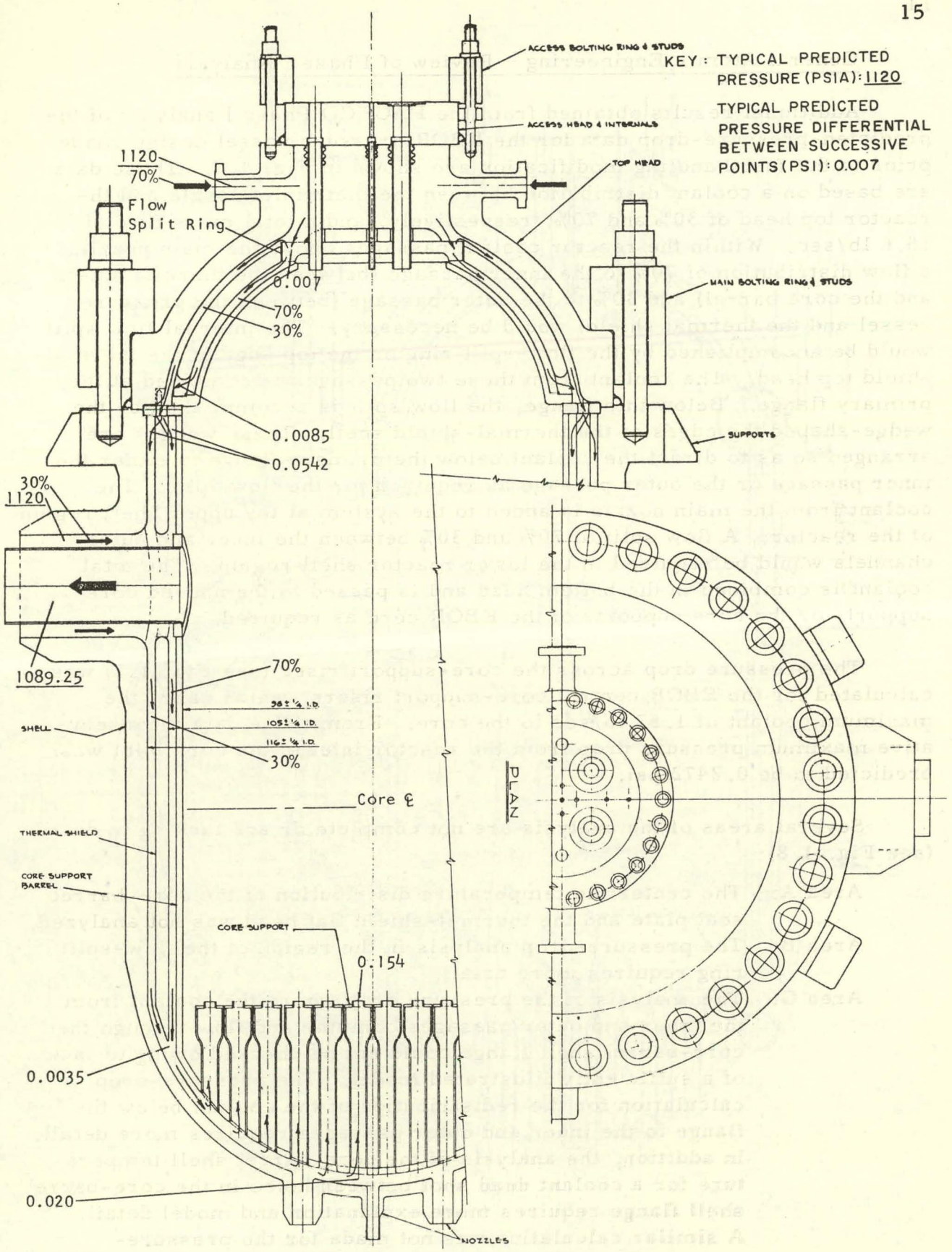

Fig. 1.7--Predicted pressures for pressure vessel and associated components

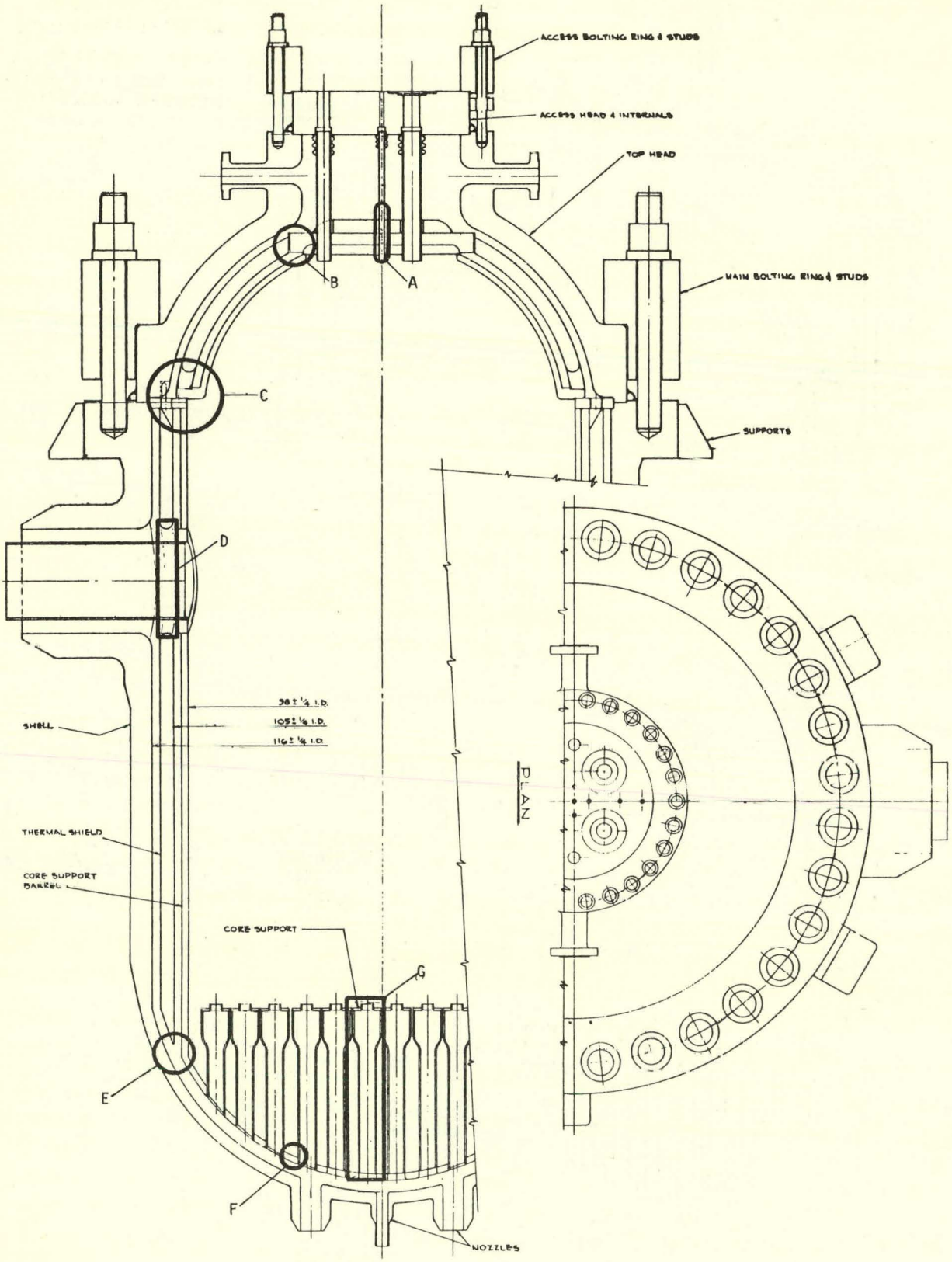

Fig. 1.8--Pressure-vessel areas requiring additional analysis (areas are marked A through G)

Area D: The effect of the coolant entering at the main nozzle was not analyzed. Provision for maintaining a 70% and 30% coolant distribution between the inner and outer passages below the main nozzle has not been made. An analysis of the coolant distribution and resulting temperature variation circumferentially from top to bottom at the outlet nozzle was not reported.

Area E: The temperatures of the pressure vessel and the core barrel at the lower end of the thermal shield were not analyzed.

Area F: The temperature level and heat load of the core-barrel bottom head was not taken into account in the analysis of the core lower support riser.

Area G: Thermal analysis of the core lower support risers under the EBOR core was not reported.

In addition to these deficiencies in specific areas, several general deficiencies were noted: (1) thermal analysis of the thermal shield was not reported; (2) analysis of the effect of a coolant dead spot caused by coolant maldistribution on the core barrel and pressure-vessel shell was not reported; and (3) the effect of dimensional tolerances was not considered in the analysis. Detailed comments on the deficiencies of the Phase I analysis have been transmitted to PACECO for action. The analysis will be reworked to incorporate changes in the design of the pressure vessel and internals resulting from the change in the fuel-handling concept.

A summary of the results of the detailed stress analysis performed by PACECO in the Phase I analysis is given in Fig. 1.9. This analysis was based on the design conditions and allowable stresses given in Table 1.2. Included in Fig. 1.9 are the maximum peak stress intensities computed at points of structural discontinuity. It can be seen that they are everywhere less than the allowable stresses given in Table 1.2. The allowable membrane stresses are those defined by the ASME Boiler and Pressure Vessel Code. The allowable peak stresses are 90% of the yield strength or 60% of the ultimate strength in tension, whichever is less when the temperature is below the creep range for the material in question. In the creep range, the allowable has been taken as equal to the allowable membrane stress defined by the ASME Code.

Thermal Analysis of Core Support Grid

The preliminary thermal analysis of the core support grid (discussed in the previous quarterly progress report[2]) has been completed. The detailed results of this analysis[4] show the maximum temperature of the grid to be 870°F, with a temperature variation of 40°F between parts of the structure at the EBOR design condition.

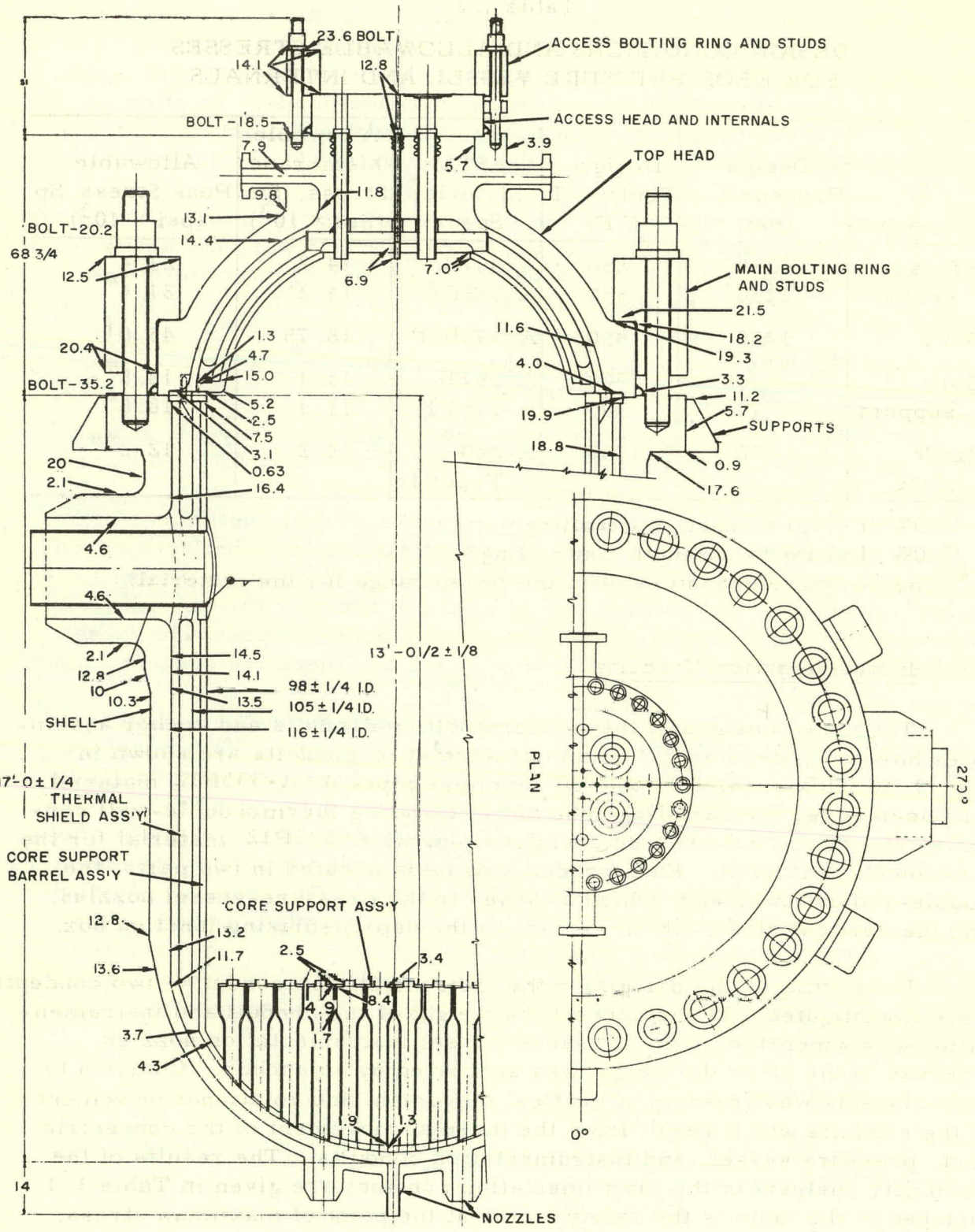

Fig. 1.9--Maximum peak stress intensities for EBOR pressure vessel and internals (stresses × 10^3 psi)

Table 1.2

DESIGN CONDITIONS AND ALLOWABLE STRESSES
FOR EBOR PRESSURE VESSEL AND INTERNALS

Component	Design Pressure, p (psi)	Design Temp., T (^{o}F)	ASTM Material Spec.	Allowable Membrane Stress, Sm (psi × 10^3)	Allowable Peak Stress, Sp (psi × 10^3)
Pressure vessel	1250	850	A-387B	14.2	21.4*
	1250	850	A-336F2	14.2	21.4*
Bolts	1250	850	A-193B16	18.75	45.0†
Core support	70	900	A-387B	13.1	18.8*
	70	900	A-336F2	13.1	18.8*
Riser plate	70	1050	A-240—Type 316	12.2	12.2**

*90% of yield strength controlling.
†60% of ultimate strength controlling.
**The design temperature is in the creep range for the material.

Instrumentation Conduits

The detail designs of the instrumentation conduits and anchor assemblies have been developed. The instrumentation conduits are shown in Fig. 1.10. Six-inch, Schedule 80 seamless pipes of A-335P12 material will be used for the sampling-tube and calibrating thermocouple-well conduits, and 8-in., Schedule 80 seamless pipe of A-335P12 material for the thermocouple conduit. Each conduit will be fabricated in two parts: the double-radius lower end, which attaches to the pressure-vessel nozzles, and the vertical riser, which extends to the depressurizing junction box.

In arriving at the design for the instrumentation conduits, two concepts were investigated. In one concept the weight of the conduit and instrumentation was supported by the pressure-vessel instrumentation nozzles, whereas in the other the weight was supported by an anchor. Common to both concepts was freedom of vertical movement and rotational movement of the conduits, which result from the thermal movement of the concentric duct, pressure vessel, and instrumentation conduits. The results of the flexibility analysis of the instrumentation conduits are given in Table 1.3. Included in the table is the safety factor at the point of maximum stress, based on a piping-code allowable stress of 21,600 psi.

On the basis of these results, a decision was made to use constant support anchors for all conduits. These constant support anchors (shown

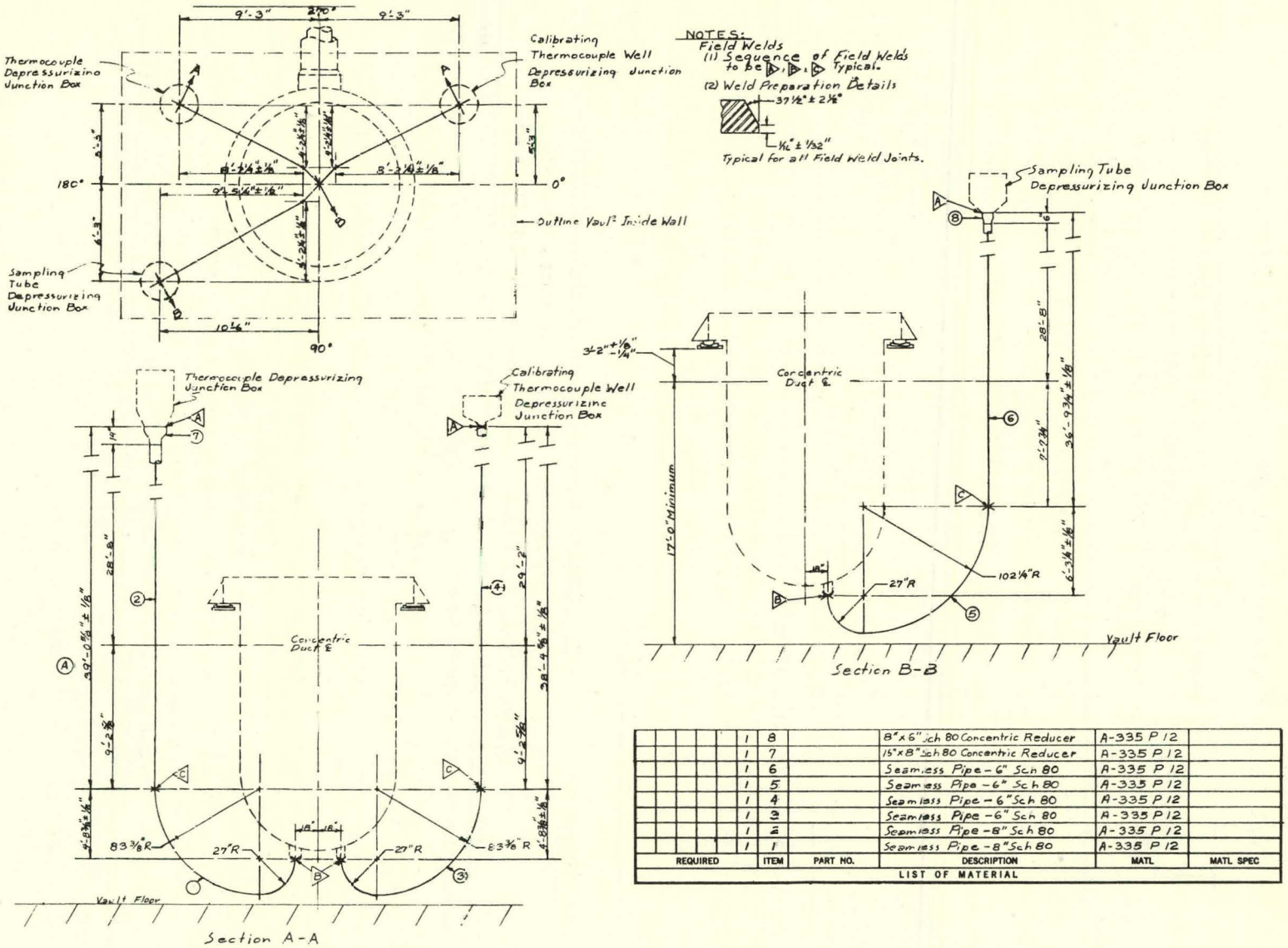

REQUIRED	ITEM	PART NO.	DESCRIPTION	MATL	MATL SPEC
			LIST OF MATERIAL		
1	8		8"x6" Sch 80 Concentric Reducer	A-335 P 12	
1	7		15"x8" Sch 80 Concentric Reducer	A-335 P 12	
1	6		Seamless Pipe - 6" Sch 80	A-335 P 12	
1	5		Seamless Pipe - 6" Sch 80	A-335 P 12	
1	4		Seamless Pipe - 6" Sch 80	A-335 P 12	
1	3		Seamless Pipe - 6" Sch 80	A-335 P 12	
1	2		Seamless Pipe - 8" Sch 80	A-335 P 12	
1	1		Seamless Pipe - 8" Sch 80	A-335 P 12	

Fig. 1.10--EBOR instrumentation conduits

Table 1.3

FLEXIBILITY ANALYSIS OF INSTRUMENTATION CONDUITS

Conduit	Without Anchor		With Anchor	
	Location of Max. Stress	Safety Factor	Location of Max. Stress	Safety Factor
Sampling-tube conduit	Anchor	0.6	Anchor	6.2
Thermocouple conduit	Pressure-vessel nozzle	1.3	Anchor	7.5
Calibrating thermocouple-well conduit	Pressure-vessel nozzle	1.8	Anchor	11.0

in Figs. 1.11a and 1.11b) will support the weight of the conduits, instrumentation, and junction boxes over the full vertical travel predicted for the conduits. In conjunction with the constant supports, the horizontal deflection of each conduit is resisted by the sleeve mounted on the upper biological shield. The sleeve configuration is sized to allow axial movement and torsional rotation of the conduit without binding.

The purchase equipment specifications for the instrumentation conduits and the anchor assemblies have been approved and released for transmittal to the architect-engineer. A report on the flexibility analysis of the instrumentation conduits and the anchors will be prepared.

CONTROL-ROD DRIVES (K. A. Trickett, B. C. Hawke)

Research and Development (Task 10) (B. C. Hawke, F. C. Dahms)

EBOR Experimental Control-rod-drive Mechanism

Life testing of the control-rod drives was continued in accordance with the procedures outlined in the last quarterly report.[2] Testing was concluded on completion of the fifth life cycle.

The five-life-cycle test comprised the following control-rod-drive operations:

1. 136,200 oscillations of approximately 1/8-in. amplitude. This is equal to 272,400 starts and stops of the positioning motor.
2. 150 fast insertion strokes of 10% full rod travel.
3. 30 slow insertion strokes of 10% full rod travel.
4. 180 slow withdrawal strokes of 10% full rod travel.

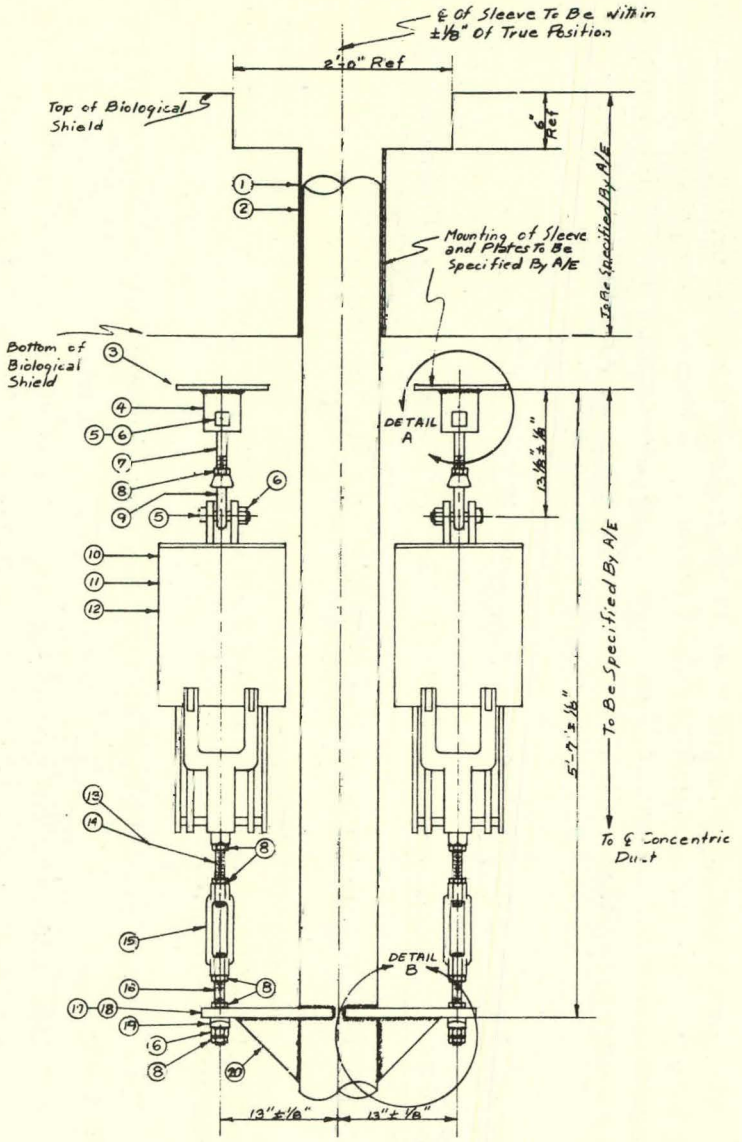

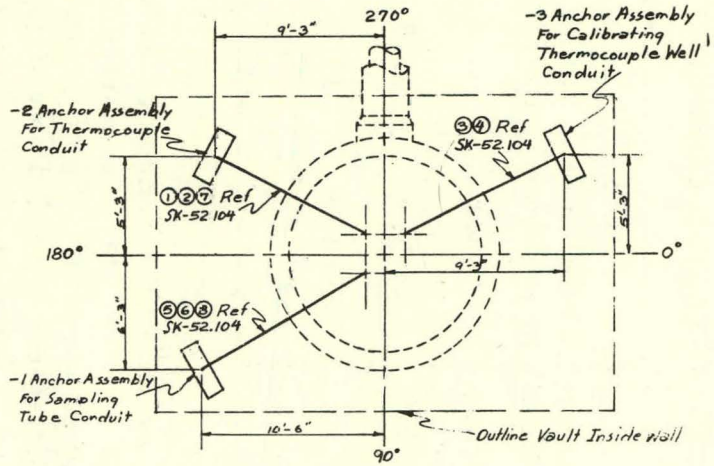

REQUIREC			ITEM	PART NO.	DESCRIPTION	MATL	MATL SPEC
2	2	2	20		Plate 1/2" x 7" per Detail B	Steel	
2	2	2	19	Sleweк Catalog No. 9	Spherical Washer # 10571-1 5/16" # 1 3/8" ID x 1/2" Thk or Equal		Steel
	2		18		Plate 1" x 4" per Detail B	Steel	
2		2	17		Plate 1" x 4" per Detail B	Steel	
2	2	2	16	GRINNELL CATALOG PH 58	Hanger Rod-Fig 140-1" x 10" x 8" thd or Equal	Carbon Steel	
2	2	2	15	GRINNELL CATALOG PH 58	Turnbuckle-Fig 230-1" Rod Size or Equal	Forged Steel	
	2		14	GRINNELL CATALOG PH 58	Hanger Rod-Fig 140-1" x 10" x 5" thd. or Equal	Carbon Steel	
2		2	13	GRINNELL CATALOG PH 58	Hanger Rod-Fig 140-1" x 18" x 7" thd or Equal	Carbon Steel	
		2	12	GRINNELL CATALOG PH-58	Constant Spring Support-Fig 80V-Type C-Mod R-Size 12 or Equal		
	2		11	GRINNELL CATALOG PH-58	Constant Spring Support-Fig 80V-Type C-Mod R-Size 18 or Equal		
2			10	GRINNELL CATALOG PH 58	Constant Spring Support-Fig 80V-Type C-Mod R-Size 18 or Equal		
2	2	2	9	GRINNELL CATALOG PH 58	Weldless Eye Nut-Fig 290-Size 3-1" or Equal	Forged Steel	
12	12	12	8		ASA Reg Hex Jam Nut-1"	Steel	
2	2	2	7	GRINNELL CATALOG PH 58	Welded Eye Rod-Fig 278-1" x 8" x 4" thd or Equal	Carbon Steel	
6	6	6	6		ASA Reg Hex Nut - 1"	Steel	
4	4	4	5		ASA Reg Sq Hd Bolt-1" x 4 1/2" Lg	Steel	
2	2	2	4	GRINNELL CATALOG PH 58	Hanger-Fig 66-1" Rod or Equal	Carbon Steel	
2	2	2	3		Plate To Be Specified By A/E	Steel	
	1		2		Sleeve 9" ± 1/8" ID x .25" Wall	Steel	
1		1	1		Sleeve 7" ± 1/8" I.D x .25" Wall	Steel	
1	2	3			Assembly		

LIST OF MATERIAL

Fig. 1.11a--Instrumentation-conduit anchor assembly

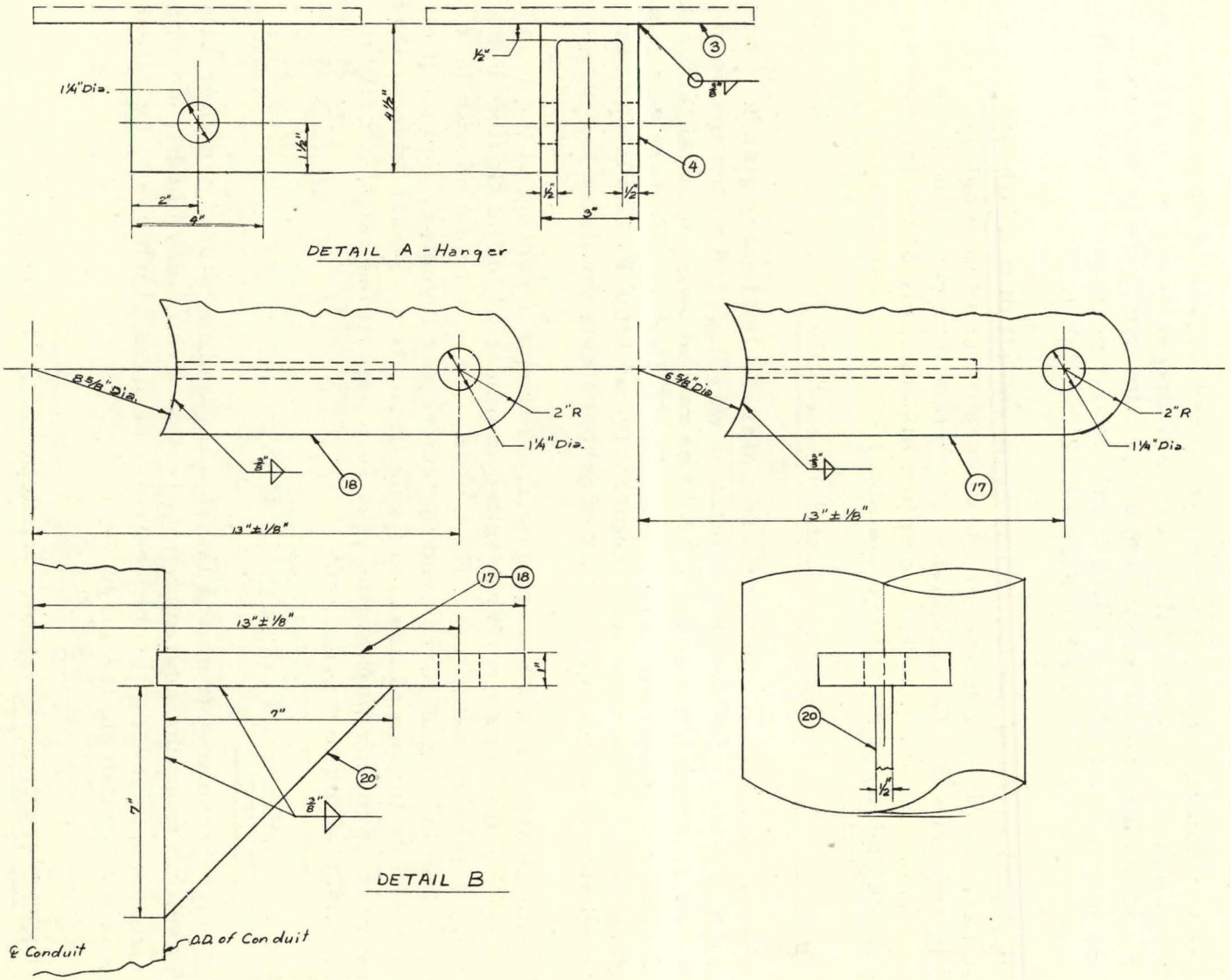

Fig. 1.11b--Details of instrumentation-conduit anchor assembly

5. 30 slow withdrawal strokes from the rod "full-in" position, consisting of 5 each of 50%, 60%, 70%, 80%, 90%, and 100% full rod travel.

(Operations 2 through 5 represent a total of 4, 000 in. of rod travel.)

6. 30 scrams from various positions of rod insertion.

Seventy-five additional scrams were performed for preliminary checkout and to establish the reproducibility of scram characteristics. A series of scrams was performed on completion of the fifth life cycle to determine times for insertion of 5% rod worth from various positions of rod withdrawal. These test results are plotted in Figs. 1. 12 through 1. 14.

The final phase of the fourth life cycle and all of the fifth life cycle were run at maximum permissible loop pressure and temperature, i. e., 1200 psig and 1200°F. On conclusion of the test program, the drive was still functioning satisfactorily; a complete disassembly of the mechanism will be made and all parts will be examined for wear and deterioration.

Control-rod-drive Environmental Test Facility

During the quarter, the improved water-cooled heater glands[2] performed satisfactorily, although a limitation was imposed on the maximum temperature to which the autoclave could be raised owing to local temperature conditions of the Teflon insulation. The Teflon temperature was found to be about 125°F at an autoclave temperature of 1200°F, and it was not considered safe to go higher for fear of jeopardizing the drive test program.

Contamination of the helium gas (from frequent venting of the loop to the atmosphere for repair work) resulted in oxidation of the flexible heater connectors within the autoclave. Each connector was replaced with four strands of 1/8-in. copper wire, and the entire gas inventory was purified to a level of 7 to 10 ppm of total oxidizing impurities. Apart from further ruptures of compressor diaphragms, the loop performed satisfactorily for the remainder of the test program.

Design for Construction (Task 61) (B. C. Hawke)

Changes resulting from the latest fuel-handling study, together with those resulting from the environmental test program, have been incorporated in the production drawings of the control-rod drive which are to be released for use in manufacturing the drive.

COMPONENT HANDLING (K. A. Trickett, T. J. Larson)

Research and Development (Task 11) (T. J. Larson)

Modification of the STF Instrument Bridge

The conceptual design of the STF instrument bridge has been completed,

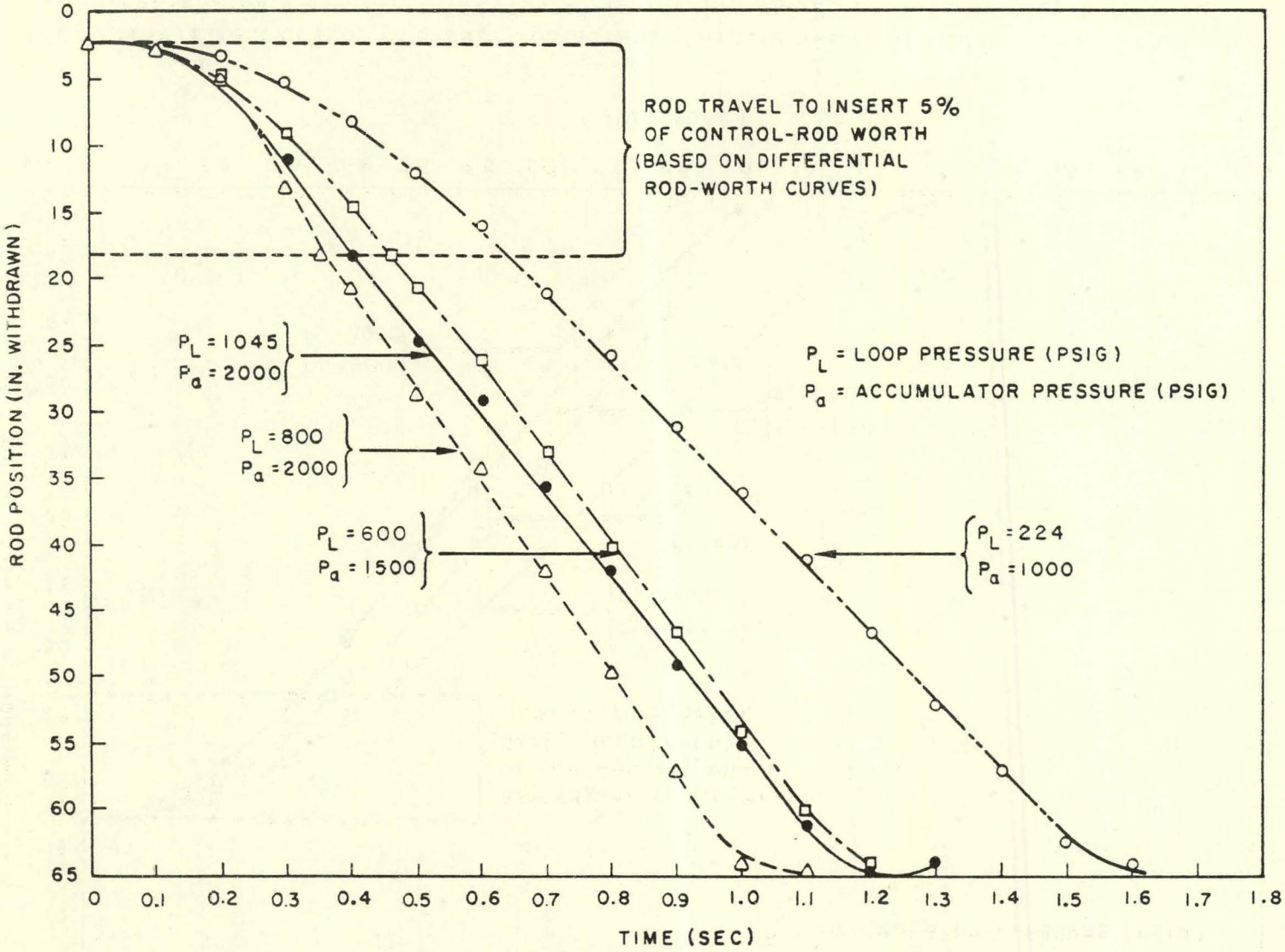

Fig. 1.12--Effect of loop pressures on scram characteristics of EBOR control-rod-drive mechanism (data are for scram tests 10, 13, 18, and 21 performed March 7, 1962)

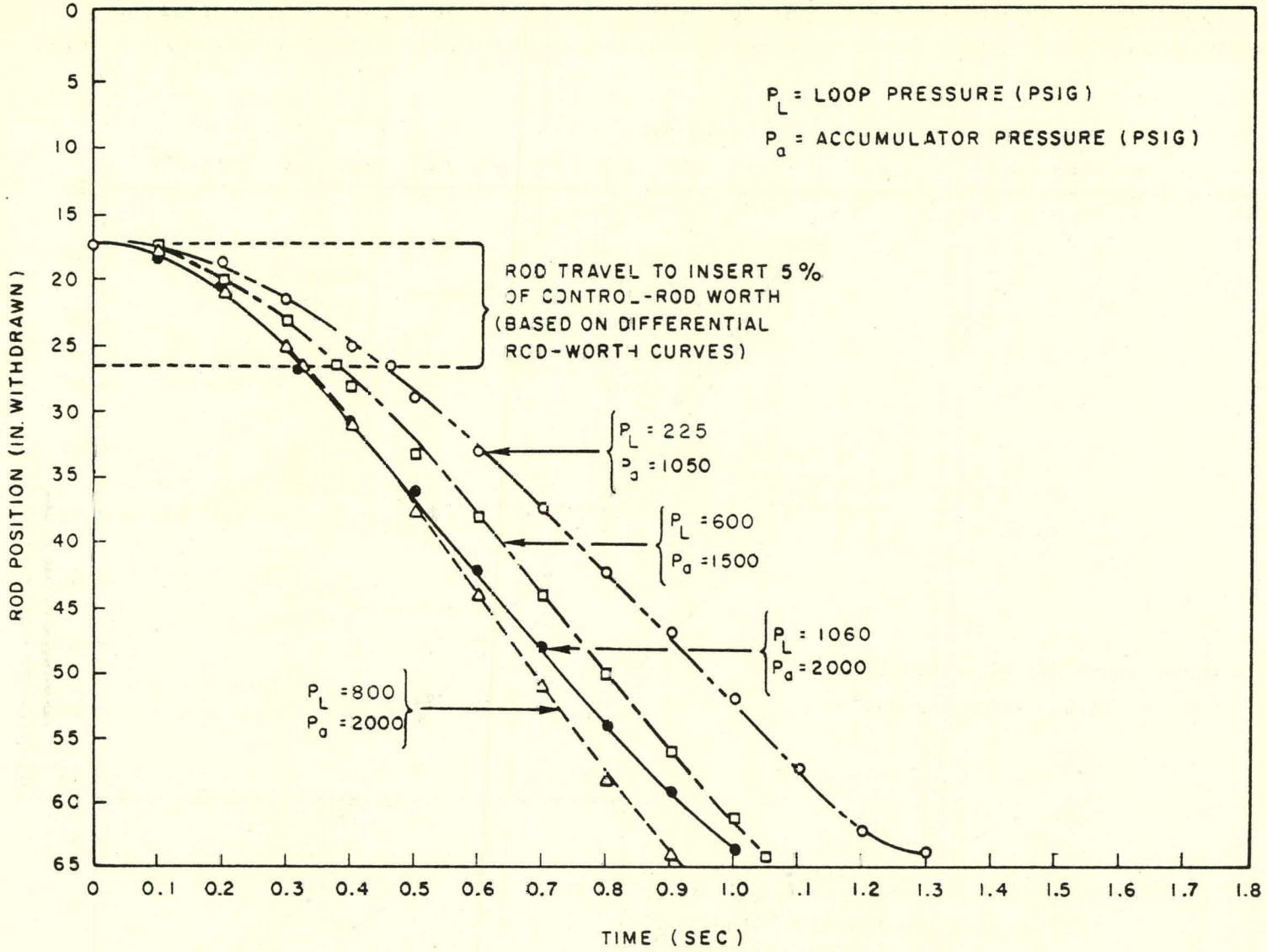

Fig. 1.13--Effect of loop pressures on scram characteristics of EBOR control-rod-drive mechanism (data are for scram tests 11, 14, 17, and 20 performed March 7, 1962)

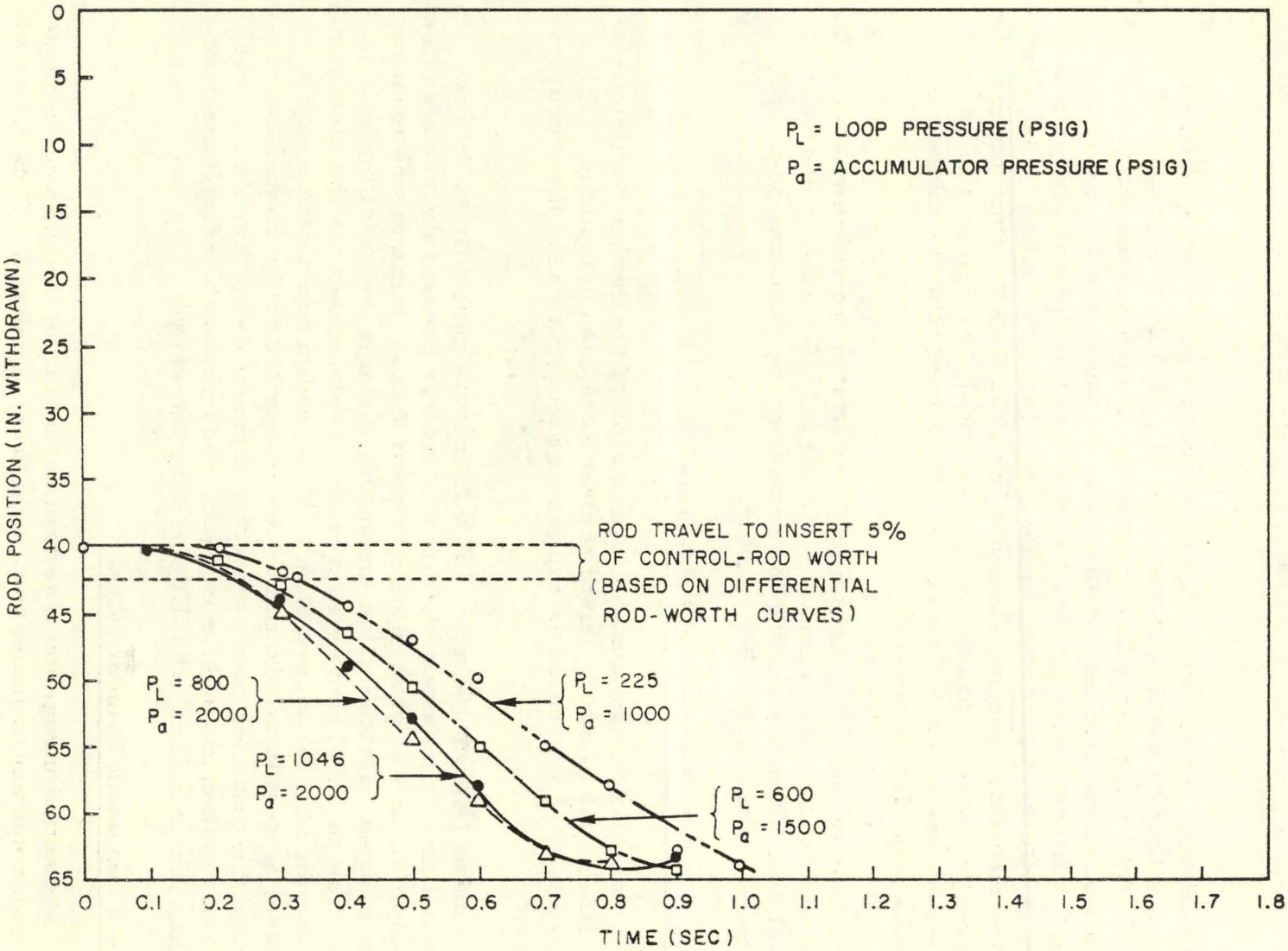

Fig. 1.14--Effect of loop pressures on scram characteristics of EBOR control-rod-drive mechanism (data are for scram tests 12, 15, 16, and 19 performed March 7, 1962)

and a determination has been made of the design requirements necessary to convert the existing bridge in the shield test pool facility to a core component handling tool. This information was a necessary input to the preparation of an equipment specification for the accomplishment of the modification.

The modified instrument bridge will function generally as follows. During dry-handling of the EBOR core (see Fig. 1. 15), the bridge will remove individual components in air from the reactor vessel and place them into a lead transfer cask. In the case of core elements, provision for cooling components during transit to the cask will be provided in order to remove the afterheat generated in the fuel. No such cooling is required for reflector elements, control elements, or grid plates. After the transfer cask has been transported to the fuel-storage pool, the bridge will remove core, reflector, and control elements and load them into the submerged storage racks provided in the pool.

In addition to removing these components from the reactor, the modified bridge will load core components into the transfer cask at the fuel-storage pool and, after positioning the cask over the refueling port, will reinstall them in place within the reactor.

Transfer-cask Portable Shield Shutter

The conceptual design and a determination of the design requirements for the transfer-cask portable shield shutter have been completed. This information was used to prepare an equipment specification for the procurement of the shutter.

The shutter (shown in Fig. 1. 16) will operate generally as follows. Since the handling of components within the reactor pressure vessel requires the removal of an access plug in the shutdown shield, some means must be provided to prevent radiation from emanating through the resulting hole in the shield. The shielded shutter serves as a replacement for the biological shielding provided by the access plug. When used in combination with a transfer cask, it serves in addition to accurately locate the centerline of the cask over the refueling port or control-element drive thimble, to level the cask, and to allow passage of radioactive components through the shutdown shield without loss of over-all shielding integrity.

Core-component Transfer Cask

The conceptual design and a determination of the design requirements for the core-component transfer cask have been completed. This information was a necessary input to the preparation of an equipment specification for the procurement of the cask.

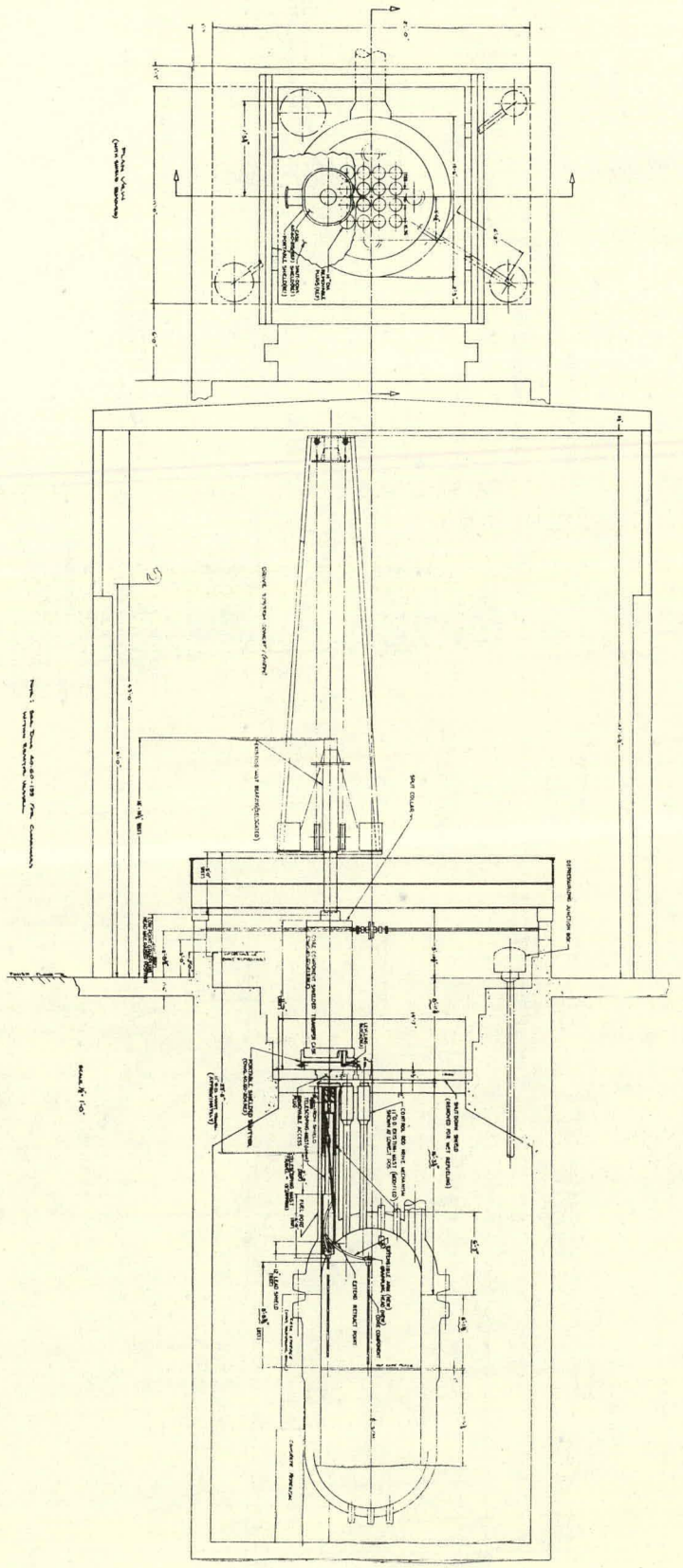

Fig. 1.15--Reactor component handling arrangement

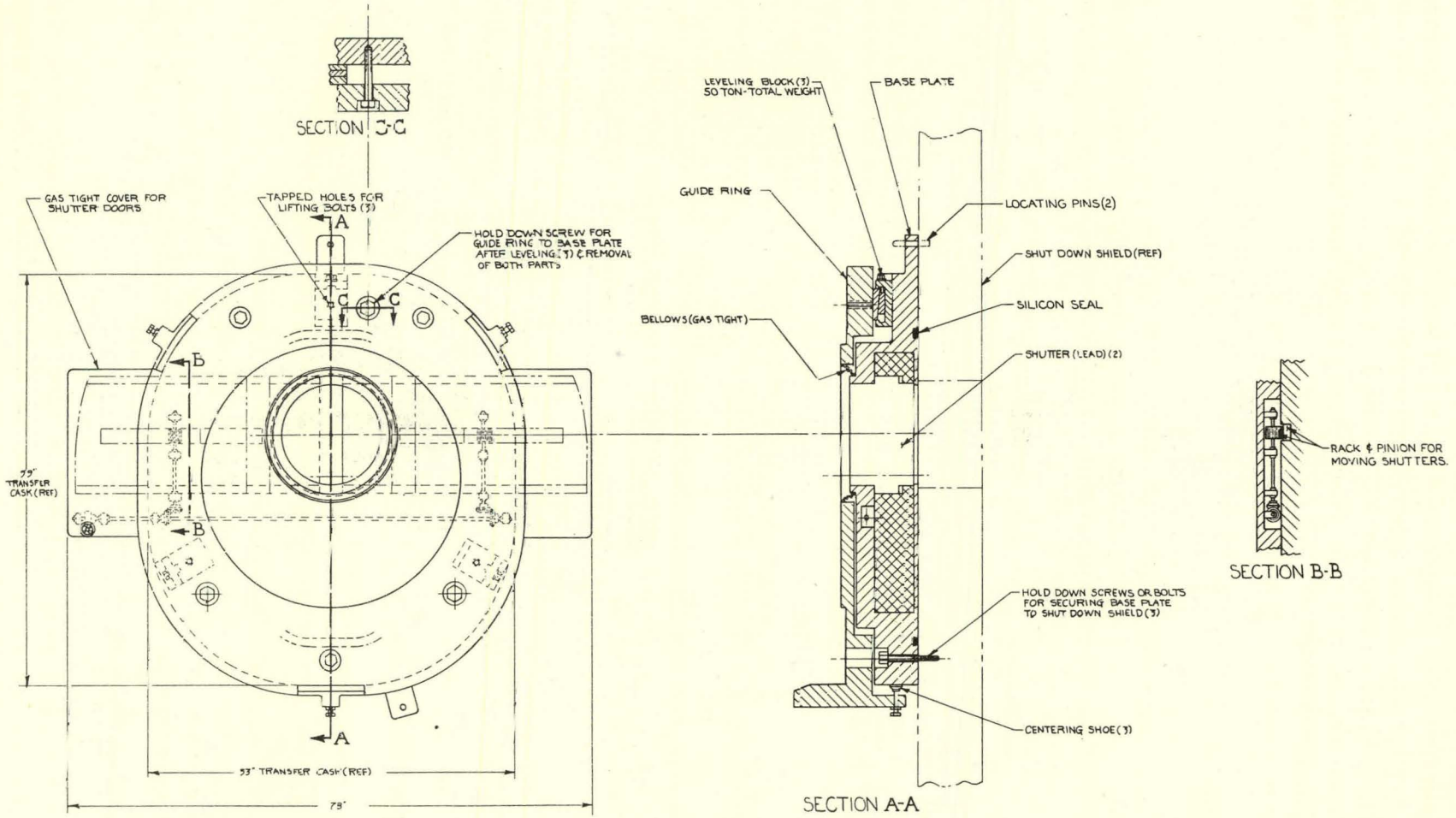

Fig. 1.16--Conceptual design of transfer-cask portable shield shutter

The transfer cask (shown in Fig. 1. 17) will be used to transport radioactive core components in air between the EBOR and the fuel-storage pool. During transfer, the cask will provide biological shielding to protect personnel from exposure to radiation, will prevent the release of fission products to the atmosphere, and will protect the core components against possible mechanical damage from handling loads.

General

Work is in process on the conceptual design and the definition of design requirements for the shield plug cask, the control-rod-drive transfer cask, the intermediate cooling station, and the remote-viewing system.

Design for Construction (Task 60) (T. J. Larson)

Modification of the STF Instrument Bridge

The equipment specification which defines the modifications necessary to convert the STF instrument bridge to a core component handling tool has been completed. The specification has been sent to vendors with a request for bids by April 30, 1962.

Transfer-cask Portable Shield Shutter

The equipment specification which defines the requirements for the transfer-cask portable shield shutter has been completed and sent to purchasing for bid invitations.

Core-component Transfer Cask

The equipment specification which defines the requirements for the core-component transfer cask is in the process of final review.

Information for Architect-Engineer Title II Design

Design information for the architect-engineer Title II package was prepared covering the following previously reported areas[5]:

1. Location and orientation of the shutdown shield.
2. Requirements for the control-rod-drive storage cell.
3. Requirements for the handling-tool storage racks.
4. Requirements for the transfer-cask foundation.

Safeguards Report

Information has been obtained on fuel-cladding temperature/time history during the transport of fuel in the transfer cask. (This information has been issued in an addendum to the Preliminary Safeguards Report.)

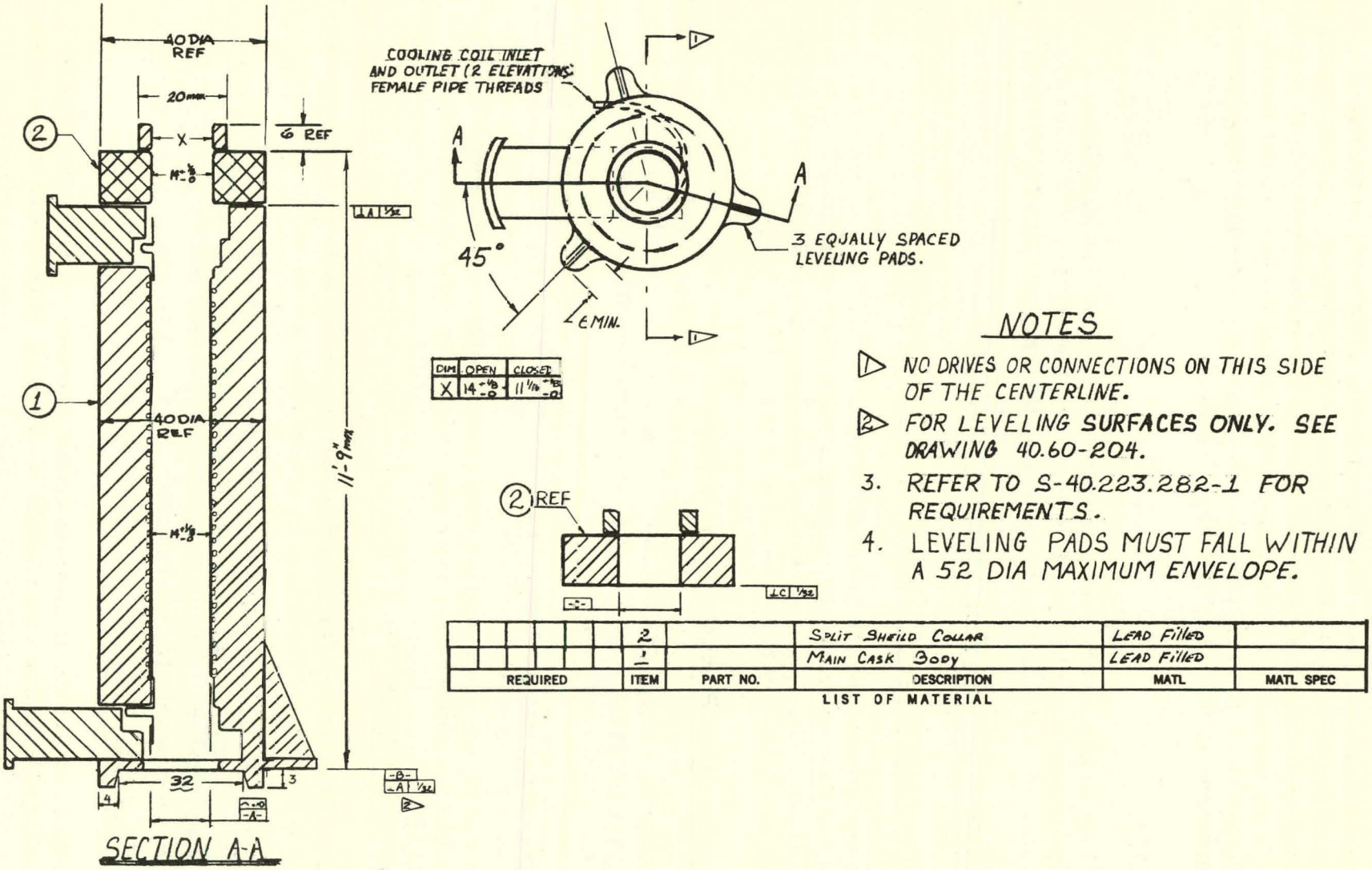

REQUIRED	ITEM	PART NO.	DESCRIPTION	MATL	MATL SPEC
2	2		Split Shield Collar	Lead Filled	
1	1		Main Cask Body	Lead Filled	

LIST OF MATERIAL

Fig. 1.17--Core-component transfer cask

The time/temperature analysis was based on the previously reported[2] investigation of core-element temperatures during transfer. Assuming failure of the cask cooling system and ignoring the loss of heat from the cask to its surroundings (an ultraconservative assumption), 113 hr would be required for the cladding of an uncooled element to reach its melting point.

REACTOR INSTRUMENTATION (W. Lones)

Research and Development (Task 14)

Connector Contact Test

The connector contact test is in progress, and contact-noise data and data related to reading inaccuracies (if any) introduced by the contacts will be forthcoming.

Trial Fabrication of In-core Sensors and Connectors

Trial fabrication of the core-element connectors pointed up the high cost of fabricating the Geminol P/N contacts and the failed-fuel detection tube connection. Therefore, in order to reduce costs, the threads on the contact stems were eliminated, and the failed-fuel tube connection was changed from Hastelloy X to stainless steel.

Design for Construction (Task 62)

Most of the work under this task has been directed toward the completion of the instrumentation design and the writing of purchase specifications. The specifications for the nuclear and safety system and the failed-fuel-detection system have been issued to the purchasing department and transmitted to vendors.

The final drawings for the thermocouple and calibrating thermocouple-well depressurizing junction box have been completed and have undergone dimensional check. The drawings for the sampling-tube depressurizing junction box are presently being checked.

EXPERIMENTAL ENGINEERING (H. C. Hopkins)

Hanford Loop (Task 20)

On January 6, 1961, a 19-rod-bundle test fuel element was inserted into the Hanford DR-1 gas loop. The test element consists of 19 fuel pins,

each approximately 15 in. long by 3/8 in. in diameter, of $BeO-UO_2$ fuel clad with Hastelloy X and has a thermal power putput of 35 kw. The detailed design and operating conditions have been discussed in a previous quarterly progress report.[6]

The test element has demonstrated the ability of EBOR fuel pins to operate satisfactorily at a maximum cladding temperature of 1500°F and above. Current plans are to remove the element in June, 1962, after 18 months in-pile and an estimated time of 7000 hr at high temperature, including 1200 hr at 1700°F.

As of March 1, 1962, a maximum cladding temperature of 1500°F and above had been maintained for 5069 hr , including 1226 hr at 1700°F. During this time, the element was thermal-cycled 38 times. The loop is monitored for release of fission products by means of two proportional counters mounted on the external piping and by examination of helium samples with a single-channel gamma analyzer set for the principal gamma from Xe^{133}. Both of these monitors have remained at normal background level, which indicates that the cladding has remained sound and that there has been no fission-product leakage.

REFERENCES

1. Quirk, J., F. H. Lofftus, and J. V. Furth, Strength and Structure of Sintered BeO Moderator Ceramics, General Atomic, Report GA-2727, October 24, 1961
2. MGCR Quarterly Progress Report for the Period Ending December 31, 1961, General Atomic, Report GA-2847.
3. Malek, G. J., Radial Temperature Distribution in a Square-Annular Shaped Block, General Atomic, Report GAMD-2739, October 25, 1961.
4. MGCR Project Staff, MGCR Project Monthly Technical Progress Report, January, 1962, General Atomic, Report GACD-2932.
5. EBOR Project Staff, EBOR Project Monthly Technical Progress Report, February, 1962, General Atomic, Report GACD-3017.
6. MGCR Quarterly Progress Report for the Period Ending September 30, 1961, General Atomic, Report GA-2568.

II. REACTOR PHYSICS

EXPERIMENTAL PHYSICS (Task 13) (W. B. Wright, A. J. Goodjohn)

Critical experiments in the simulated water-flooded condition were summarized in the last two quarterly progress reports.[1][2] At the end of this experimental program, a new critical-assembly building was constructed to provide more adequate shielding in preparation for dry-core experiments. A description of this building and the dry-core experimental program has been given in Supplement 3 to the Safeguards Report, which was issued during this period.[3]

Dry-core experiments in the new building were begun on January 9, 1962. The properties of two basic cores were investigated. The first of these had a unit-cell arrangement in which fuel was lumped to approximately the same extent as in the EBOR. Therefore, this core is referred to as the "standard core," and most of the experiments performed during this quarter were carried out with this configuration. The second core had a unit-cell configuration in which the fuel was lumped to a much greater extent than in the EBOR and is referred to as the "lumped core." This core provided a more stringent test of the analytical homogenization techniques and served as an additional check of the design methods. Both cores contained distributed boron-stainless steel shims to hold down the excess core reactivity.

Reactivity Experiments in the Standard Core

The standard core was composed of 24 unit cells constructed as shown in Fig. 2.1, and it contained 46.91 kg of U^{235}. With 45 mils of boron-stainless steel in each fuel channel, the core reactivity excess was 0.53 dollar. Various experiments were performed with this configuration and are reported below.

Operational Experiments

The worths of the fuses and safety rods were measured as soon as the first core became critical and are listed in Table 2.1.

The perturbations in reactivity created by fuse voids and control-rod voids were measured. In the case of the fuse and horizontal control-rod void, the measurements were made by determining the worth of beryllium

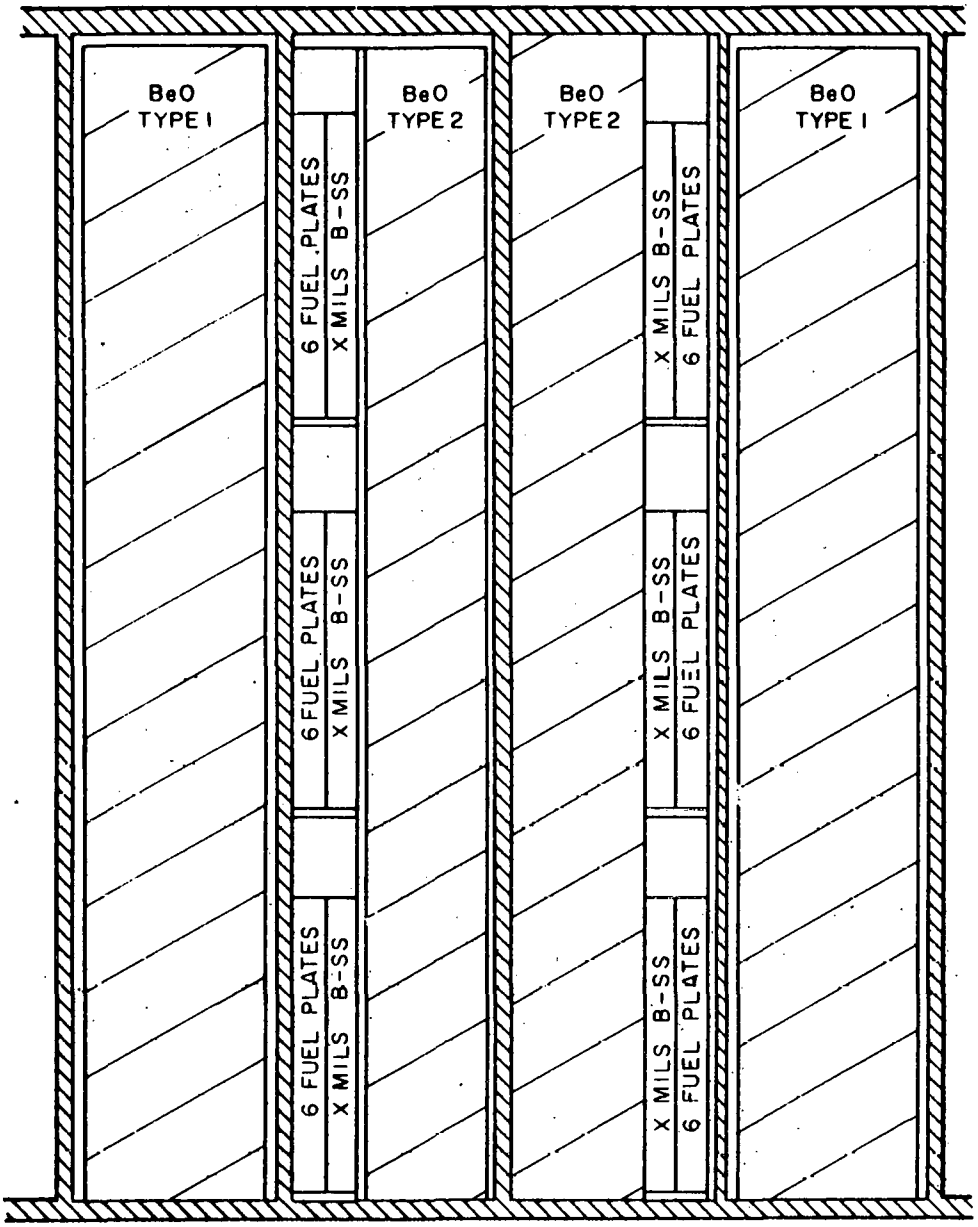

Fig. 2. 1--Unit cell for standard core configuration

oxide in the void locations. Since this was not possible in the case of the vertical control-rod voids, voids of like dimensions were introduced in both halves of the core at distances from the centerline that bracketed the positions of the vertical control rods. The worth of these simulated control-rod voids as a function of position is shown in Fig. 2.2. The results of the measurements of these reactivity perturbations are given in Table 2.2 in terms of the increase in core reactivity that would have occurred had these voids been filled with beryllium oxide.

Table 2.1

WORTH OF SAFETY DEVICES

Device	Worth (dollars)
Vertical rods	8.50
Five fuses	2.70
Horizontal rod	0.80

Table 2.2

WORTH OF ROD AND FUSE VOIDS

Void Type	Worth (dollars)
Upper fuse, center	0.34
Upper fuse, off-center	0.31
Lower fuse, off-center	0.33
Horizontal rod	0.29
Vertical rods	3.10
Total void	5.01

In addition to the void measurements, the reactivity coefficient of boron-stainless steel was measured as a function of position throughout the core, to determine the core symmetry and the distributed worth of the boron-stainless steel. Figure 2.3 shows a core map with the various unit-cell positions. Table 2.3 lists the reactivity coefficient of the boron-stainless steel in the various unit cells. For the distributed reactivity coefficient measurement of boron-stainless steel, one 5-mil piece was added to each of the six fuel channels within a unit cell.

An estimate was made of the reactivity loss caused by streaming. The normal arrangement of fuel channels wherein the alignment of the various channels yields a possible streaming path in both the vertical and

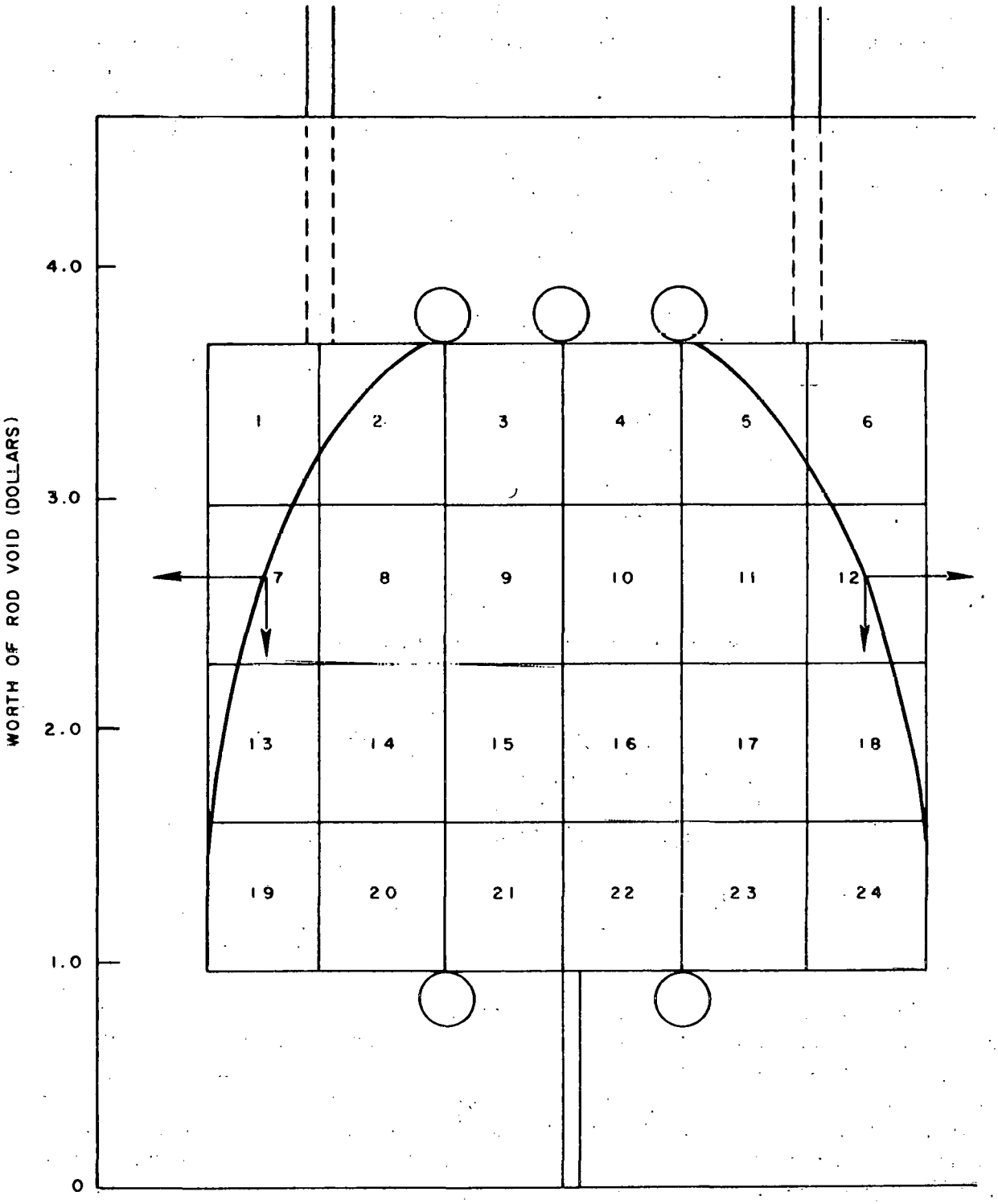

Fig. 2.2--End view of dry core

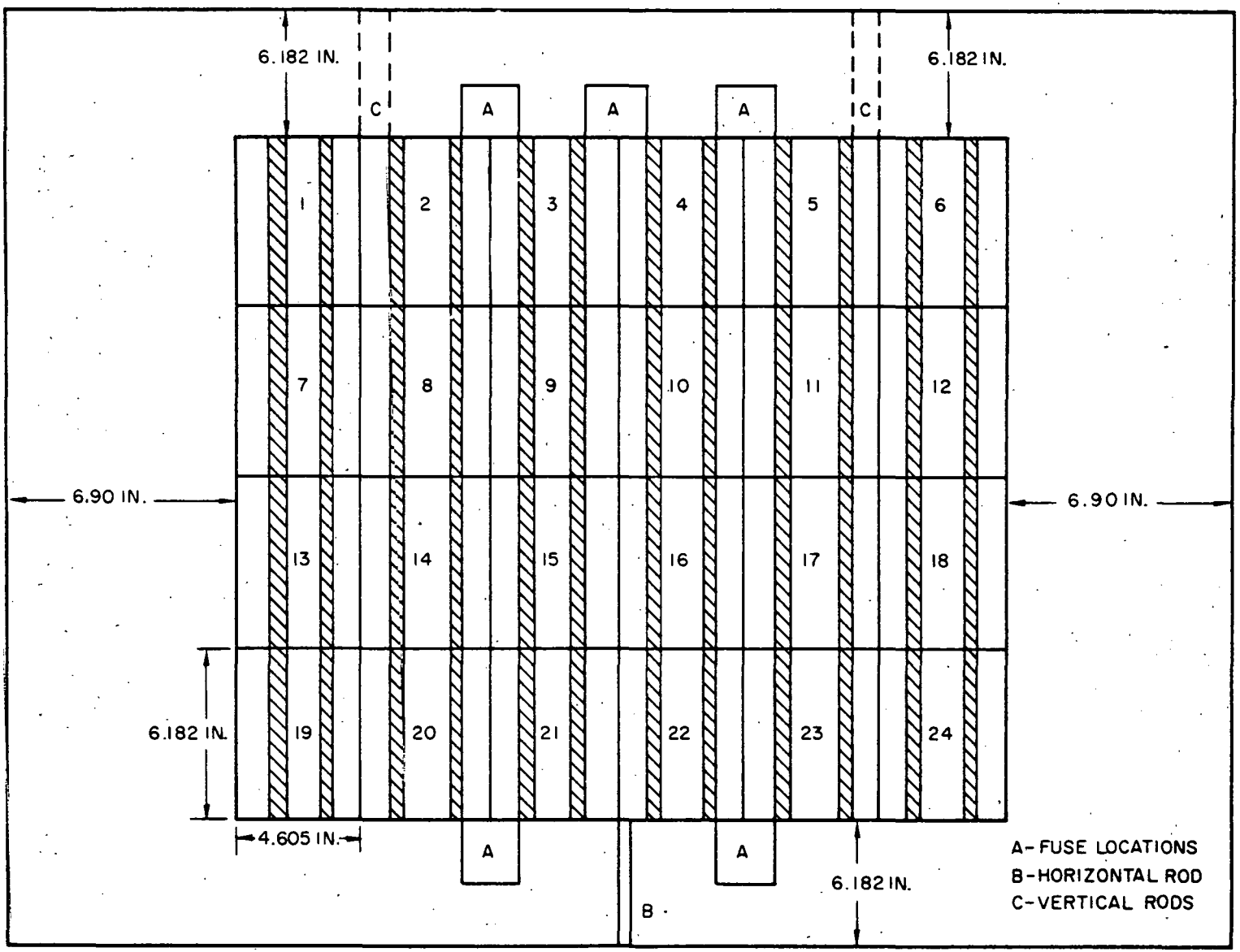

Fig. 2.3--Core map

Table 2. 3

REACTIVITY COEFFICIENT OF BORON-STAINLESS STEEL

Unit Cell	Worth* (dollars)	Unit Cell	Worth* (dollars)
1	0. 0631	3	0. 111
6	0. 0730	7	0. 088
19	0. 0620	8	0. 124
24	0. 0640	9	0. 181
2	0. 083	Total core	2. 60

*For 5 mils of stainless steel in each channel.

axial directions is shown in Fig. 2. 3. In these streaming experiments, the fuel channels in four of the unit cells were rearranged in three steps as shown in Fig. 2. 4. In Step A, the fuel channels were arranged as in the standard core. In Step B, the fuel channels and No. 2 BeO blocks were interchanged in alternate rows of unit cells. In Step C, the remaining unit cells were interchanged. In each case, the excess core reactivity was determined. In Steps A and C, the reactivity loss caused by streaming was the same and the change in reactivity was a measure of only the rearrangement of beryllium oxide and fuel. Half of this reactivity change would be that expected in Step B with no streaming present. The difference between the measured reactivity change in Step B and half of the change in Steps A to C is the reactivity loss caused by streaming. Using the relative worth of boron-stainless steel in each column of cells, the total streaming effect in the vertical direction was computed as 0. 17 dollar. A summary of the measurements is given in Table 2. 4.

Table 2. 4

VERTICAL-DIMENSION CORE-STREAMING MEASUREMENTS

Step	Core Excess Reactivity (dollars)	Change from A (dollars)
A	0. 061	0. 0
B	0. 244	0. 183
C	0. 390	0. 329

NOTE: Streaming = 0. 183 - (0. 329/2) = 0. 019; total vertical streaming = 0. 17 dollar, based on the relative worth of boron-stainless steel.

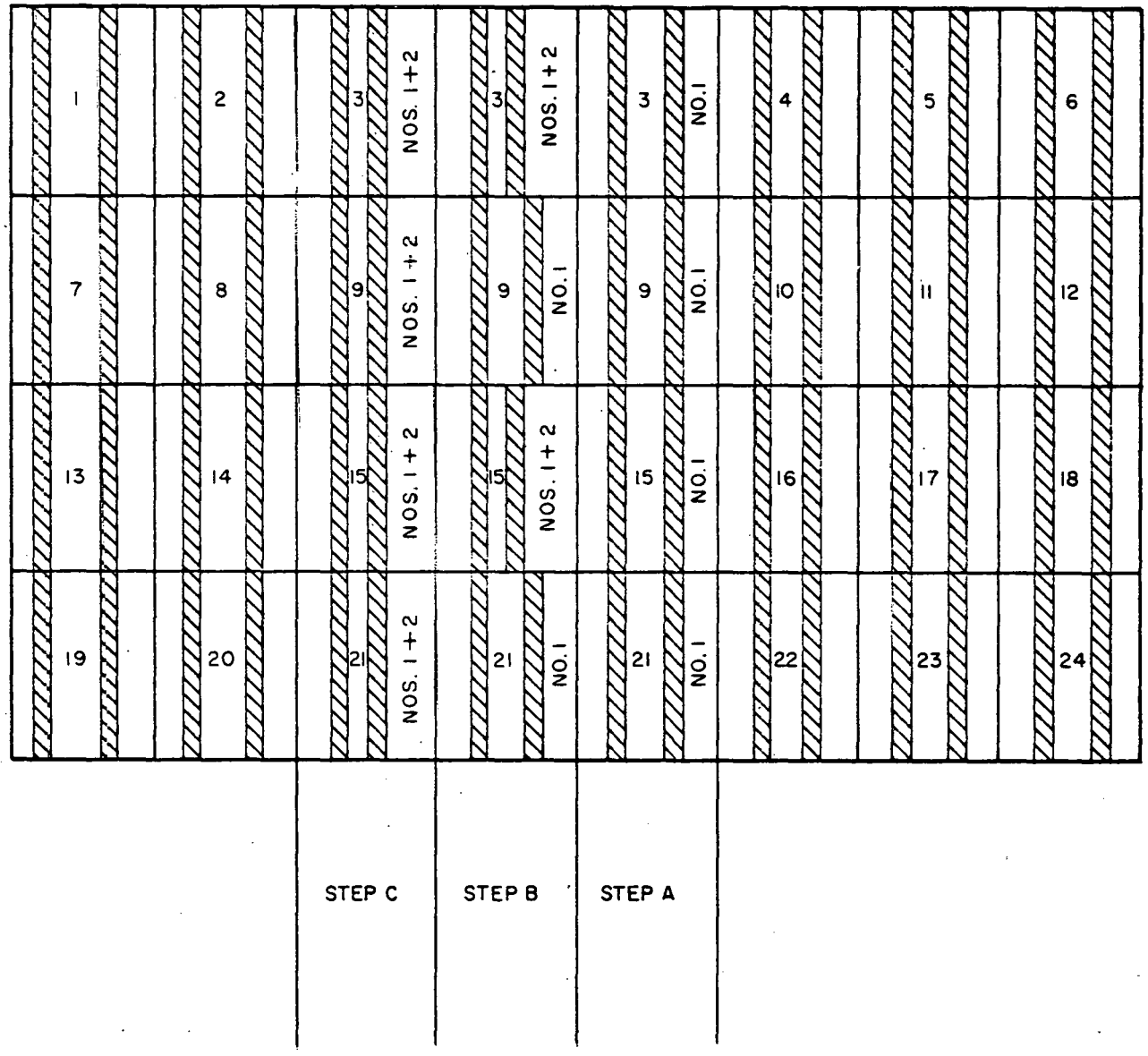

Fig. 2.4--Core streaming measurements

A streaming measurement similar to that made for the vertical dimension could have been made for the axial dimension of the core but would have required the cutting of fuel foils and channels. Therefore, since streaming appeared to be only a minor perturbation to the core, the assumption was made that streaming is inversely proportional to the length of the possible streaming path. Axial streaming was thus assumed to be worth 0.13 dollar and the total streaming correction for the standard core was 0.30 dollar.

Using the measured values of void worths and the loss in reactivity caused by streaming, the excess core reactivity with all voids filled with beryllium oxide, with a uniform boron-stainless steel distribution, and with no streaming would be 4.40% $\delta k/k$, based on β_{eff} - 0.0075. This value should be noted carefully because a calculation of the reactivity of the critical assembly by our analytical techniques, in which all voids are filled with BeO, there is no streaming, and boron-stainless steel distribution is uniform, should show a reactivity excess of this magnitude. Similarly, a calculation in which only the vertical-rod voids are filled with BeO, there is assumed to be no streaming, and the distribution of boron-stainless steel is uniform, but which has the explicit voids due to the fuses and the horizontal rod, should show a reactivity excess of 2.92%.

Slab Void Experiments

Because the EBOR has discrete slab control-rod voids that cut both the core and the reflector, slab voids were incorporated in this core as shown in Fig. 2.5, and the boron-stainless steel was removed until the core was again critical. In addition, measurements were also made with the voids completely filled with beryllium oxide and partially filled with beryllium oxide.

In the first of these measurements, the voids were filled with No. 1 blocks (1.060 in. wide) after the addition of boron-stainless steel throughout the core. In the second measurement, No. 2 blocks (0.655 in. wide) were substituted for the No. 1 blocks, leaving a slab void approximately 0.4 in. wide. The reactivity loss caused by streaming in this void was measured by a method similar to the one described above. In Step 1, the core reactivity was determined with all of the No. 2 blocks lined up toward the core center. In Step 2, the No. 2 blocks were moved to the other side of the slot in alternate rows. In Step 3, the blocks were lined up away from the core center. The reactivity loss caused by streaming is the difference between one-half the reactivity change in Steps 3 and 1 and the reactivity change in Step 2. The results showed a 0.031-dollar loss in reactivity because of streaming through a 0.4-in. slab void. A summary of these measurements is given in Table 2.5.

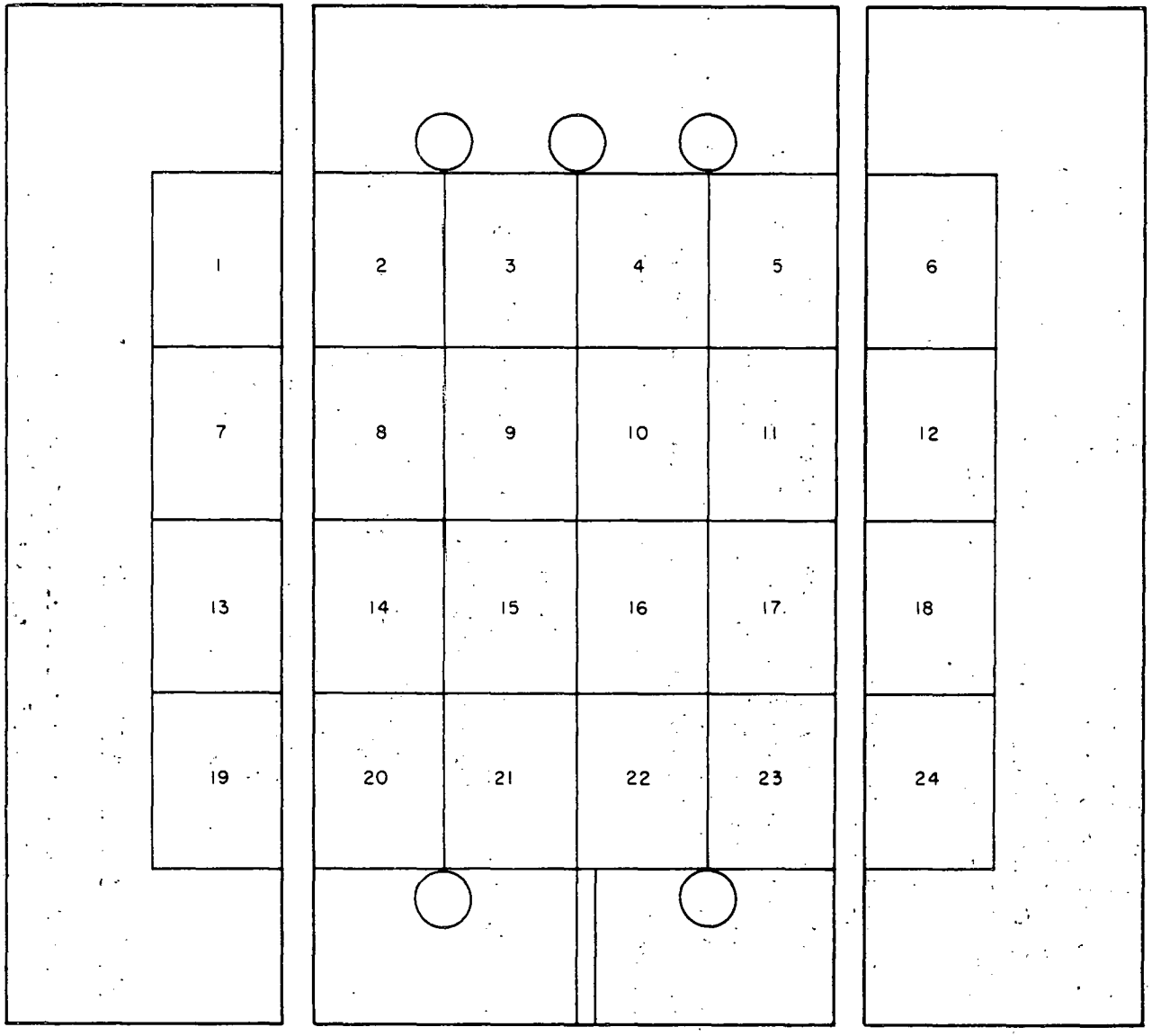

Fig. 2.5--Slab void experimental arrangement

Table 2.5

SLAB-VOID STREAMING MEASUREMENTS

Condition	Core Excess Reactivity (dollars)	Change from I (dollars)
No. 2 BeO toward core center	0.090	0.0
No. 2 BeO alternated	0.1094	+0.0194
No. 2 BeO away from center	0.0665	-0.0235

NOTE: Streaming = 0.0194 - [(-0.0235/2)] = 0.031 dollar.

Reflector Measurements

The side-reflector thickness was changed in two steps and the core excess reactivity was determined by either a subcritical measurement or removal of the boron-stainless steel. In the first step, one row of No. 1 BeO blocks was removed from each side of the reflector, and in the second step, another row of BeO blocks was removed. The change in reactivity due to the change in reflector thickness is shown in Table 2.6.

Table 2.6

CHANGE IN CORE REACTIVITY AS A FUNCTION OF REFLECTOR THICKNESS

Side Reflector Thickness (in.)	Reactivity Change (dollars)
Standard (6.906)	0.0
5.755	-1.21
4.604	-2.75

Slab Control-rod Measurements

Slab rods 12 in. wide and 38 in. long were inserted at the core center, as shown in Fig. 2.6, by removing beryllium oxide in this location. The reactivity loss due to the removal of beryllium oxide was 1.87 dollars. After this void had been obtained, three slab rods were inserted in the core and the core was brought to criticality by the removal of boron-stainless steel. The first rod was composed of dysprosium tiles encased in an aluminum box; the second rod was composed of strips of boron-stainless steel of a thickness chosen to match the optical thickness of the dysprosium

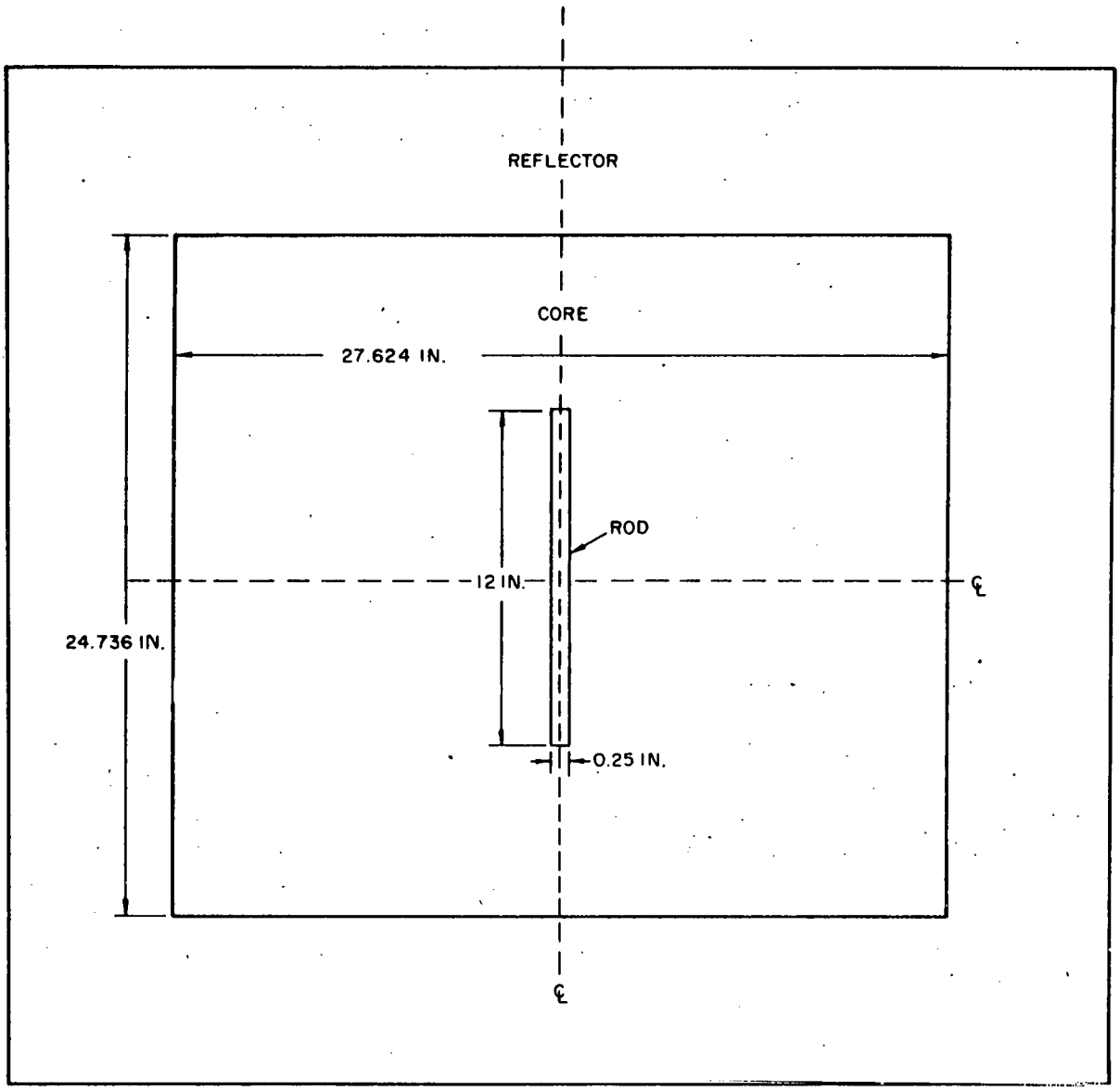

Number Densities of Rod Material

Rod	N_{Al}	N_B	N_{Fe}	N_{Cr}	N_O	N_{Dy}
Dy_2O_3	0.1001	-----	-----	-----	0.1268	0.003011
B-SS	0.09195	0.004434	0.06112	0.0160	-----	-----
Boral	0.04	0.03758	-----	-----	-----	-----

Fig. 2.6--Slab rod experimental arrangement

rod at 2200 m/sec; and the third rod was composed of boral. The number densities of the various rod materials are given in Fig. 2.6, adjusted to a rod thickness of 0.25 in. The estimated rod worths in the standard core (containing 45 mils of boron-stainless steel in each cell) are listed in Table 2.7.

Table 2.7

ESTIMATED ROD WORTHS

Rod Type	Estimated Worth (dollars)
Dy_2O_3	5.80
Boron-stainless steel	5.23
Boral	9.10

Core Reactivity Values

The excess reactivity values and the corresponding values of k_{eff} for all the standard cores constructed are given in Table 2.8, adjusted by (1) the worth of the vertical control-rod voids, (2) loss in reactivity caused by streaming, (3) the reactivity coefficient of boron stainless steel applied to cells not containing the noted boron-stainless steel (when necessary), and (4) the excess reactivity of the cores measured by period or subcritical measurements. Column 2 of Table 2.8 lists the thickness of boron-stainless steel in each fuel channel. In computing the reactivity values, it was assumed that $\beta_{eff} = 0.0075$.

Reactivity Experiments in the Lumped Core

The lumped core was composed of 24 unit cells constructed as shown in Fig. 2.7 and containing 46.91 kg of U^{235}. With 30 mils of boron-stainless steel in each fuel channel, the core reactivity excess was less than 0.37 dollar. As in the standard core, slab rods 12 in. wide and 38 in. long were inserted at the core center, as shown in Fig. 2.6, by removing beryllium oxide in this location. The reactivity loss caused by the removal of beryllium oxide was 1.75 dollars. With this void, three slab rods were inserted in the core and the assembly was brought to criticality by the removal of boron-stainless steel. These rods were identical with those described above and had the number densities given in Fig. 2.6. The adjusted excess reactivity values and the corresponding values of k_{eff} for all of the lumped cores constructed are given in Table 2.9.

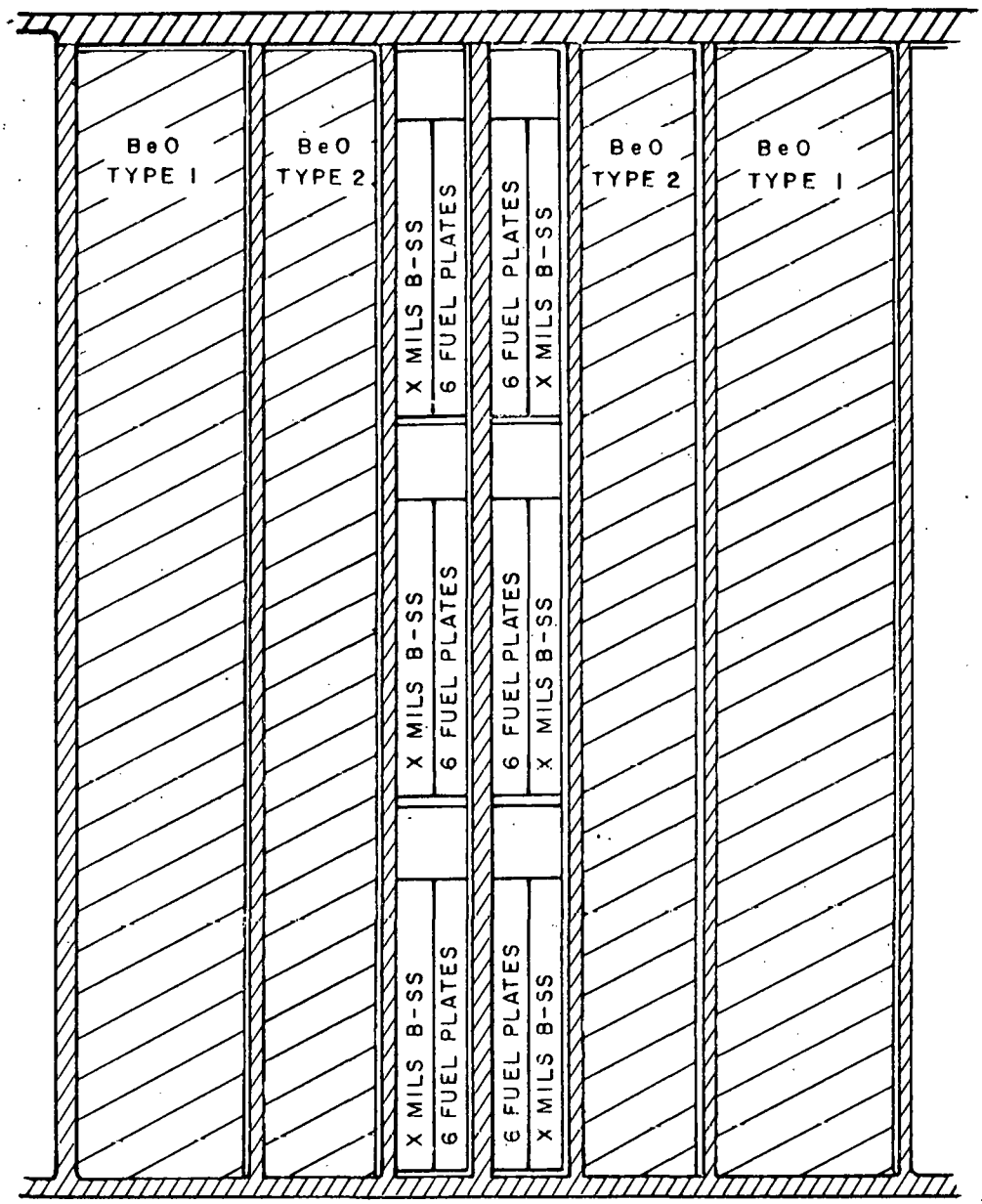

Fig. 2.7--Unit cell for lumped core configuration

Table 2.8

STANDARD-CORE REACTIVITY VALUES

Conditions	B-SS Thickness in Each Channel (mils)	Core Excess Reactivity (% δk/k)	k_{eff}
Clean standard core	45	2.92	1.0300
Side reflector change			
5.755 in.	45	2.00	1.0204
4.604 in.	40	2.40	1.0246
Void (Fig. 5)			
1.090 in.	40	1.02	1.0103
0.435 in.	45	2.59	1.0266
Void filled with BeO	50	2.18	1.0223
Dy_2O_3 rod at center	30	4.43	1.0464
Boron-stainless steel rod at center	30	4.85	1.0510
Boral rod at center	20	5.80	1.0616

Table 2.9

LUMPED-CORE REACTIVITY VALUES

Conditions	B-SS Thickness in Each Channel (mils)	Core Excess Reactivity (% δk/k)	k_{eff}
Clean lumped core	30	2.24	1.0229
Dy_2O_3 rod at center	20	3.22	1.0333
Boron-stainless steel rod at center	20	3.55	1.0368
Boral rod at center	10	6.04	1.0643

Cell Homogenization Measurements

Detailed manganese activation measurements were made in unit cells in both the standard and the lumped cores. It was found that for these epithermal cores, wherein the mean free path for neutrons is higher than in the simulated water-flooded cores reported previously, foil interaction effects were important and care was necessary to assure that the presence

of too many foils across the cell in any one activation did not perturb the measured flux distribution. These effects were investigated experimentally by varying the number of manganese foils used in any one activation. As a result, it was found necessary to do a series of activations with only a few foils inserted in the cell in each run. The detailed distribution was determined by normalizing the various runs to the same power level. The difference in distributions, measured with few and many foils, is shown in Fig. 2.8.

Since the unit cell (No. 9 of Fig. 2.2) in which the activations were made was off-center, the detailed distribution is superimposed on an overall core flux gradient pertaining to the gross radial leakage. The distributions in both halves of the cell are shown in Fig. 2.9, where they are compared with the calculated values of the manganese foil activities.

NUCLEAR DESIGN (Tasks 22 and 51) (A. J. Goodjohn, H. A. Vieweg, L. R. Amyot, A. D. McWhirter, J. R. Seibold, W. B. Wright)

Analysis of Critical Experiments

Two reports describing the analysis of the simulated-water-flooded critical experiments were issued.[4][5] During the present quarter, the methods used in the nuclear design of the EBOR were examined in detail, using the experimental data from the dry-core experiments discussed under Task 13. A number of investigations were made on various parts of the analytical methods, and the gross aspects of the analysis were checked by computing the total core reactivities for a number of critical configurations. These investigations can be classified as (1) studies of fuel-cell homogenization techniques and (2) calculation of gross core-reactivity values.

Fuel-cell Homogenized Constants

The method used in the EBOR design studies to homogenize fuel cells consists of a DSN calculation in 22 energy groups (10^7 to 0.005 ev) of which 12 groups are epithermal (> 2.1 ev) and 10 are thermal. The initial calculation is performed with microscopic cross sections derived from GAM and GATHER spectra, based on homogenized fuel-cell number densities. Microscopic DSN cross sections can be obtained from the resulting self-shielded spectrum, and the DSN calculation can be repeated to obtain iterated macroscopic constants for the homogenized cell. The use of a crystalline (as opposed to a free-gas) kernel for beryllium oxide and the number of thermal groups used in the calculation could also affect the homogenization results. Two additional factors peculiar to the critical assembly are the large amount of aluminum present and the fact that the fuel height is less than the height of the unit cell, as seen in Figs. 2.1 and 2.7.

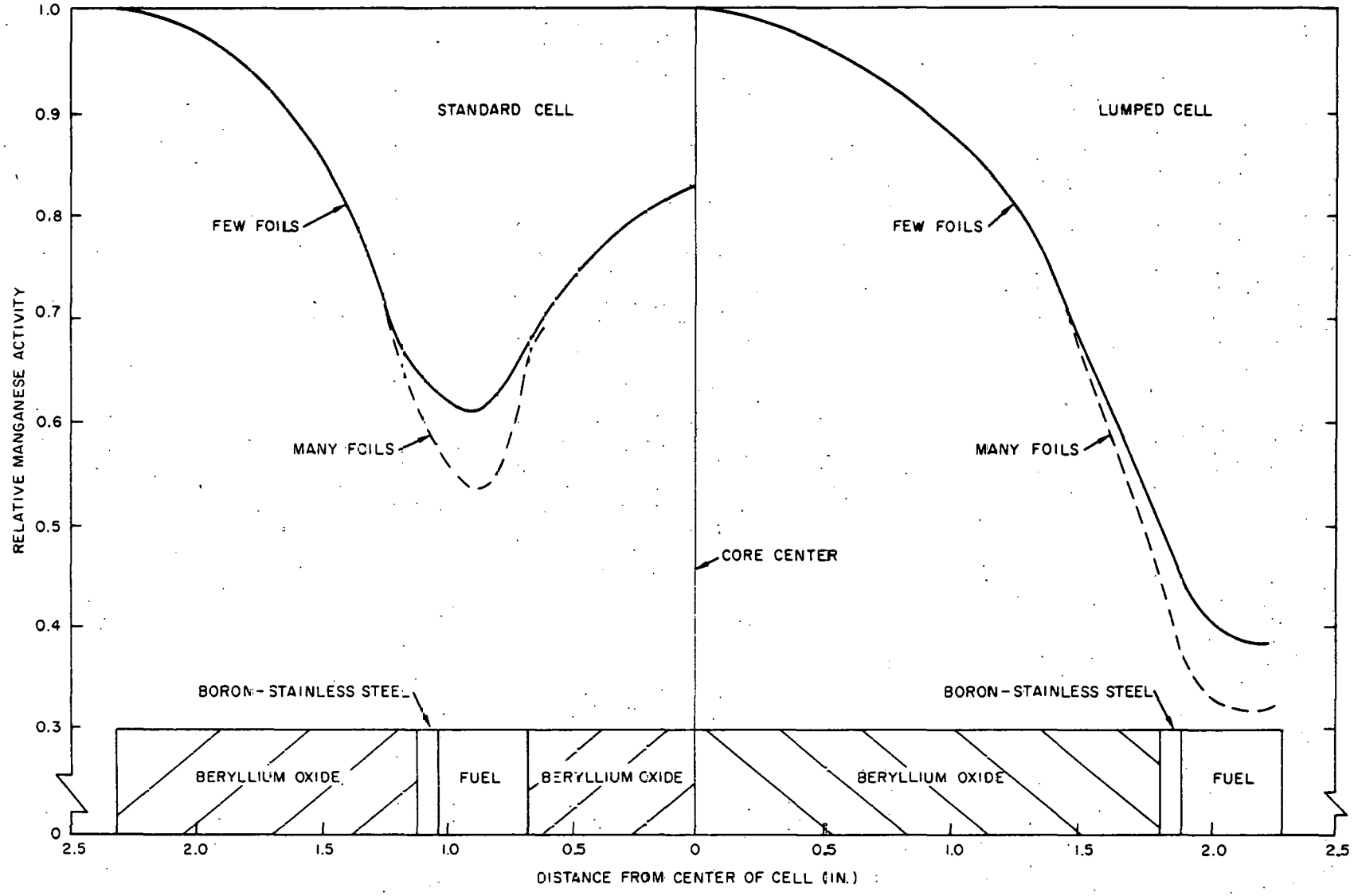

Fig. 2.8--Manganese activity distribution measurements

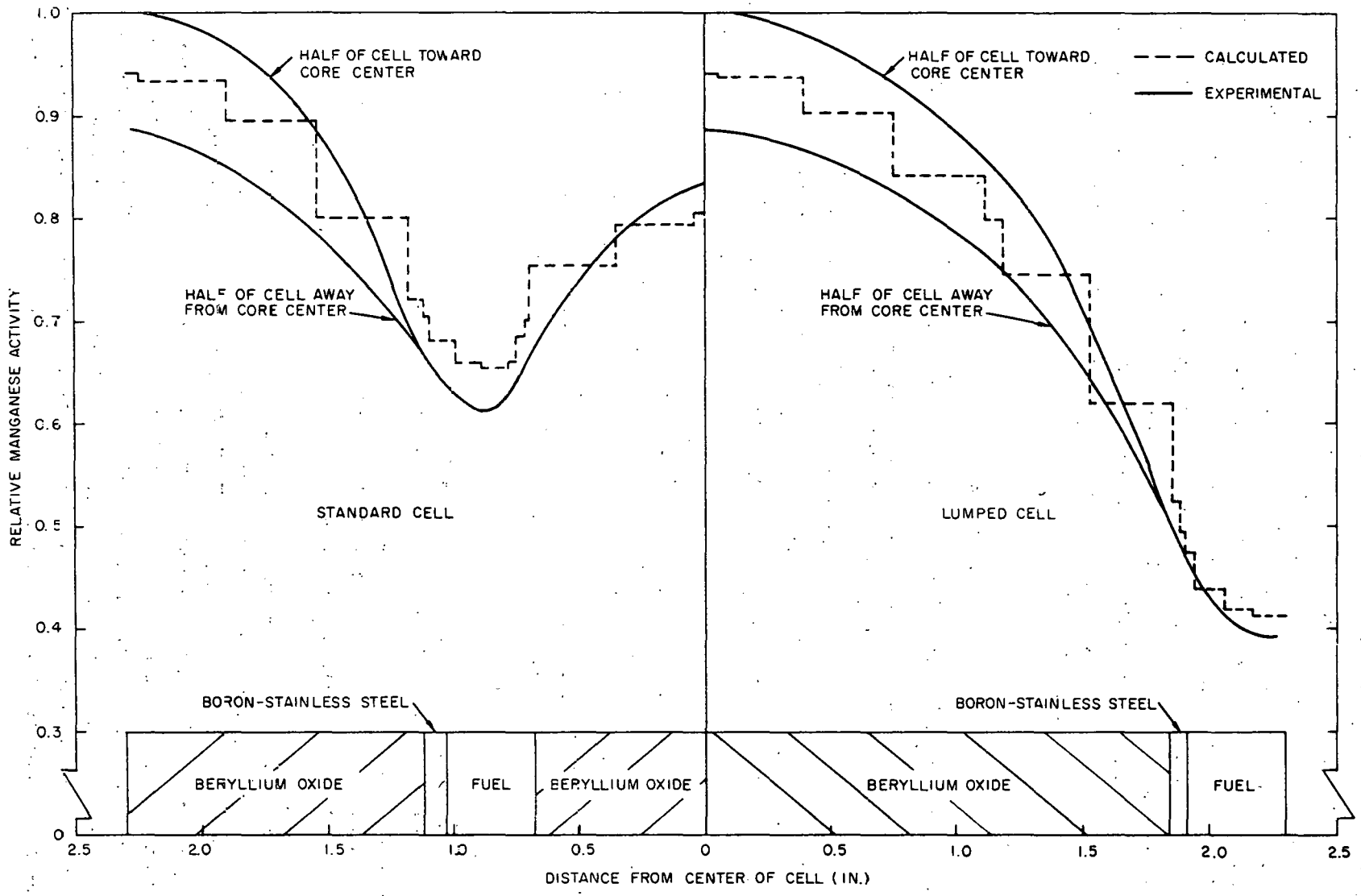

Fig. 2.9--Comparisen of experimental and calculated manganese activations

Using the geometry and composition of the standard core, comparisons were made between iterated and noniterated cross sections, between gas- and crystalline-kernel cross sections, and between the use of 10 and 18 thermal groups. In addition, a DSN calculation was made in which the fuel height was considered to be the same as that of the unit cell, rather than diluting the fuel region by the ratio of fuel height to cell height. After the analytical program had started, a slight change was made in the high-energy cross sections for aluminum, and this effect was investigated. Table 2. 10 presents the results of these calculations in terms of two-group constants derived from GAM and GATHER. The estimate of k_{eff} is based on a geometric buckling of 0. 0018 cm^{-2}.

Table 2. 10

COMPARISON OF VARIOUS HOMOGENIZATION CALCULATIONS

Case	Epithermal Groups (10^7 to 2. 1 ev)			Thermal Groups (2. 1 to 0. 005 ev)		Estimated k_{eff}
	ηf	$\tau(cm^2)$	p	ηf	$L^2(cm^2)$	
Noniterated gas kernel	1. 2850	116. 68	0. 18741	1. 3784	16. 393	1. 0498
Iterated gas kernel	1. 2867	116. 32	0. 18961	1. 3886	16. 201	1. 0532
Iterated crystalline kernel	1. 2867	116. 32	0. 18961	1. 3806	17. 179	1. 0516
18 thermal groups*	1. 2867	116. 32	0. 18961	1. 3805	17. 081	1. 0517
New aluminum data*	1. 2927	117. 18	0. 19043	1. 3806	17. 179	1. 0540
Fuel height increased*	1. 2827	116. 56	0. 20021	1. 3854	18. 018	1. 0493

*All with iterated crystalline kernel.

These results indicate very little difference between the various methods. The increased fuel height is physically unrealistic; however, the comparison does show that little, if any, error results from the diluted representation, since the homogenized constants are evidently insensitive to the geometric approximation used.

One other aspect of the homogenization technique was investigated. This was the approximation made in both the nuclear design and the critical assembly analysis, that each unit cell in the core can be homogenized prior to the criticality calculations, as though it were in an infinite medium of like-unit cells. In other words, the fact that a cell may be next to the reflector or at the core center is not taken into account in the homogenization. To check the validity of this approximation, a DSN calculation was performed on the entire core in which the rows of unit cells were represented explicitly. Self-shielding factors were obtained for each row of cells (designated as

center, middle, and outer in Table 2. 11) and GAM and GATHER constants were obtained for each position. With reference to Fig. 2. 2, the cells considered were as follows:

Cell No. 10 approximately center,
Cell No. 11 approximately middle,
Cell No. 12 approximately outer.

The results of the calculations are given in Table 2. 11 in terms of the ratios of thermal and epithermal values of ηf to those obtained for a cell in an infinite medium of like cells (design method). The results show that little or no error due to cell location in the core is involved in the present design method of cell homogenization.

Table 2. 11

DEPENDENCE OF HOMOGENIZED CONSTANTS ON FUEL-CELL POSITION WITHIN THE CORE

Position	Epithermal $[(\eta f)/(\eta f)_\infty]$	Thermal $[(\eta f)/(\eta f)_\infty]$
Center	1. 0003	1. 0014
Middle	1. 0009	1. 0018
Outer	1. 0009	1. 0000

As a final check on the homogenization techniques, the detailed manganese activations for both the standard and lumped cores were obtained with 15-region DSN calculations, using iterated, crystalline-kernel cross sections and the 22-energy-group structure in use in the EBOR design. A comparison of the calculated and experimental results is given in Fig. 2. 9. In both cores, 60% to 70% of the manganese activity was caused by neutrons above 167 ev; therefore, resonance self-shielding corrections may be necessary. These corrections are now being calculated and, if significant, will lead to better agreement than that indicated in Fig. 2. 9.

Methods of Calculating Gross Core Reactivity

The method used in the EBOR design studies to compute core reactivities incorporates 2DXY computations utilizing 12 energy groups--6 epithermal and 6 thermal. Since 2DXY performs the calculation with P-0 transfer only, a comparison was made with DSN between eigenvalues obtained with P-0 and P-1 transfer. In addition, the effects of using a crystalline kernel for BeO and of changing the number of thermal and epithermal groups were determined.

Eigenvalues were computed for the various cases listed, using the geometry and composition of the standard core. The change in reactivity in each case from that obtained from the standard design method (crystalline kernel, 12 groups, P-0 transfer) is listed in Table 2. 12.

Table 2. 12

COMPARISON OF VARIOUS CALCULATIONAL METHODS FOR GROSS CORE REACTIVITY

Case	Other Features	Reactivity Change (% δk/k)
Gas kernel	12 groups, P-0 transfer	+0. 41
P-1 transfer	12 groups, crystalline kernel	+0. 34
10 thermal groups	6 epithermal groups, crystalline kernel	+0. 18
18 thermal groups	6 epithermal groups, crystalline kernel	+0. 01
12 epithermal groups	6 thermal groups, crystalline kernel	Not completed

It can be seen from these results that none of the factors are of much importance. A change in the number of epithermal groups is not expected to be of major importance, but computations are in progress to check this effect. On the basis of present information, however, it appears that criticality calculations on the critical assembly performed with 12-group, 2DXY computations should be adjusted by +0. 34% from P-1 transfer and +0. 22% from the change in the high-energy data for aluminum. The net result would be +0. 56% in the calculated eigenvalue for the critical assembly. This adjustment has been incorporated into all of the following calculations on core reactivity values.

Core Reactivity Values

Seven of the standard-core experiments have been calculated with the methods in use in the EBOR design. Macroscopic homogenized constants were derived from GAM and GATHER, using self-shielding factors from 22-group iterated DSN problems. The beryllium oxide crystalline kernel was incorporated in the thermal-group calculations, and the standard 12-energy-group structure was used. All problems were run with 2DXY (converged to 10^{-5}) and control rods, when present, were represented explicitly in the calculation. The axial leakage was entered as group-dependent leakage in each problem. The experimental, calculated, and adjusted values of k_{eff} are listed in Table 2. 13.

Table 2. 13

COMPARISON OF CALCULATED AND EXPERIMENTAL VALUES OF CORE REACTIVITIES

Conditions	Experimental k_{eff}	Calculated k_{eff}	Adjusted k_{eff}
Clean standard core	1.0300	1.0535	1.059
Void (Fig. 5)			
1.090 in.	1.0103	1.0390	1.024
0.435 in.	1.0266	1.0487	1.054
Void filled with BeO	1.0223	1.0422	1.049
Dy_2O_3 rod at center	1.0464	1.0523	1.058
Boron-stainless steel rod at center	1.0510	1.0633	1.069
Boral rod at center	1.0616	1.0592	1.065

It is seen from these results that the adjusted k_{eff}'s differ by as much as 3% from the experimental values, with the unrodded cores yielding the largest difference. The reason for such a discrepancy is difficult to pinpoint. First, it is difficult to imagine a single block of fundamental data that could yield such a large difference and, in general, all of the errors in the fundamental data would appear to cancel in an over-all effect. Second, the analytical techniques are being put to severe tests in calculating the criticality--indeed, more severe in many cases than the corresponding EBOR calculations. However, investigations of the effects of (1) changing thermal-energy-group structure, (2) incorporating P-1 scattering as opposed to diffusion-theory-type approximations, (3) possible differences arising from space-energy problems in cell homogenization as a function of position, and (4) incorporating an assumed crystalline-kernel effect do not clarify the discrepancies; all except the last are elaborations of our present techniques. Experimental and analytical work is continuing. Increasing the number of high-energy groups in the calculations has given some indication of decreasing the calculated k_{eff}'s. These calculations are only preliminary.

Methods Development

Minor modifications were made in the $(SFD)^2$ and COMBO codes mentioned in the last quarterly progress report.[2]

The $(SFD)^2$ code, which computes self-shielding factors for use in the GAM and GATHER codes on the basis of the results of DSN cell calculations, was changed to permit the use of fluxes punched from the DSN code in binary form as direct input, thus avoiding the necessity of transcription of printed output from the DSN calculations. Utilization of these

fluxes required the addition of the cell radii to the input for $(SFD)^2$, and the code was made to read the same radii input used for the DSN calculations. Other modifications were added to reduce the amount of input required for consecutive problems having the same group structure, number of materials, geometrical configurations, and radii, and differing only in concentrations and fluxes.

The COMBO code and its associated versions of the GAM and GATHER codes were modified to make the code compatible with a standard IBM FORTRAN system, to reduce the number of records written on tape in GAM and GATHER, and to include an identification scheme appearing in columns 73 to 80 on the punched cards from the COMBO code.

Minor compatibility modifications were made in all of the codes used in the analytical program associated with the EBOR to adjust to the operation of the new IBM-7090, which is now in operation at General Atomic. It now appears that the analytical techniques used for the static analysis of the EBOR nuclear design are adequate and that further major work in this area will not be necessary.

EBOR Nuclear Analysis

Temperature-coefficient Studies

Temperature coefficients of reactivity have been obtained at room temperature, operating temperature, and a maximum temperature of 2000°F. A basic change in the method of defining the coefficients was incorporated in the analysis. Rather than attempt to describe the various components of the temperature coefficient in terms of differential variations with temperature of simple four-factor-type formulas, it was decided that for such a heterogeneous, epithermal, reflector-moderator system as the EBOR it would be better to describe the coefficients in terms of the total reactivity change associated with successive temperature increments in various physical components of the core. This method is certainly a more realistic and practical method, since definite time delays are involved in the temperature variation in various components following a power variation associated with a reactivity change. In terms of this method of analysis, the components of the temperature coefficient are defined as follows:

1. Prompt coefficient. This coefficient is associated with a temperature variation of the fuel-bearing region only. Doppler broadening of the U^{238} and U^{235} resonances and a thermal base effect, caused by the temperature change of that fraction of the beryllium oxide moderator that is mixed as a diluent with the fuel, are the factors that are incorporated when determining this coefficient.
2. Core-delayed coefficient. The subsequent temperature variation in the rest of the core moderator is the only effect incorporated

in this coefficient. Since the core is so epithermal, the thermal base effect that describes this coefficient is expected to be small.

3. Reflector-delayed coefficient. A possible temperature variation in the reflector following a power and temperature variation in the core will be significantly delayed and is the third component in the temperature-coefficient analysis. The effect is again a thermal base effect and, since the reflector is large, the loss of absorption in the reflector when the temperature rises and the somewhat thermal spectrum becomes harder, results in an expected positive reflector-delayed coefficient.
4. Over-all temperature coefficient. The over-all coefficient, as defined by this method, is the sum of all three previously mentioned components and is the result of a uniform temperature variation (necessarily slow) in all parts of the core and reflector. The cold-to-hot reactivity swing is determined step by step by the over-all coefficient.

A summary of the results of these studies was prepared for the preliminary safeguards report for the EBOR. Tables 2.14 and 2.15 summarize the results for the 100 kg U^{235}, 60 kg U^{238}, and 90 kg U^{235}, 70 kg U^{238} loadings, respectively. The prompt coefficient is smaller than was previously indicated because a substantial number of fissions occur in U^{235} before the neutrons are slowed down to the U^{238} resonance-absorbing region. Thus, the U^{238} Doppler broadening coefficient is modified by a factor involving the competition between U^{235} and U^{238} for resonance-energy neutrons. The core-delayed coefficient is negative but small, as anticipated; the reflector-delayed coefficient is positive, as anticipated. The prompt negative coefficient is the largest component at all temperatures investigated and is the overriding aspect of the over-all total coefficient. Doppler broadening of the U^{235} resonances has not been incorporated into the analysis at the present time. This effect is expected to be negative also and will therefore enhance the prompt negative coefficient. Preliminary investigations in this area are described later in this section.

Table 2.14

EBOR TEMPERATURE COEFFICIENTS
FOR 100 kg U^{235}, 60 kg U^{238} LOADING

Temperature		Temperature Coefficient ($\delta k/k \times 10^5/^\circ C$)			
$^\circ K$	$^\circ F$	Prompt	Prompt and Core-delayed	Reflector-delayed	Total
300	81	-2.3	-2.6	+0.8	-1.8
980	1300	-1.2	-1.4	+0.2	-1.2
136.7	2000	-1.0	-1.7	+0.1	-1.6

Table 2. 15

EBOR TEMPERATURE COEFFICIENTS
FOR 90 kg U^{235}, 70 kg U^{238} LOADING

Temperature		Temperature Coefficient ($\delta k/k \times 10^5/^oC$)			
^oK	^oF	Prompt	Prompt and Core-delayed	Reflector-delayed	Total
300	81	-2.5	-2.9	+1.0	-1.9
980	1300	-1.4	-1.7	+0.3	-1.4

The temperature coefficients were calculated by computing the reactivity at ±50°C temperature changes on the hot and cold design temperatures, taking into account self-shielding and spectrum changes. The coefficient was then calculated by taking $\delta k/k$ for any two temperatures of interest and dividing by the temperature difference. The final calculation of reactivity was done with the GAZE code, in which the core is treated as an infinitely long cylinder. No changes in axial leakage were taken into account, and the control rods were not included; the effect of the former is certainly small and the effect of the latter has yet to be investigated. The effect of assuming cylindrical geometry was checked by computing the 980°K temperature coefficient for the 100 kg U^{235} and 60 kg U^{238} loading, using the 2DXY code, which is a two-dimensional XY-geometry code. The temperature coefficients thus obtained were essentially the same as those obtained with the simpler cylindrical approximation.

The 300°K coefficients were determined, using the crystalline-model scattering kernel for beryllium oxide thermalization. The comparison between these results and the results obtained with the free-gas-model kernel is given in Table 2. 16. The difference between the two methods shows up mainly in the reflector-delayed effect. The somewhat more epithermal reflector spectrum, as calculated with a crystalline kernel for beryllium oxide, displays a smaller temperature variation.

These results are all calculated on the basis of temperature-produced changes in the nuclear characteristics of the core, and the thermal expansion of the core elements. The expansion of the lower grid plate would influence reactivity, since it defines the voids between fuel elements and in the rod channels. However, it is upstream of the core and its temperature change would be a very much delayed effect. Therefore, it is not included but is treated separately as a bulk coefficient. The magnitude of the bulk coefficient between 300°K and 980°K has been estimated to be -1.0×10^5 $\delta k/k\ ^oC$.

Table 2. 16

COMPARISON OF TEMPERATURE COEFFICIENTS OBTAINED WITH FREE-GAS AND CRYSTALLINE KERNELS AT 300°K

	Temperature Coefficient ($\delta k/k \times 10^5/°C$)	
	Free Gas	Crystal
Prompt	-2. 3	-2. 3
Prompt and core-delayed	-3. 0	-2. 6
Reflector-delayed	+1. 6	+0. 8
Total	-1. 4	-1. 8

An investigation was started on the effect on the prompt temperature coefficient of Doppler broadening of resonances in U^{235}. Resonance-integral calculations using the Adler-Nordheim-Hinman techniques were normalized to the proper infinitely dilute values at room temperature by the addition (or subtraction) of background cross sections in the appropriate energy groups in the GAM code. GAM calculations were then run at various temperatures with a homogeneous medium having the EBOR cell compositions, with the appropriate scattering cross sections per U^{235} atom, with the mean chord length, and with the lumped nuclei density. The U^{235} loading was 100 kg and the U^{238} loading was 60 kg. The results from the GAM code are described in terms of the quantity ηf over the energy range 1. 44 to 10^7 ev and are shown in Table 2. 17.

Table 2. 17

U^{235} RESONANCE-INTEGRAL STUDY

Temperature (°K)		ηf
U^{235}	U^{238}	1. 44 to 10^7 ev
300	300	1. 3337
300	350	1. 3312
350	350	1. 3302
980	980	1. 3024
980	1033	1. 3013
1033	1033	1. 3010

These results imply that, for the self-shielded configuration in EBOR,

the contribution to the prompt temperature coefficient of Doppler broadening of the U^{235} resonances is negative at both room temperature and operating temperature. This investigation is being continued in an attempt to estimate the magnitude of the U^{235} Doppler-broadening effect by means of more detailed multigroup calculations with the DSN and GAZE codes.

Control-rod Worth

The control-rod worths were evaluated at both room temperature and operating temperature for the clean EBOR at the beginning of life. The loading considered was 90 kg U^{235} and 70 kg U^{238}. In every case, discrete rod cross sections in 12 groups were used as input to 2DXY problems converged to 1×10^{-5}. The rod worths and the values of reactivity under the conditions investigated are given in Table 2. 18. The axial leakage was not taken into account in any of these problems.

Table 2. 18

CONTROL-ROD WORTH IN THE EBOR FOR 90 kg U^{235}, 70 kg U^{238} LOADING

Core Description	Temp. (^{o}K)	k_{eff}	Rod Worth
Unrodded	980	1. 1206	0.267
Rodded	980	0. 8625	
Unrodded	300	1. 1329	0.266
Rodded	300	0. 8712	

Power Distributions

Relative fuel-element power normalized to the average over an XY plane is shown in Fig. 2. 10 for the unrodded and the rodded cores. The radial peak-to-average power is 1. 143 in the unrodded portion of the core under hot-operating conditions.

Calculations now in progress will yield the rod worth versus insertion curve and axial power distribution. Rodded and unrodded core cross sections, homogenized over a transverse plane from the pertinent 2DXY output, will be fed into a series of axial GAZE problems in which the effect of the reflector is accounted for by adding appropriate core leakage cross sections in all twelve groups to the core absorption cross sections in the same groups. The two-dimensional GAMBLE code will be used to check the most important cases.

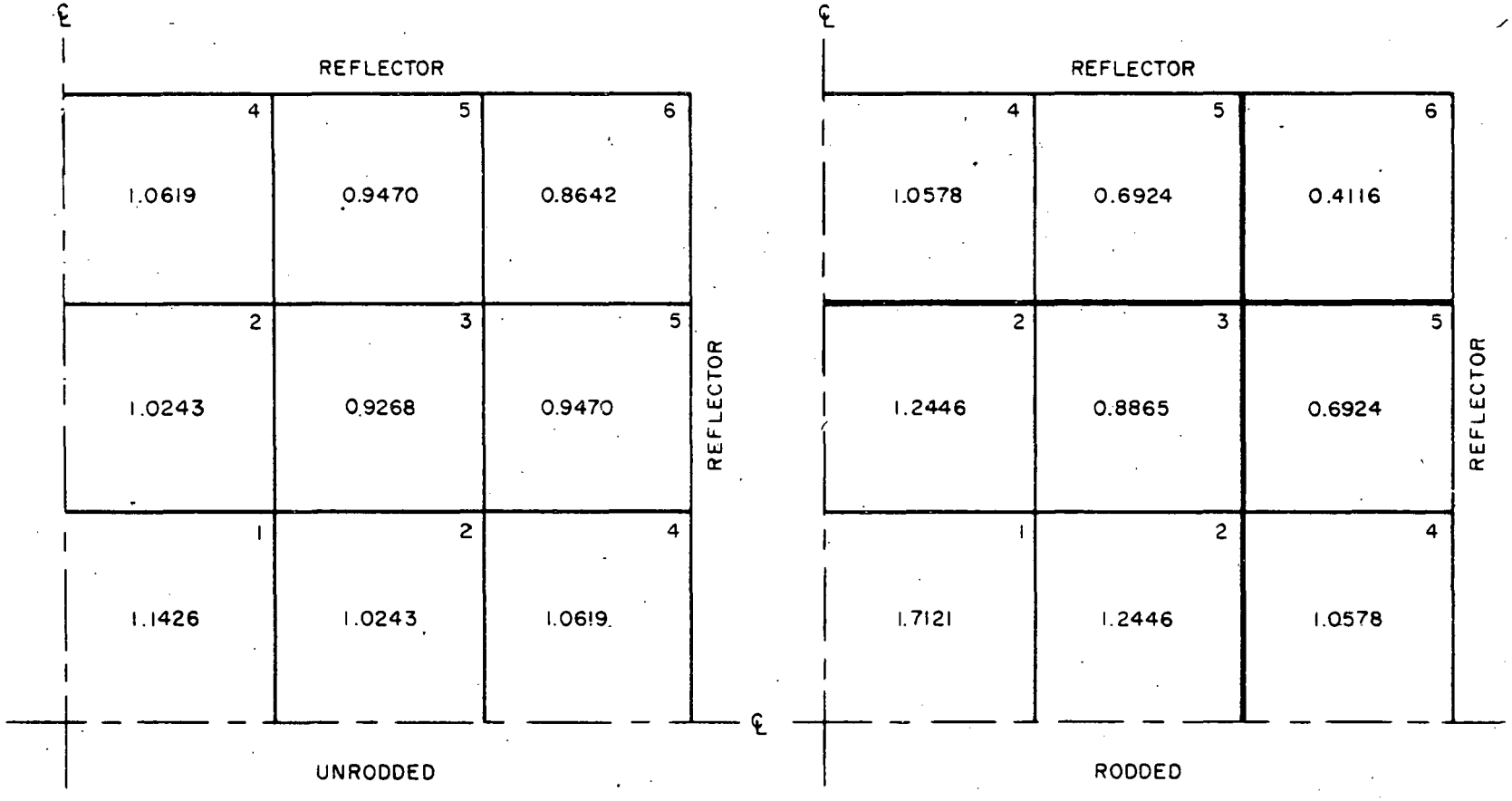

Fig. 2.10--Radial power distributions in the clean EBOR at beginning of life at 980°K, with loading of 90 kg U^{235} and 70 kg U^{238} (normalized to average over XY plane)

Analysis of a Livermore BeO Critical Experiment

A report has been published[6] containing the results of calculations of the reactivity of a bare, clean critical experiment with a BeO:U ratio of 247 performed at Livermore.[7] These calculations followed the same lines and used the same data as those for the EBOR, in order to put the methods and data to a preliminary test. Before starting the calculations, it was realized that such a test would by no means be conclusive, since there are several features of the EBOR which are not contained in such a simple system. Nevertheless, agreement with the experiment would provide some measure of confidence in the beryllium oxide and U^{235} cross-section data, although uncertainties in leakage would reduce the effectiveness of this test. Table 2.9 in the last quarterly progress report[2] compares the parameters of the experiment with those of the EBOR. In addition to the test of the data, the experiment provided a convenient place to determine the effects of certain variations in the calculational methods. These variations were as follows:

1. Use of crystalline-model and gas-model kernels.
2. The effect of leakage on the spectrum used to obtain constants.
3. Different methods of obtaining the XY-leakage constants.
4. Replacement of diffusion theory by P-1 transport theory.
5. Comparison of P-0 and P-1 transport theory.
6. Use of $\sum_T$ instead of $\sum_{TR}$ in P-0 transport theory.

The detailed results of and conclusions drawn from the above calculations are given in the preliminary EBOR safeguards report.

The results of the reactivity calculations are summarized in Table 2.19. The XY leakage in each case is obtained by a 2DXY calculation and the reactivity calculation is determined by a one-dimensional calculation of the type indicated in Table 2.19. The results indicate good agreement with the experiment, in that a discrepancy in the k_{eff} of only 2% means that the critical height is inaccurate by only 0.5 in. out of 20.2 in. One might expect, from looking at the results, that had the XY calculation been a P-1 rather than a P-0, the P-1 calculation would have been even closer. A neutron balance for the P-1 calculation appears in Table 2.20.

Table 2.19

SUMMARY OF CALCULATIONS OF LIVERMORE CRITICAL EXPERIMENT

Method	k_{eff}
Diffusion theory (GAZE)	0.979
P-0 transport theory (DSN)	0.981
P-1 transport theory (DSN)	0.985

Table 2.20

NEUTRON BALANCE--LIVERMORE CRITICAL EXPERIMENT
(DSN P-1 Calculation with 2DXY Transverse Leakages)

Group	Energy (ev)	Flux	Absorption	Fission	XY Leakage	Z Leakage	Total Leakage
1	10^7 to 1.35×10^6	8.688	-0.040843	0.0033032	0.050036	0.032638	0.082674
2	1.35×10^6 to 1.83×10^5	16.616	0.0069436	0.0062061	0.056925	0.038111	0.095036
3	1.83×10^5 to 3.36×10^3	27.157	0.026614	0.021564	0.076257	0.052934	0.12919
4	3.36×10^3 to 167.0	16.293	0.076969	0.052001	0.044154	0.030768	0.074922
5	167.0 to 17.6	8.851	0.15737	0.09591	0.023356	0.016209	0.039565
6	17.6 to 2.38	4.816	0.091922	0.049326	0.012597	0.0087858	0.021383
7	2.38 to 1.44	1.017	0.0056375	0.0043877	0.0026962	0.0018818	0.004567
8	1.44 to 0.414	2.316	0.04609	0.038228	0.0060598	0.0042099	0.01027
9	0.414 to 0.16	1.436	0.069001	0.056188	0.0036322	0.0023808	0.006013
10	0.16 to 0.04	1.114	0.074633	0.063149	0.0026942	0.0018257	0.0045199
11	0.04 to 0.01	0.14	0.01523	0.012902	0.0003187	0.00021682	0.00053552
12	0.01 to 0	0.01067	0.0016305	0.001374	0.00002728	0.00001858	0.00004586
Total			0.5312	0.40454	0.27875	0.18998	0.46873

Evaluation of Crystalline Kernel Effect

The effect on reactivity of changing from the scattering kernel associated with the gas model of the BeO moderator to the more accurate crystalline kernel was evaluated for the EBOR at 300°K with a loading of 100 kg U^{235} and 60 kg U^{238}. The DSN problems, which were run for cell cross section homogenization, and the GAZE problems, which supplied the values of reactivity, were converged to 10^{-5} in all cases. The comparison was made in the cylindrical S-4 and S-8 approximations. The results are shown in Table 2.21. It will be seen that, because of the epithermal nature of the core spectrum, the gas model is a very good approximation even at room temperature.

Table 2.21

COMPARISON OF CRYSTALLINE AND FREE-GAS SCATTERING KERNELS

Kernel	S_n Approximation	k_{eff}
Gas	4	1.1821
	8	1.1831
Crystal	4	1.1809
	8	1.1844

Fuel-element Manufacture, Storage, and Transfer Criticality Problems

Calculations were made to determine safe geometries and batch sizes for the manufacture, storage, and transfer of EBOR fuel elements The problems involved in avoiding a criticality accident are as follows:

1. Limitation of the UO_2 batch size during manufacture of the fuel pellets.
2. Storage of the manufactured fuel pellets prior to insertion in the fuel element.
3. Storage and shipping of the manufactured fuel elements in "bird-cages."

During pellet manufacture, the UO_2 is washed in water as one of the steps to obtain a uniform grain size. Under such conditions, a critical mass is formed with 1100 g of U^{235} in oxide form with a $H:U^{235}$ ratio of 400 in a spherical geometry surrounded by an infinite water reflector. The batch size is most conveniently set in multiples of 300 g of U^{235}, since the UO_2 is received in batches of this size. Therefore, the batch size for pellet manufacture is limited to 300 g of U^{235} to allow for double batching errors.

It was proposed to store the manufactured fuel pellets on 10 in. by 10 in. by 1 in. polystyrene foam "cards," which would be wrapped and sealed in a clear plastic, such as polyvinyl chloride. Polystyrene foam, although a hydrocarbon, has a density of only 0.03 g/cm^3, so that the mass of hydrogen present as a moderator is very small. By storing 180 pellets in each card, it would be possible to store enough fuel for 44 fuel elements in any configuration without reaching a criticality situation, provided that (1) water does not get in between the cards, (2) the polystyrene does not soak up water, and (3) the polystyrene maintains its low density and foamlike structure. If these conditions cannot be met, the cards could be arranged on a flat horizontal surface (such as the floor) in layers, with the restriction that the total height of the fuel pins must be 1-1/2 in. or less; this means a maximum of three layers on cards 1/2 in. thick. Some provision should also be made to tie down the cards to ensure the stability of the planar array. These recommendations are based on the data contained in TID-7016.[8]

Fuel elements are contained in metal boxes lined with a low-density packing material to prevent damage during handling. The fuel-element boxes are stored and shipped in "bird-cages," which are metal frames designed to maintain a specified distance between the fuel elements. Calculations have shown that it is possible to pack two fuel elements in each box by allowing up to 1/2 in. of packing material around each element. However, it was felt that unless it was more advantageous to store two element boxes in one bird-cage, the elements should be stored separately. The spacing of fuel-element boxes should be maintained at a minimum of 12 in. and the bird-cages could be stacked horizontally up to three layers high.

These recommendations are based on multigroup one-dimensional calculations with constants derived from GAM and GATHER. No self-shielding effects were taken into account, as the configurations were all assumed to be completely homogenized. No credit was taken for neutron absorption in U^{238}, which varies from about 5% to 20% of the total source neutrons, depending on the lumping. The geometry was assumed to be spherical with an infinite water reflector, except in calculations of the fuel-element transfer and storage, where the geometry was either an infinite cylinder or slab. The basic rule in avoiding criticality was that in any configuration the mass of U^{235} present should be less than 75% of that needed to attain criticality, allowing for double batching, unless the configuration was shown to always be safe. The calculation was made with the optimum amount of water present intimately mixed with the fuel.

Shielding and Heat Generation

As the EBOR enters into the final stages of nuclear and mechanical design, a more comprehensive examination of heat generation and shielding

data becomes possible. A series of calculations using the latest design and composition data available has been initiated. Results will be incorporated into the final heat generation and shielding reports for the EBOR and will serve to confirm, modify, and expand the existing data.

Calculations were made for the purpose of establishing a possible level of contamination for a fuel-handling cask during transfer of a ruptured fuel element. Table 2.22 summarizes the results for fission products which are either gaseous or which may be volatile in the vicinity of operating temperatures. Activity was based on equilibrium conditions for an average fuel pin, except for the long-lived isotopes, for which a 600-day build-up was assumed.

Table 2.22

FISSION-PRODUCT ACTIVITY IN A SINGLE EBOR FUEL PIN

Isotope	Activity (curies/pin)		Temp. to Vaporize at Atm Pressure (^{o}K)
	10 Hr After Shutdown	3 Days After Shutdown	
Xe^{131m}	4.37	4.30	Gaseous at room temperature
Xe^{133m}	19.33	11.81	
Xe^{133}	816.24	653.35	
Xe^{135m}	122.62	0.22	
Xe^{135}	631.87	11.06	
Total Xe	1594.43	680.74	
Kr^{83m}	11.64		Gaseous at room temperature
Kr^{85m}	35.98		
Kr^{85}	3.87	3.87	
Kr^{87}	1.61		
Kr^{88}	36.16		
Total Kr	89.26	3.87	
I^{131}	426.02	304.30	430
I^{132}	544.16	311.46	
I^{133}	610.39	7.79	
I^{134}	15.84		
I^{135}	268.50	0.43	
Total I	1864.91	623.98	
Cs^{136}	8.07	7.02	900
Cs^{137}	25.96	25.96	
Total Cs	34.03	32.98	
Rb^{88}	40.45		865

Table 2.22--continued

Isotope	Activity (curies/pin) 10 Hr After Shutdown	Activity (curies/pin) 3 Days After Shutdown	Temp. to Vaporize at Atm Pressure (^{o}K)
Ba^{137m}	23.81	23.81	1667
Ba^{139}	6.50		
Ba^{140}	785.81	681.99	
Total Ba	816.12	705.80	
Sr^{89}	579.96	560.27	3000
Sr^{90}	29.36	29.36	
Sr^{91}	354.42	4.19	
Sr^{92}	581.75		
Total Sr	1545.49	593.82	
Mo^{99}	741.21	375.90	1320
Te^{125m}	0.16	0.16	1250
Te^{127m}	7.48	7.41	
Te^{127}	28.64	26.31	
Te^{129m}	46.36	43.86	
Te^{129}	46.36	43.86	
Te^{131m}	6.61		
Te^{131}	7.64		
Te^{132}	528.05	300.72	
Te^{133m}	0.81		
Te^{133}	0.82		
Te^{134}	0.07		
Total Te	673.00	422.32	
TOTAL ACTIVITY (gaseous plus volatile)	7398.88	3439.38	

Flux Depression and Spectrum Data for the MGCR-2 Capsules

The MGCR-2-type capsules containing beryllium oxide plus various additives are being irradiated in the central E-5 position of the GETR. As part of an auxiliary effort to establish the magnitude of the flux-time irradiation for the capsule and some of the neutron physics properties of the irradiation, spectrum and flux depression calculations were performed. Our standard techniques of spectra determinations by means of the GAM and GATHER codes and the depression calculations by means of the multigroup-transport-theory DSN code were used.

Figures 2.11, 2.12, and 2.13 respectively, show as 22-group histograms the calculated central unperturbed GETR group flux spectrum, the perturbed spectrum in the GETR during capsule irradiation in the region immediately adjacent to the capsule, and the average group flux spectrum in the BeO capsule during irradiation. Figure 2.14 shows the unperturbed high-energy GETR spectrum in sufficient detail for the future calculation of activation data. The only normalization in the spectrum calculations has been to the integrated fast unperturbed flux in the energy range 0.18 Mev $\geq E \geq$ 10 Mev, where the value of 3.41×10^{13} neutrons/cm^2-sec has been used as the basis for all other fluxes. Table 2.23 is a summary of the flux depression factors for each of the 22 groups used in the DSN calculations.

Table 2.23

SUMMARY OF FLUX DEPRESSION FACTORS USED IN DSN CALCULATIONS

Group	Energy Limits (ev)	Ratio of Avg. to Unperturbed Flux
1	10^7 to 3.68×10^6	0.576
2	3.68×10^6 to 1.35×10^6	0.756
3	1.35×10^6 to 4.98×10^5	0.841
4	4.98×10^5 to 1.83×10^5	1.093
5	1.83×10^5 to 4.09×10^4	1.206
6	4.09×10^4 to 3.36×10^3	1.174
7	3.36×10^3 to 748.0	1.106
8	748.0 to 167.0	1.074
9	167.0 to 61.4	1.066
10	61.4 to 17.6	1.080
11	17.6 to 5.04	1.078
12	5.04 to 2.38	1.060
13	2.38 to 1.44	1.083
14	1.44 to 0.876	1.220
15	0.876 to 0.414	1.215
16	0.414 to 0.16	1.767
17	0.16 to 0.1	1.461
18	0.1 to 0.065	1.101
19	0.065 to 0.04	0.898
20	0.04 to 0.025	0.785
21	0.025 to 0.01	0.697
22	0.01 to 0.005	0.604

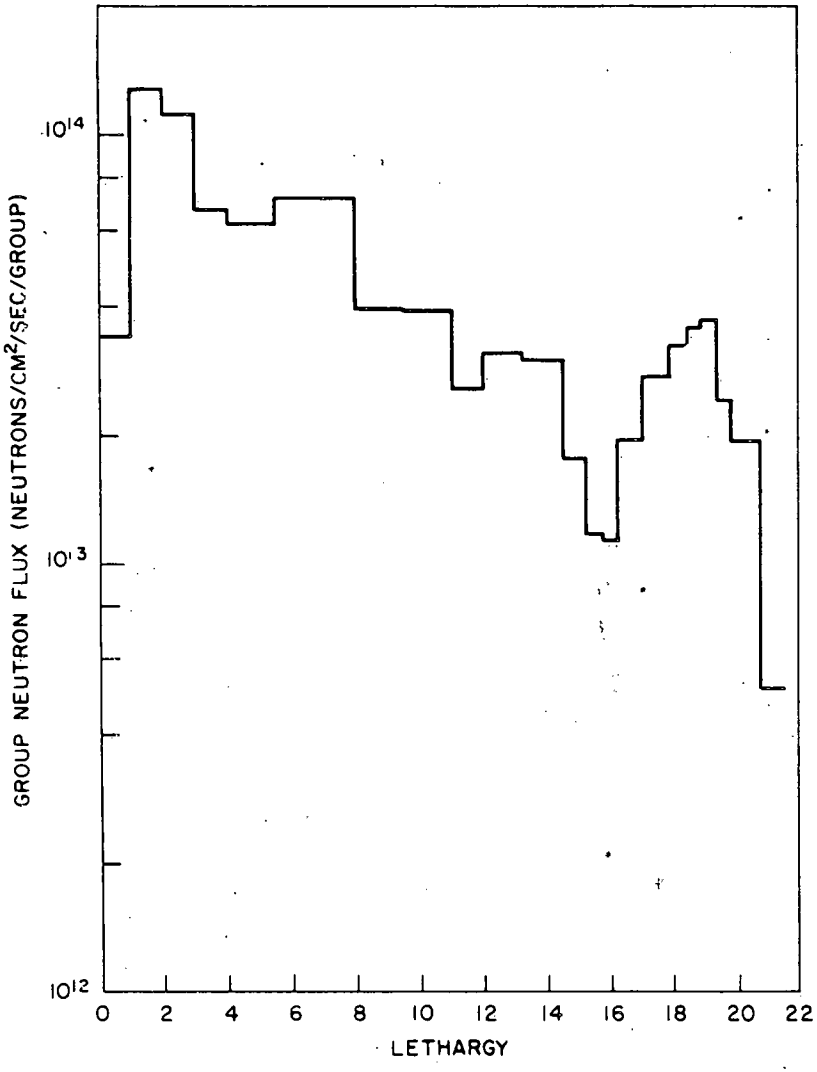

Fig. 2.11--GETR neutron flux unperturbed spectrum, central E-5 position, normalized to 3.41×10^{14} neutrons/cm^2-sec, with E > 0.18 Mev

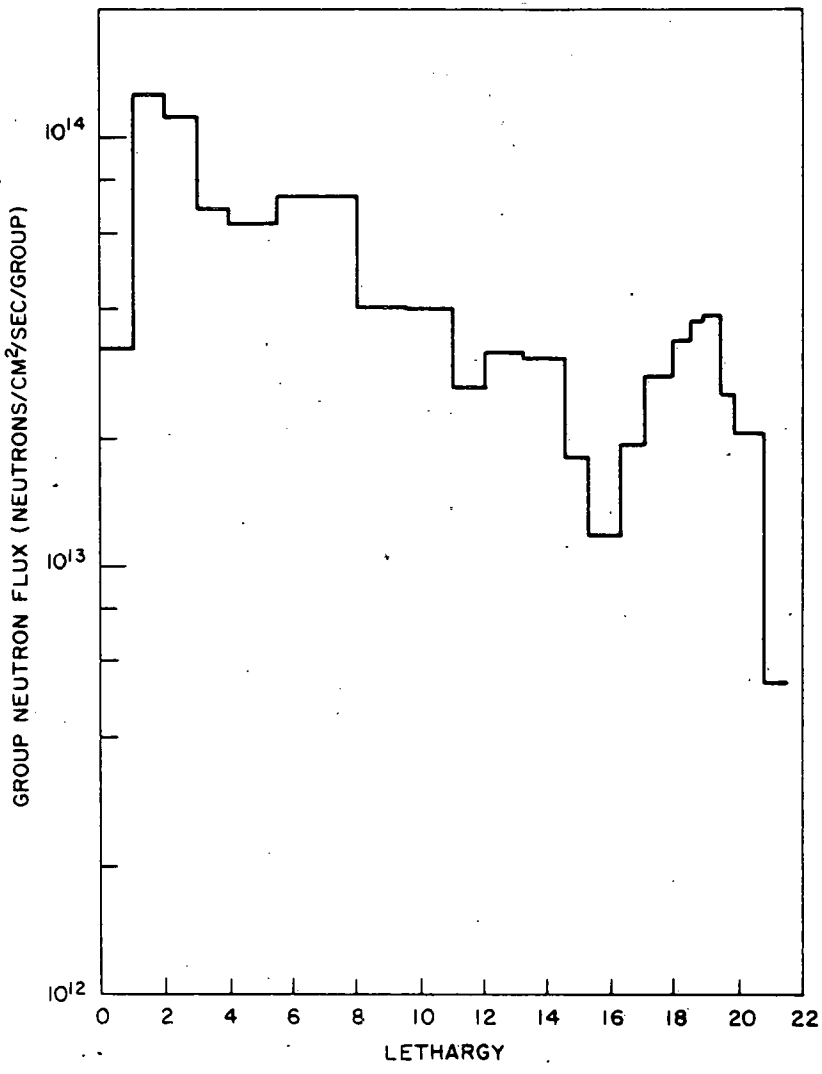

Fig. 2.12--GETR neutron flux perturbed spectrum in region adjacent to MGCR-2 capsule during irradiation

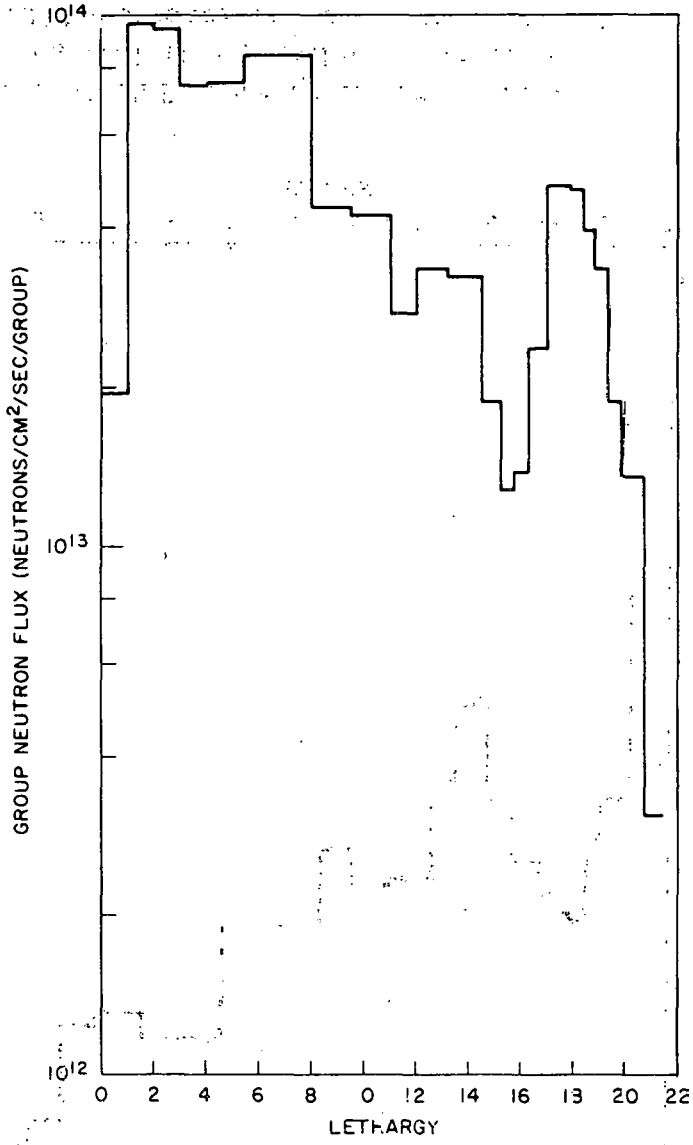

Fig. 2.13--Average neutron flux in MGCR-2 capsule during irradiation in position E-5 in GETR

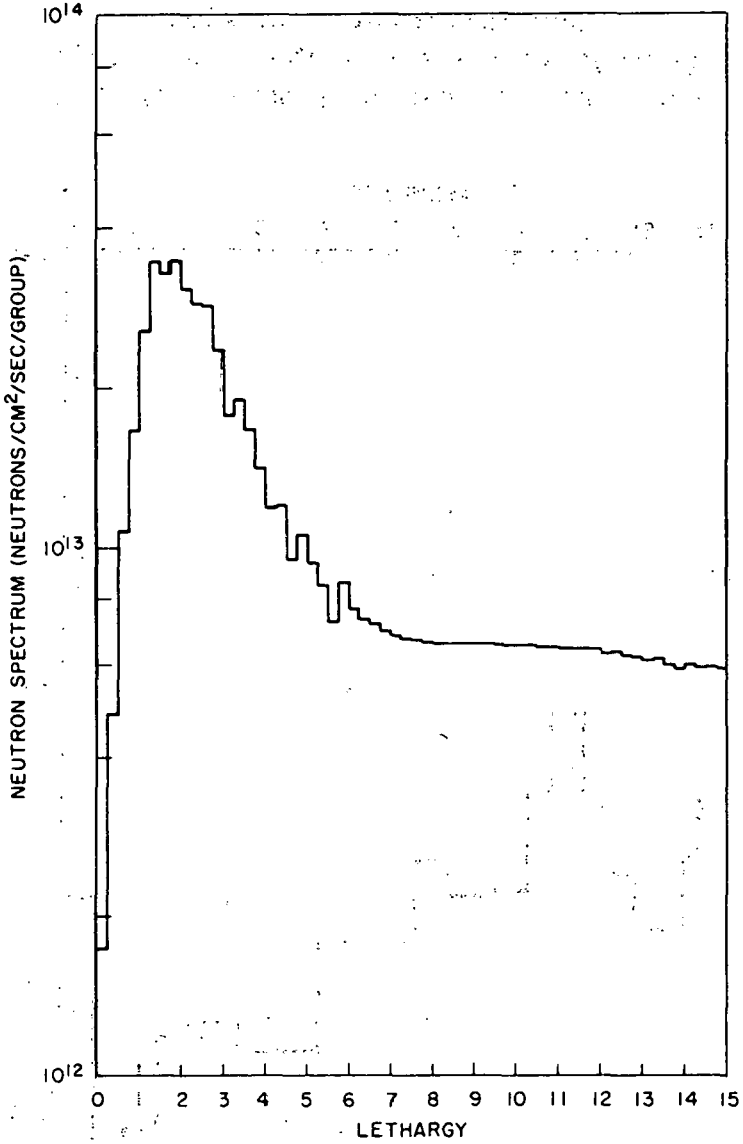

Fig. 2.14--GETR quarter lethargy group unperturbed spectrum in center region

Data for MGCR-7 and -8 Capsules in WTR

The MGCR-7 and MGCR-8 capsules will be identical and will be irradiated in a reflector position in the WTR near the core-reflector interface. Four different specimens of varying concentrations of Dy_2O_3–Al_2O_3 will be included in each capsule.

Calculations similar to those performed on the MGCR-2 capsule in the GETR were made to determine spectrum and flux depression data. Absolute magnitudes of neutron fluxes were obtained from normalization of Westinghouse flux data (>821 kev) at the core centerline. The compilation of the data for these capsules is presently under way. Most of the difficulties have now been overcome and the use of the techniques established for the EBOR nuclear design in capsule irradiation calculations appears to yield data which previously could not be obtained for these capsules.

REFERENCES

1. Quarterly Progress Report for the Period Ending September 30, 1961, General Atomic, Report GA-2568.
2. Quarterly Progress Report for the Period Ending December 31, 1961, General Atomic, Report GA-2847.
3. Wright, W. B., Supplement 3, Safeguards Report for the EBOR Critical Experiment, General Atomic, Report GA-1100, February 13, 1962.
4. Wright, W. B., The Homogenization of Heterogeneous Slab Lattices Containing BeO and Hydrogen, General Atomic, Report GAMD-2871, January, 1962.
5. Wright, W. B., Experiments and Analysis on Beryllium Oxide Moderated Cores Containing Hydrogen, General Atomic, Report GAMD-2873, January, 1962.
6. McWhirter, A. D., Analysis of a Livermore BeO Critical Experiment, General Atomic, Report GAMD-3008, March, 1962.
7. Kloverstrom, F. A., et al., Critical Measurements on Near-Homogeneous, BeO-Moderated, Oralloy-Fueled Systems, University of California Research Laboratory, Report UCRL-5369, Pt. 1, July, 1959; Nuclear Sci. and Eng., Vol. 8, 1960, p. 221.
8. Nuclear Safety Guide, TID-7016, Revision 1, 1961.

THIS PAGE

WAS INTENTIONALLY

LEFT BLANK

III. MATERIALS DEVELOPMENT
(D. E. Johnson)

FUEL-MATERIALS DEVELOPMENT (Task 04) (F. H. Lofftus, W. Morris)

Work on the development of BeO-coated BeO–UO_2 fuel compacts was resumed during the present quarter, following the completion of the fabrication of the BeO specimens for the MGCR-2 irradiation capsule. Previous efforts in this area during the past year were directed toward the application of impervious BeO coatings to BeO–UO_2 fuel compacts by slurry-spray or slurry-dip methods. The effort during the next quarter will be directed toward the application of impervious coatings by a direct compaction method using a steel die. It is anticipated that sufficient information will be available by the end of the next quarter to evaluate the relative merits of these three fabrication processes. At that time the process that appears to have the greatest potential for development into a production process will be selected for more intensive study.

MATERIALS FOR PROPULSION PLANT (Task 19)

Metallic-materials Development (W. L. Wyman, J. Wunderlich, R. Wallace, N. Baker)

The objective of this subtask is to develop methods for the prevention of self-welding of metal contact surfaces which are heated in the reactor coolant atmosphere. Before preventive action is suggested, the time–temperature–contact pressure relations that effect self-welding of various materials must be established. Materials of interest are as follows:

1. Carbon steel (SA-212B).
2. 1 Cr–1/2 Mo steel (SA-387B).
3. Ferritic stainless steel (Type 430).
4. Austenitic stainless steel (Type 304).
5. Inconel.
6. Hastelloy X.
7. Inconel X.
8. Colmonoy.
9. Flame-sprayed Hastelloy X (tungsten carbide and chromium carbide).

For experimental purposes, the lower limit of the interface pressure has been arbitrarily selected as 100 psi and the upper limit for the interface pressure has been selected as the stress required to produce 1% creep in

10,000 hr. All tests are being conducted in pure helium (less than 50 ppm impurity). Metallographic examination of diffusion boundaries will be made. A device was fabricated to measure the torsion required to separate the bonded specimens and the results that have been obtained to date are summarized in Table 3.1. These results show an almost linear relationship for the increase in the bonding of A-212 to A-212 with increasing temperature at a constant load of 100 psi. An increase of pressure from 100 psi to 500 psi at 1500°F caused welding of A-212 to Type 304 stainless steel and of Type 304 stainless steel to itself. Changing the test time from 100 hr to 500 hr at 100-psi contact pressure gave the same result.

Table 3.1

TORSION DATA FOR SPECIMENS FROM SELF-WELDING TESTS

	Exposure Conditions			Torque to Separate Self-welded Specimens (in.-lb)		
Test No.	Temp. (°F)	Time (hr)	Pressure (psi)	A-212 to A-212	A-212 to 18/8	18/8 to 18/8
1	1,800	100	100	108.6	5.0	52.2
2	1,500	100	100	48.6	Not welded	
3	1,200	100	100	7.2	Not welded	
4	1,800	100	50	19.8	91.2	10.8
5	1,200	100	1,200	84.6	Not welded	
6	1,500	500	100	64.6	124.5	43.2
7	1,500	100	500	187.8	195.0	13.5
8	800	1,000	34,000	In furnace		
9	1,200	10,000	1,200	In furnace		
	Exposure Conditions			Torque to Separate Self-welded Specimens (in.-lb)		
Test No.	Temp. (°F)	Time (hr)	Pressure (psi)	Inconel to Inconel	Inconel to 304	304 to 304
10	1,200	100	1,200	Welded (not tested)	Not welded	Not welded

Fission-product Plateout (L. Zumwalt, E. Anderson, D. Busch, J. Moses, W. Snow)

The objective of this subtask is to measure the plateout of selected fission-product isotopes from a simulated EBOR coolant stream. The resulting data will be used to evaluate the problems that are associated with (1) the failure of a fuel-pin cladding and (2) the use of vented fuel pins.

Three runs to test iodine plateout on AISI 304 stainless steel,

Mk 74-78

NSIC 2388

ASTM 387B low-alloy steel, and AISI 1030 carbon steel have been completed. Samples in the form of 0.5 in. by 1.75 in. plates were exposed in dry helium to a total of 2330 μg of I^{131} at a partial pressure of 1×10^{-6} atm for 65 hr. The samples were held in a quartz tube maintained at temperatures which decreased smoothly from 750° to 235°C (1380° to 455°F). The inlet helium carrier gas contained 100 ppm O_2, 370 ppm N_2, and 4 to 6 ppm H_2O. Helium flow over the samples was laminar (u = 1.62 ft/min at 750°C, N_{Re} = 64).

The logarithm of the plateout of iodine (or metal iodides formed) appears to be roughly inversely proportional to absolute temperature. The relationship is shown in Figs. 3.1, 3.2, and 3.3, and the test results are presented in Table 3.2. The "apparent Arrhenius activation energy" was obtained from the plot of log plateout versus 1/T. This quantity is of questionable physical significance but at least is a parameter indicating the magnitude of the temperature effect. Calculations of apparent activation energies and plateout concentrations indicate that the plateout mechanism may be somewhat independent of the type of steel used.

Table 3.2

PLATEOUT TEST RESULTS

Run	Material	Average Plateout* (μg I/cm^2)	AAAE† (kcal/mole I)
1	AISI 304 stainless steel	3.3	5.5
2	ASTM 387B low-alloy steel	4.2	6.2
3	AISI 1030 carbon steel	4.4	4.2
			Av. 5.3

*Over temperature range from 750° to 235°C.

†Apparent Arhhenius Activation Energy.

Before exposure to iodine, samples were degreased in a chlorinated solvent, dried, and exposed at temperature to the helium-carrier gas for 65 hr. Substantial oxidation and scaling occurred at temperatures above 500°C. Corrosion of Type 387B low-alloy steel appeared to be greater than that of Type 1030 carbon steel. Corrosion of both steels was greater than that of Type 304 stainless steel. Heat discoloration of the 304 stainless steel was observed above 500°C; oxidation and scale formation occurred at 750°C.

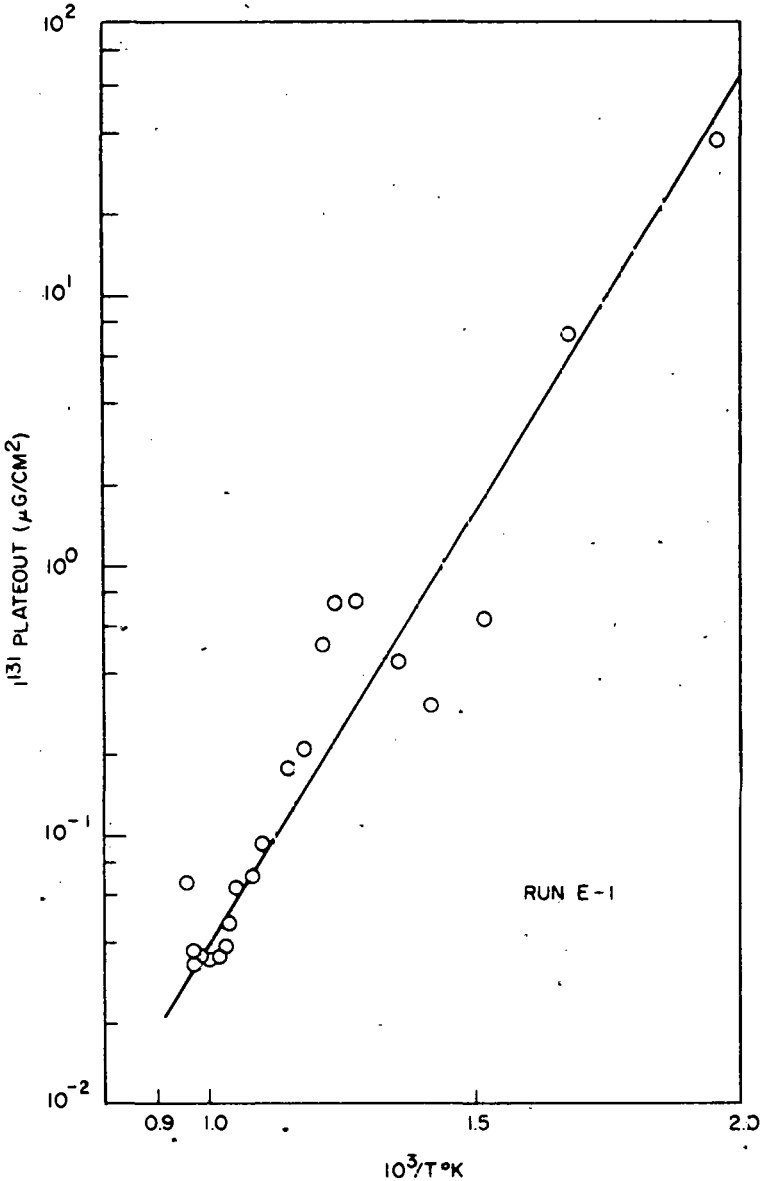

Fig. 3.1--Plateout of I^{131} on Type 304 stainless steel

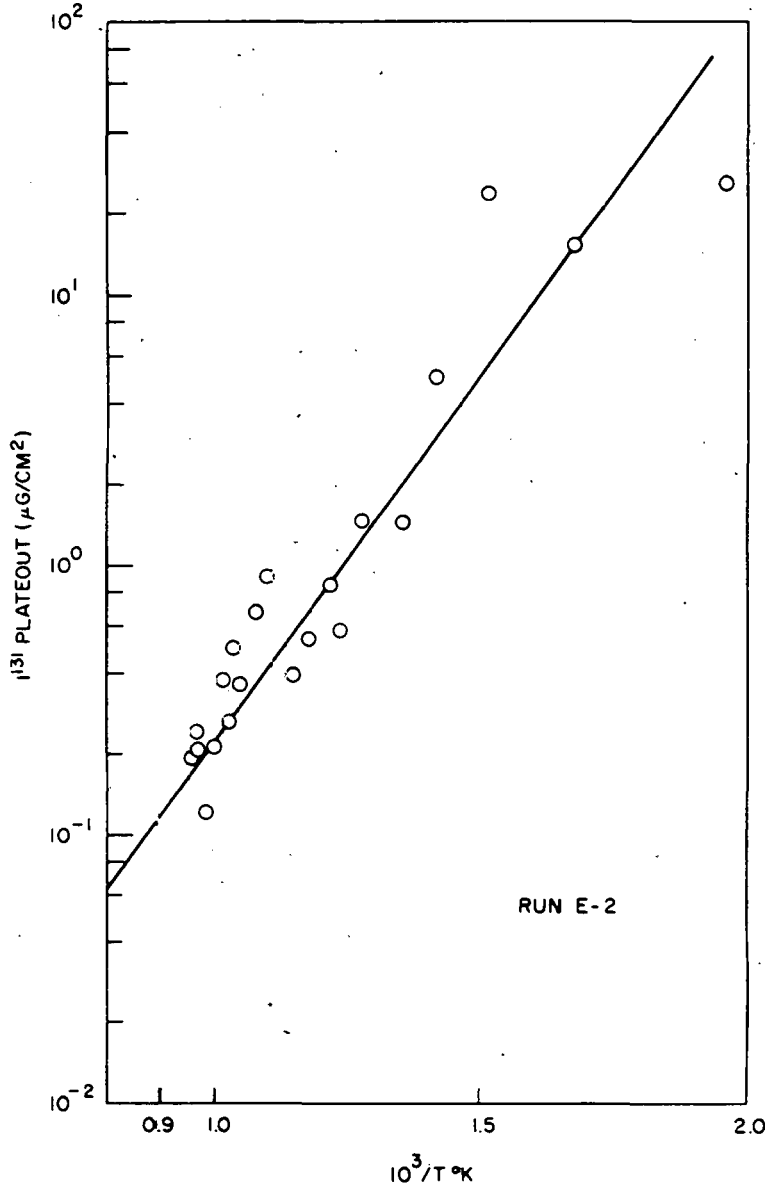

Fig. 3.2--Plateout of I^{131} on Type 387B steel

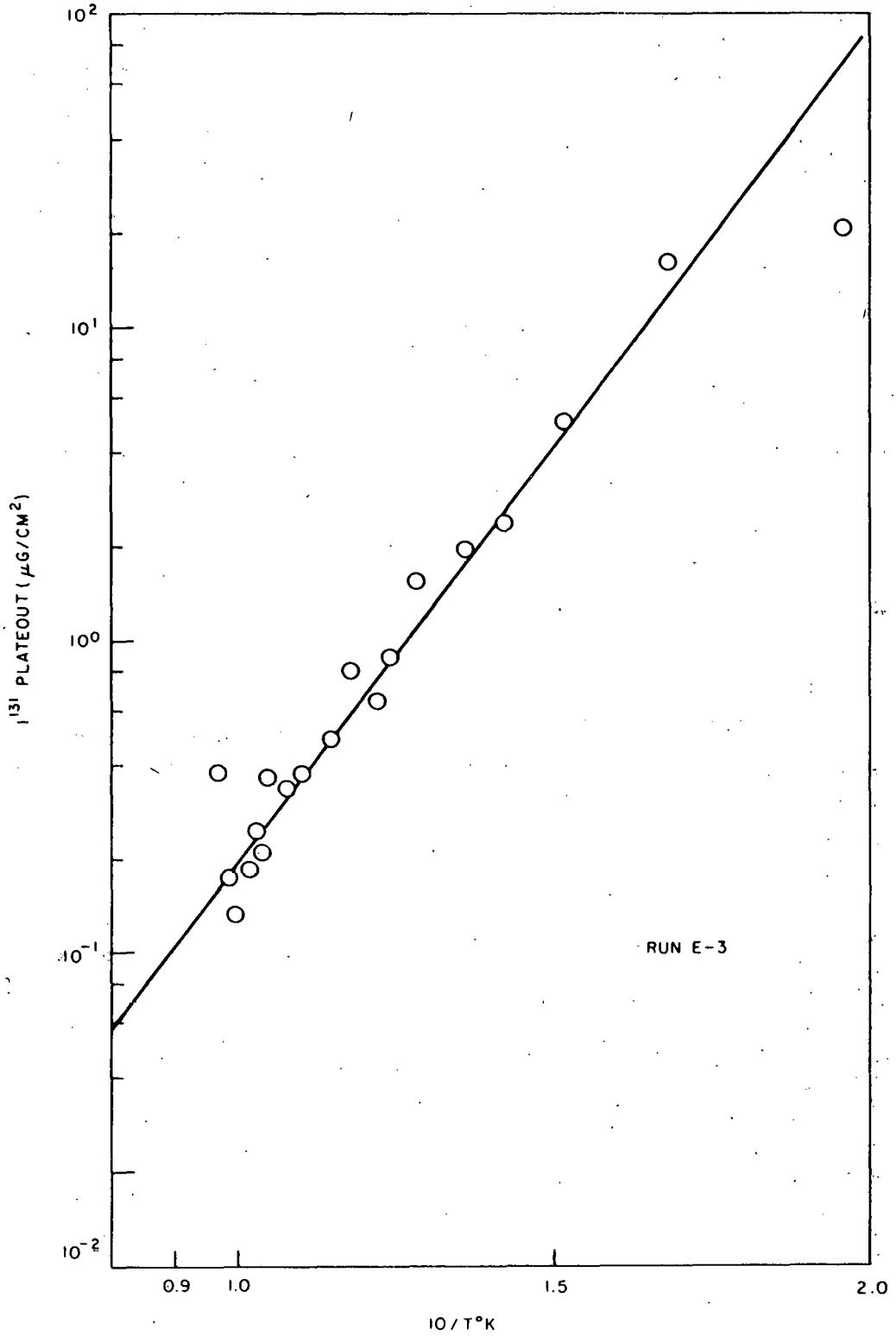

Fig. 3.3--Plateout of I^{131} on low carbon steel (Type 1030)

To study the corrosion reactions further, two gas chromatographs and a moisture monitor were used to measure O_2, N_2, CH_4, CO, CO_2, and H_2O inlet and exit concentrations during the sample-preparation stage for run E-3 before the introduction of iodine. The samples were Type 1030 carbon steel. After 48 hr of exposure at temperature (750°C to 235°C), the incoming oxygen was apparently reacting with the carbon in the steel to produce a corresponding amount of CO and CO_2. Prior to this "equilibrium" situation, the total amount of CO and CO_2 produced greatly exceeded that which could result from reaction with the incoming O_2. Carbon monoxide and carbon dioxide were formed when the maximum temperature exceeded 570°C. None of the incoming oxygen reacted at temperatures below 100°C. Inlet and exit O_2 concentration reactions occurred (or the CO and CO_2 were not released from the metal) between 250° and 570°C.

The inlet and exit nitrogen concentration remained at 260 ppm throughout the run. The inlet H_2O concentration appeared to be about 4 to 6 ppm. Up to 330 ppm of methane was detected in the exit gas during the first 1.3 hr of operation. A small amount of hydrogen was present in the exit gas during much of the run. Exposed samples have been submitted for metallographic analysis.

FUEL-MATERIALS IRRADIATIONS (Task 23) (D. E. Johnson, D. Guggisberg)

The objective of this task is to determine the performance capabilities of EBOR-type BeO—UO_2 fuel materials under conditions of high-temperature reactor irradiation.

MGCR-4 Capsule

The MGCR-4 fuel-irradiation capsule was designed for studying the effect of fuel particle size on the performance of the fuel pellets during reactor irradiation at temperatures and heat-flux conditions that are of interest for EBOR program applications. Fuel pellets for the capsule were fabricated at General Atomic and are composed of 30 vol-% UO_2 dispersed in BeO. The UO_2 is present in the form of fine (~10 μ in diameter) particles in some pellets, and in the form of coarse (~150 μ in diameter) particles in other pellets. The irradiation of the capsule began on June 16, 1961, and was uneventful during the present quarter. Nine of the original ten thermocouples are still functioning in a normal manner. A peak fuel-cladding surface temperature of approximately 1640°F is being maintained.

MGCR-BRR-9 Capsule

The MGCR-BRR-9 capsule was designed and fabricated at Battelle Memorial Institute under the terms of a subcontract; it is being irradiated

in the MTR. The capsule contains BeO–UO_2 fuel pellets that are identical to those being irradiated in the MGCR-4 capsule described above. The irradiation of this capsule began on November 9, 1961. Its operation since that date has been normal. A peak fuel-cladding surface temperature of approximately 1600°F is being maintained.

NONFUEL-MATERIALS DEVELOPMENT (Task 24)

BeO Irradiation (D. E. Johnson, F. H. Lofftus, D. Guggisberg, B. Czech)

The objective of this subtask is to measure the effect of irradiation on the behavior of BeO moderator ceramics during reactor irradiation.

The fabrication of the BeO specimens for the MGCR-2 capsule was completed at General Atomic during the quarter. The fabricated specimens are presently being ground to the required finished dimensions by an outside company.

An improved device for the measurement of the thermal diffusivity of the BeO specimens has been developed. The measurement of the thermal diffusivity of the specimens that will be used in the capsule and also of the control specimens is under way for the hot-pressed materials and for 15 cold-pressed and sintered specimens that have been procured from manufacturers.

Absorber Materials Irradiation (D. E. Johnson, B. Czech, J. Furth, B. Morris)

The objective of this subtask is to develop absorber materials for use in the EBOR-type reactor-control rods.

The fabrication of the MGCR-7 capsule for the irradiation of control-rod absorber materials was completed during the quarter. Specimens contained in the capsule are composed of alumina with 5, 27, 47, and 67 wt-% dysprosium oxide. The capsule will be shipped to the test reactor site when the approval of the AEC has been received.

Fuel-cladding Materials Development (W. L. Wyman, J. Wunderlich, W. Ellis)

The objective of this subtask is to develop the technology of using Hastelloy X as a fuel-cladding material for the EBOR type of reactor.

The EBOR is designed to use fuel pins composed of a Hastelloy X tube 0.375 in. in diameter and 0.020 in. in wall thickness creep-shrunk onto UO_2–BeO fuel pellets. In this application, the cladding is sized onto the pellets at high temperature and pressure in a gas autoclave. After the cladding has been creep-shrunk onto the pellets, the temperature in the

autoclave is reduced, with the result that a high residual stress is generated in the cladding because of the difference in the coefficients of thermal expansion for the fuel and cladding materials.

During the quarter, the residual stress in the fuel cladding that results from the above procedure was measured by strain-gauge techniques. This residual strain was found to be in the region of 950 to 1100 μ in./in. Using the standard stress–strain relationship, the stress corresponding to this strain was calculated to be approximately 28,600 psi. Since the relationship

$$S = E\alpha$$

is valid only if the proportional limit is not exceeded, it was necessary to determine a precise value for the proportional limit of the Hastelloy X. The results of the determination are presented in Fig. 3.4 and show that the material exhibits a proportional limit of 29,800 psi.

The value of 28,600 psi for the residual stress in creep-shrunk fuel cladding was obtained by applying strain gauges to the cladding and subsequently removing the cladding from around the strain gauge, thereby allowing relaxation. As a check on this method, a second set of specimens was tested using internal gas pressure to produce the strain in the cladding; strains were again measured with electrical-resistance strain gauges. The thin-wall pressure-vessel formula was used to compute the stress values for the cladding, and a value for the proportional limit of 27,000 psi was obtained. It is believed that this slightly lower value for the proportional limit may be the result of a low rate of load application in the internally pressurized specimens.

From the results of the experiments, it was concluded that the residual stress in the fuel-pin cladding is near the proportional limit for Hastelloy X.

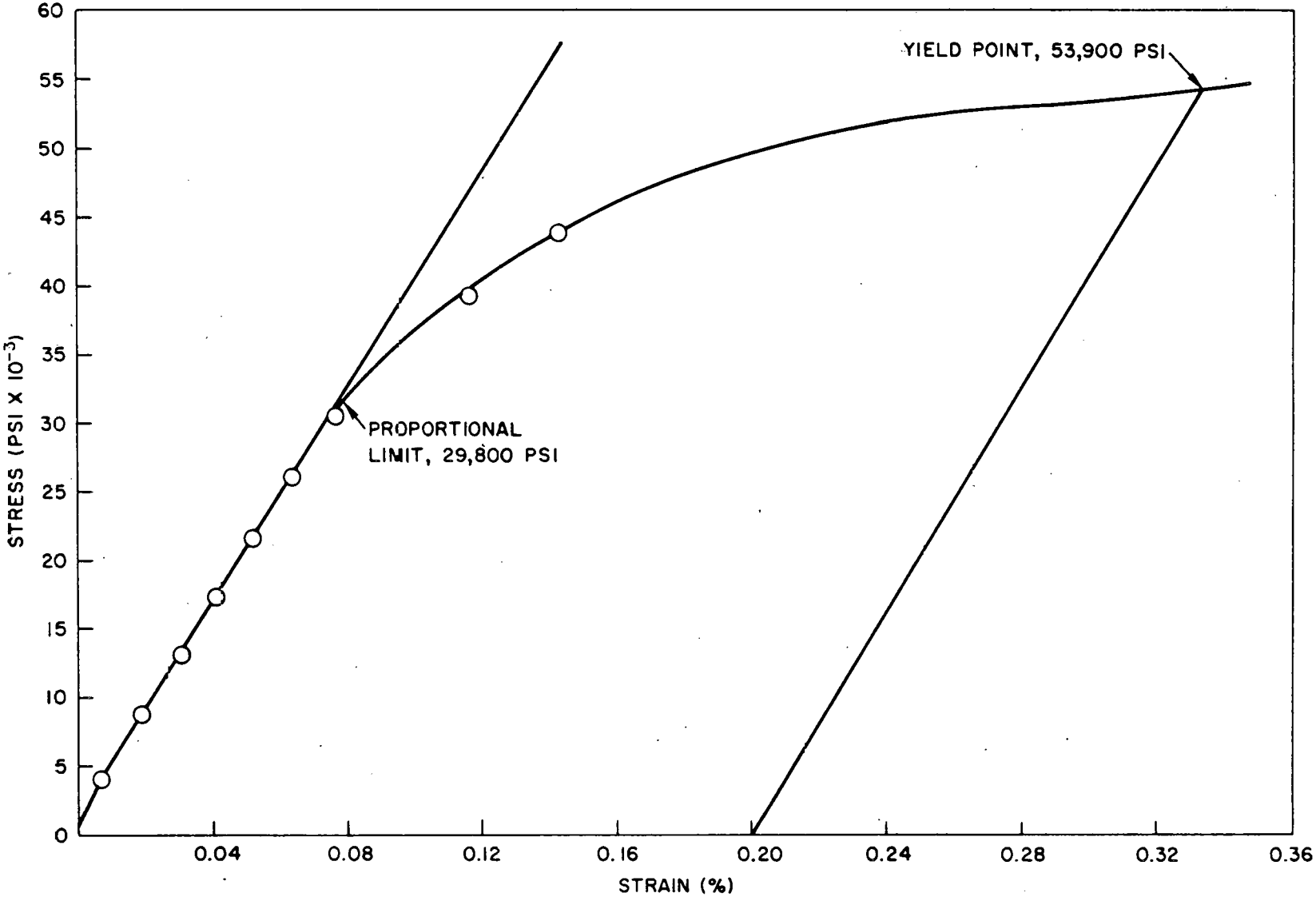

Fig. 3.4--Stress-strain curve for Hastelloy X after creep shrinking

THIS PAGE

WAS INTENTIONALLY

LEFT BLANK

IV. SITE DEVELOPMENT

EBOR SITE DEVELOPMENT (Task 66) (W. T. Furgerson, H. N. Wellhouser, C. H. Carson)

Preliminary design (Title I) of the EBOR site was completed by General Atomic and the architect-engineer in mid-September, 1961. Aside from some modifications necessitated by a change in the fuel-handling procedure,[1] little design work has been done on the site. Final design of the facility (Title II) will begin as soon as the AEC completes contract negotiations with the architect-engineer. Meanwhile, General Atomic is proceeding with the Title II design as far as it pertains to their portion of the project. This work is generally limited to the purchase of certain pieces of the equipment and is covered in Section I.

REFERENCE

1. MGCR Quarterly Progress Report for the Period Ending December 31, 1961, General Atomic, Report GA-2847.

EXPERIMENTAL BERYLLIUM OXIDE REACTOR PROJECT ORGANIZATION

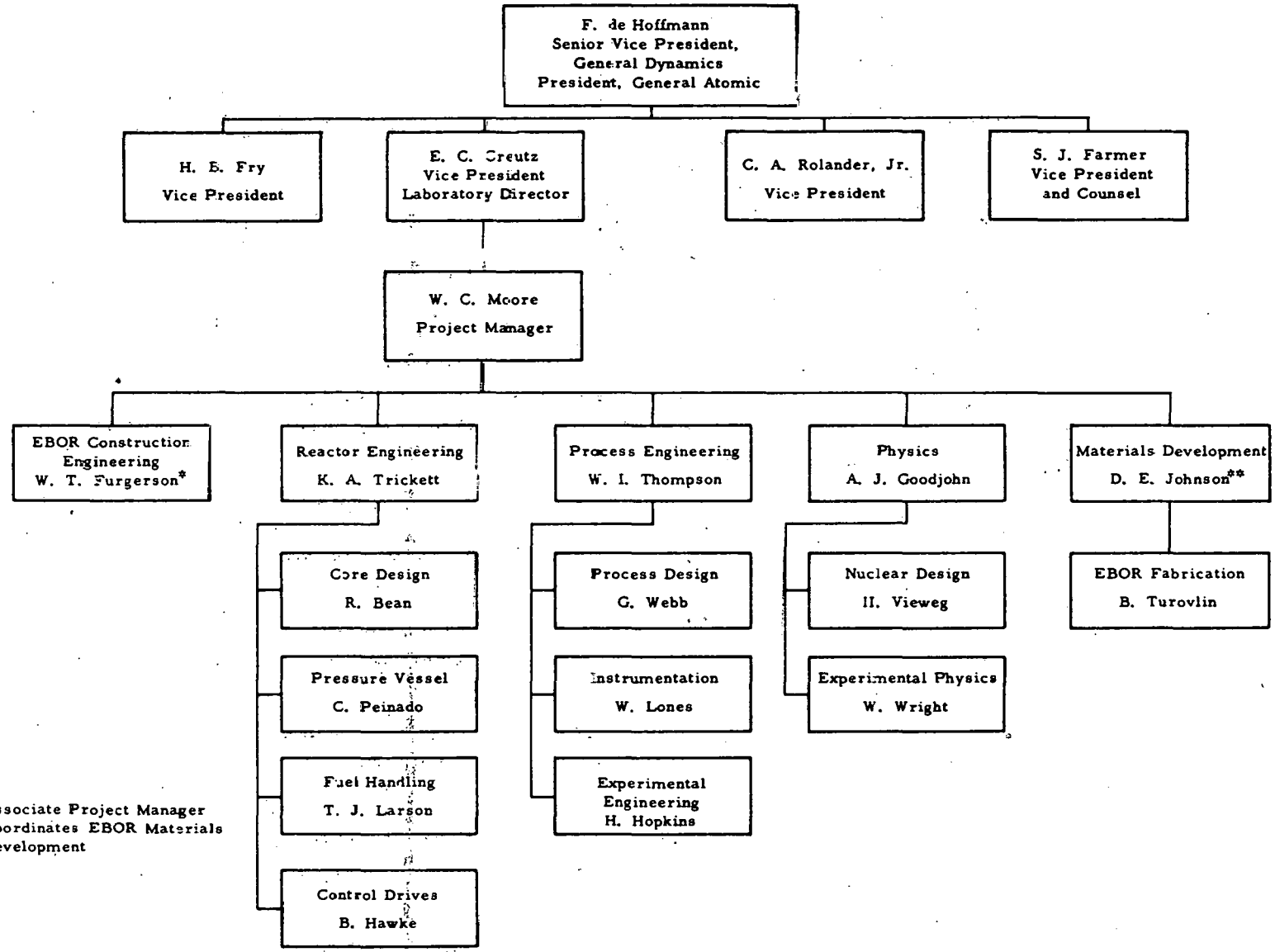

* Associate Project Manager
** Coordinates EBOR Materials Development